ENERGY RECOVERY AND TORQUE RIPPLE ANALYSIS OF DIRECT TORQUE CONTROL BASED INDUCTION MOTOR DRIVE

A Thesis submitted to Gujarat Technological University

for the Award of

Doctor of Philosophy

in

Electrical Engineering

by
Pravinkumar Dhanjibhai Patel
149997109010

under the supervision of

Dr. Saurabh N. Pandya

GUJARAT TECHNOLOGICAL UNIVERSITY
AHMEDABAD

June-2021

DECLARATION

I declare that the thesis entitled **Energy Recovery and Torque Ripple Analysis of Direct Torque Control based Induction Motor Drive** submitted by me for the degree of Doctor of Philosophy is the record of research work carried out by me during the period from **June 2014 to June 2021** under the supervision of **Dr. Saurabh N. Pandya** and this has not formed the basis for the award of any degree, diploma, associateship, fellowship, titles in this or any other University or other institution of higher learning.

I further declare that the material obtained from other sources has been duly acknowledged in the thesis. I shall be solely responsible for any plagiarism or other irregularities, if noticed in the thesis.

Signature of Research Scholar: 

Date: 04/06/2021

Name of Research Scholar: **Pravinkumar Dhanjibhai Patel**

Place: **Patan**

CERTIFICATE

I certify that the work incorporated in the thesis **Energy Recovery and Torque Ripple Analysis of Direct Torque Control based Induction Motor Drive** submitted by **Mr. Pravinkumar Dhanjibhai Patel** was carried out by the candidate under my supervision/guidance. To the best of my knowledge: (i) the candidate has not submitted the same research work to any other institution for any degree/diploma, Associateship, Fellowship or other similar titles (ii) the thesis submitted is a record of original research work done by the Research Scholar during the period of study under my supervision, and (iii) the thesis represents independent research work on the part of the Research Scholar.

Signature of Supervisor: 

Date: 04/06/2021

Name of Supervisor: **Dr. Saurabh N. Pandya**

Place: **LEC, Morbi**

Course-work Completion Certificate

This is to certify that Mr. **Pravinkumar Dhanjibhai Patel** enrolment no. 149997109010 is a PhD scholar enrolled for PhD program in the branch **Electrical Engineering** of Gujarat Technological University, Ahmedabad.

(Please tick the relevant option(s))

☐ He/She has been exempted from the course-work (successfully completed during M.Phil Course)

☐ He/She has been exempted from Research Methodology Course only (successfully completed during M.Phil Course)

☑ He/She has successfully completed the PhD course work for the partial requirement for the award of PhD Degree. His/ Her performance in the course work is as follows-

Grade Obtained in Research Methodology (PH001)	Grade Obtained in Self Study Course (Core Subject) (PH002)
BC	BB

Supervisor's Sign

(Dr. Saurabh N. Pandya)

Originality Report Certificate

It is certified that PhD Thesis titled **Energy Recovery and Torque Ripple Analysis of Direct Torque Control based Induction Motor Drive** submitted by **Mr. Pravinkumar Dhanjibhai Patel** has been examined by us. We undertake the following:

a. Thesis has significant new work/knowledge as compared already published or are under consideration to be published elsewhere. No sentence, equation, diagram, table, paragraph or section has been copied verbatim from previous work unless it is placed under quotation marks and duly referenced.

b. The work presented is original and own work of the author (i.e. there is no plagiarism). No ideas, processes, results or words of others have been presented as Author own work.

c. There is no fabrication of data or results which have been compiled/analyzed.

d. There is no falsification by manipulating research materials, equipment or processes, or changing or omitting data or results such that the research is not accurately represented in the research record.

e. The thesis has been checked using **URKUND Software** (copy of originality report attached) and found within limits as per GTU Plagiarism Policy and instructions issued from time to time (i.e. permitted similarity index <10%).

Signature of Research Scholar:  Date: 04/06/2021

Name of Research Scholar: **Pravinkumar Dhanjibhai Patel**

Place: **Patan**

Signature of Supervisor…  Date: 04/06/2021

Name of Supervisor: **Dr. Saurabh N. Pandya**

Place: **LEC, Morbi**

Copy of Originality Report

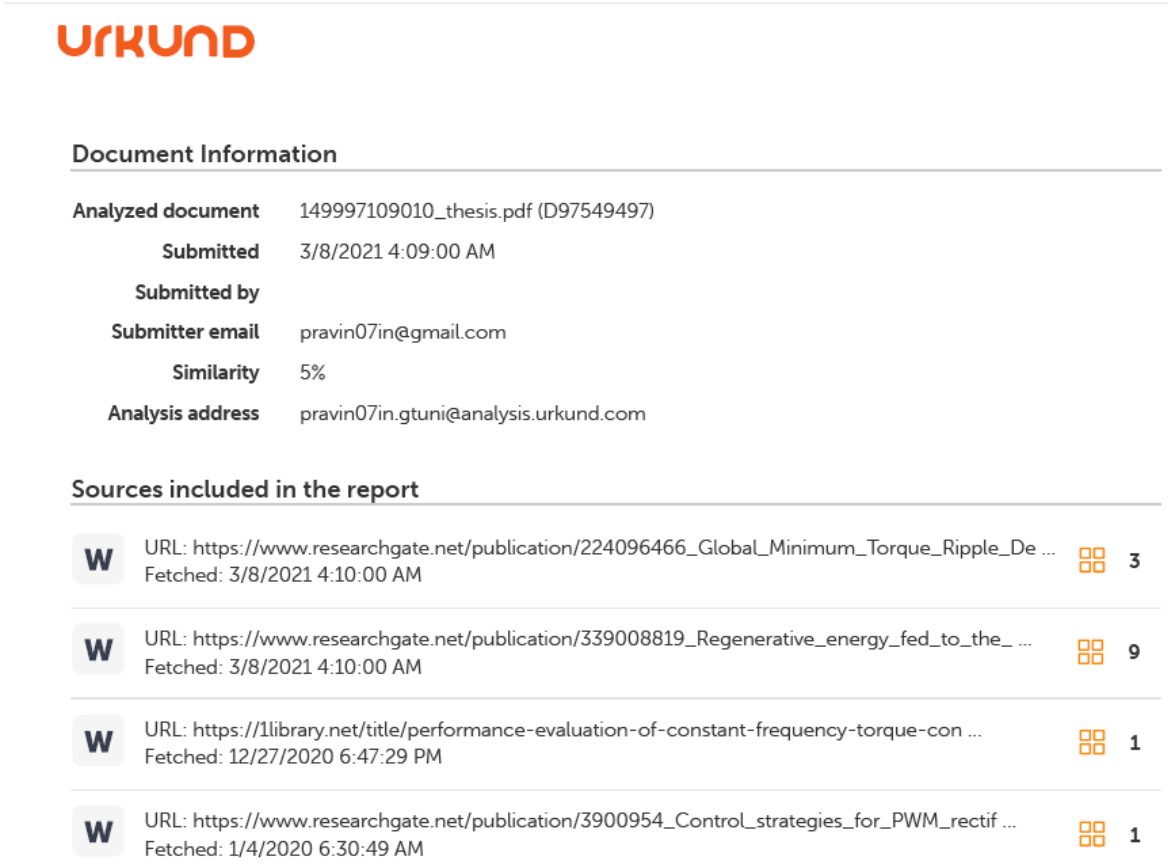

URKUND

Document Information

Analyzed document	149997109010_thesis.pdf (D97549497)
Submitted	3/8/2021 4:09:00 AM
Submitted by	
Submitter email	pravin07in@gmail.com
Similarity	5%
Analysis address	pravin07in.gtuni@analysis.urkund.com

Sources included in the report

W	URL: https://www.researchgate.net/publication/224096466_Global_Minimum_Torque_Ripple_De ... Fetched: 3/8/2021 4:10:00 AM	3
W	URL: https://www.researchgate.net/publication/339008819_Regenerative_energy_fed_to_the_ ... Fetched: 3/8/2021 4:10:00 AM	9
W	URL: https://1library.net/title/performance-evaluation-of-constant-frequency-torque-con ... Fetched: 12/27/2020 6:47:29 PM	1
W	URL: https://www.researchgate.net/publication/3900954_Control_strategies_for_PWM_rectif ... Fetched: 1/4/2020 6:30:49 AM	1

Urkund Submission ID: D97549497

File Name: Thesis_149997109010 (4.8 MB)

Word Count: 31861 word(s)

Submission Date: 8/3/2021

Similarity: 5%

PhD THESIS Non-Exclusive License to GUJARAT TECHNOLOGICAL UNIVERSITY

In consideration of being a PhD Research Scholar at GTU and in the interests of the facilitation of research at GTU and elsewhere, I, **Pravinkumar Dhanjibhai Patel** having **Enrollment No. 149997109010** hereby grant a non-exclusive, royalty free and perpetual license to GTU on the following terms:

a) GTU is permitted to archive, reproduce and distribute my thesis, in whole or in part, and/or my abstract, in whole or in part (referred to collectively as the "Work") anywhere in the world, for non-commercial purposes, in all forms of media;

b) GTU is permitted to authorize, sub-lease, sub-contract or procure any of the acts mentioned in paragraph (a);

c) GTU is authorized to submit the Work at any National / International Library, under the authority of their "Thesis Non-Exclusive License";

d) The Universal Copyright Notice (©) shall appear on all copies made under the authority of this license;

e) I undertake to submit my thesis, through my University, to any Library and Archives. Any abstract submitted with the thesis will be considered to form part of the thesis.

f) I represent that my thesis is my original work, does not infringe any rights of others, including privacy rights, and that I have the right to make the grant conferred by this non-exclusive license.

g) If third party copyrighted material was included in my thesis for which, under the terms of the Copyright Act, written permission from the copyright owners is required, I have obtained such permission from the copyright owners to do the acts mentioned in paragraph (a) above for the full term of copyright protection.

h) I retain copyright ownership and moral rights in my thesis, and may deal with the copyright in my thesis, in any way consistent with rights granted by me to my University in this non-exclusive license.

i) I further promise to inform any person to whom I may hereafter assign or license my copyright in my thesis of the rights granted by me to my University in this non- exclusive license.

j) I am aware of and agree to accept the conditions and regulations of PhD including all policy matters related to authorship and plagiarism.

Signature of Research Scholar: 

Name of Research Scholar: **Pravinkumar Dhanjibhai Patel**

Date: 04/06/2021 Place: **Patan**

Signature of Supervisor: 

Name of Supervisor: **Dr. Saurabh N. Pandya**

Date: 04/06/2021 Place: **LEC, Morbi**

Seal: **Dr. Saurabh N. Pandya**
Principal,
LEC, Morbi

Thesis Approval Form

The viva-voce of the PhD Thesis submitted by **Mr. Pravinkumar Dhanjibhai Patel** (Enrol No. 149997109010) entitled **Energy Recovery and Torque Ripple Analysis of Direct Torque Control based Induction Motor Drive** was conducted on **04/06/2021, Friday** at Gujarat Technological University.

(Please tick any one of the following option)

☑ The performance of the candidate was satisfactory. We recommend that he be awarded the PhD degree.

☐ Any further modifications in research work recommended by the panel after 3 months from the date of first viva-voce upon request of the Supervisor or request of Independent Research Scholar after which viva-voce can be re-conducted by the same panel again.

(Briefly specify the modifications suggested by the panel)

☐ The performance of the candidate was unsatisfactory. We recommend that he should not be awarded the PhD degree.

(The panel must give justifications for rejecting the research work)

PRINCIPAL
L. E. COLLEGE, MORBI.

(Dr. Saurabh N. Pandya)
Name and Signature of Supervisor with Seal

(Dr. Anton Rassõlkin)
External Examiner -1 Name and Signature

(Dr. Rajen Pudur)
External Examiner -2 Name and Signature

(Dr. Kumaravel Sundaramoorthy)
External Examiner -3 Name and Signature

ABSTRACT

The main objectives of the thesis are to obtain efficient regenerative performance and to reduce the torque ripple for Direct Torque Control (DTC) based three phase induction motor drive. Nowadays, Industrial sector needs energy saving based variable-speed drive system for efficiency improvements. Direct Torque Control is one of the most unique and proficient control techniques of the induction motor. Direct Torque Control (DTC) has the significant energy saving potential in variable speed drive system. With the use of regenerative variable speed drive system, high-inertia loads and high-speed loads with frequent accelerating/decelerating operation, it is possible to save significant amount of energy. It is found that the considerable energy wastage in the form of heat energy during the deceleration period of variable frequency drive by brake chopper resistor. In this thesis energy recovery enhancement during deceleration of DTC based three phase induction motor drive using bidirectional DC/DC converter with capacitor bank as energy storage system is simulated using MATLAB^{TM}/ SIMULINK^{TM}. The another proposed method to fed back regenerative power to supply grid using DC/AC converter for DTC based induction motor drive is simulated and results are discussed. In DTC based three phase induction motor drive, energy recovery has been analyzed with change in variables like load torque, initial speed of starting of deceleration, motor power rating and deceleration rate. Among these, the most significant variable for energy recovery during deceleration has been investigated using the Taguchi method. The losses occurred during deceleration of induction motor has been discussed.

The other problem regarding DTC technique is utilizing hysteresis comparators which produce high torque ripple and variable switching frequency. The reduction in torque ripple is obtained using Fuzzy Logic Controller (FLC) based DTC technique and Carrier Space Vector PWM (CSVPWM) DTC.

Keywords: Direct Torque Control, DTC based Induction Motor drive, regenerative power, energy recovery during deceleration, Torque Ripple Reduction, Energy regeneration, deceleration rate, Taguchi method, Fuzzy Logic Controller (FLC), Carrier Space Vector PWM (CSVPWM) DTC.

Acknowledgement

This thesis would have been impossible without the support of many people. I would express my sincere gratitude to them, for their invaluable support deserves much more than this short note of appreciation. I would like to thanks, almighty the God giving me strength and passion for doing research.

I would like to express my sincere thanks to my supervisor **Dr. Saurabh N. Pandya** for his invaluable guidance and constant encouragement during every step of my research. Due to his extensive technical support able complete my research in time. I whole heartedly give my best wishes to him and his family. I would like to express my gratitude to **Dr. Hiren H. Patel** and **Dr. Rajesh M. Patel**. It was a great honor to have them as my Doctoral Progress Committee Members. Their constructive suggestions made the thesis sound in many aspects. I would especially thank to Head of Department of Electrical Engineering and Principal, G.E.C. PATAN for providing laboratory support. I am very thankful to staff of L. E. College, Morbi during my research for their support.

I give the greatest respect and love to my parents, my wife, my daughter and my son. I want to express my highest appreciation for their support and cooperation. I would like to say thanks to my wife for encouraging me to do research and her moral support. Thanks to almighty God for giving me the ability to complete research.

Finally, I am very thankful to all of my good wishers for assisting me to achieve the most important stage in my life. I express my gratitude to all those people who helped me directly or indirectly in my research work.

Thanking you,

Pravinkumar Dhanjibhai Patel

Table of Contents

List of Abbreviations

3L-DTC	Three Level Direct torque Control
AC	Alternating Current
AI	Artificial Intelligent
ANN	Artificial Neural Network
BLDC	Brushless Direct Current
CCS-MPC	Continuous Control Set Model Predictive Control
CDTC	Conventional Direct Torque Control
CFTC	Constant Frequency Torque Controller
CMV	Common Mode Voltage
CSVPWM	Carrier Space Vector Pulse Width Modulation
DC	Direct Current
D-DTC	Duty cycle-Direct Torque Control
DOE	Design of Experiments
DOF	Degree of Freedom
DR	Deceleration Rate
DSC	Direct Self Control
DTC	Direct Torque Control
DTFC	Direct Torque and Flux Control
EMF	Electromotive Force
EV	Electrical Vehicle
FIS	Fuzzy Interface System
FLC	Fuzzy Logic Control
FOC	Field Oriented Control
FPGA	Field Programmable Gate Array
IEEE	Institute of Electrical and Electronics Engineers
IFOC	Indirect Field Oriented Control
IGBT	Insulated Gate Bipolar Junction Transistor
IPMSM	Interior Permanent Magnet Synchronous Motors
KE	Kinetic Energy
MF	Membership Functions
MMF	Magneto Motive Force
NFS	Neuro Fuzzy System
NMPC	Nonlinear Model Predictive Control
PAM	Pole Amplitude Modulation
PI	Proportional Integral
PID	Proportional Integral Derivative
PLL	Phase Lock Loop
PMSM	Permanent Magnet Synchronous Motors
PTC	Predictive Torque Control
PV	Photo Voltaic

PWM	Pulse Width modulation
RPM	Revolution per Minute
SCR	Silicon Control Rectifier
SDPM	Self-Decelerating Permanent-Magnet
SPWM	Sinusoidal Pulse Width Modulation
ST-DTC	Switching Table based Direct Torque Control
SVM	Space Vector Modulation
SVPWM	Space Vector Pulse Width Modulation
THD	Total Harmonic Distortion
TR	Torque Ripple
VSI	Voltage Source Inverter

List of Symbols

$d\psi$	Stator flux error status
dT_e	Torque error status
$V_{qs}{}^{s}$, $V_{ds}{}^{s}$	q and d axis stator voltages
$i_{qs}{}^{s}$, $i_{ds}{}^{s}$	q and d axis stator currents
$V_{qr}{}^{s}$, $V_{dr}{}^{s}$	q and d axis rotor voltages
$i_{qr}{}^{s}$, $i_{dr}{}^{s}$	q and d axis rotor currents
$\Psi_{ds}{}^{s}, \Psi_{qs}{}^{s}$	d axis and q axis stator flux linkages
$\overline{\Psi}s$	Stator flux vector
$\overline{\Psi r}$	Rotor flux vector
V_a, V_b, V_c	Stator voltages
i_a, i_b, i_c	Stator currents
f_s	Stator frequency
R_s	Stator resistance
R_r	Rotor resistance
L_s	Stator inductance
L_r	Rotor inductance
L_m	Mutual inductance
P	Number of poles
J	Moment of inertia
T_e	Electromagnetic output torque
T_l	Load torque
T_d	Dynamic torque
ω_e	Angular velocity
τ_{r6}	6^{th} harmonic torque
K	Torque constant
Ψ_{1m}	Air-gap flux
I_{5r}, I_{7r}	5^{th} and 7^{th} harmonics currents
γ	Angle between the stator and rotor flux linkage space vectors
δ	The phase angle between the air gap flux and rotor current
N	Rotor speed

ω_m	Rotor angular velocity
ω_s	Synchronous angular velocity
ω	Angular velocity
T_{fl}	Full Load Torque
K_L	Kinetic energy of the load
K_m	Motor kinetic energy
K_T	Total kinetic energy
I_L	Moment of inertia of load
I_m	Motor rotor inertia
S_1	Starting slip
S_2	Final slip
V_{dc}	DC link voltage
V_{ref}	Reference voltage
I_{cap}	Capacitor bank current
V_{cap}	Capacitor bank voltage
F	Friction factor
I_{peak}	Peak charging current
P_m	Mechanical power
P_e	Electrical power for the motor
α	Acceleration
β	Frictional coefficient
N_1	Initial Speed of deceleration
N_2	Final speed of deceleration
t_1	Initial time of deceleration
t_2	Final time of deceleration
M	Energy Multiplying factor
η	Energy recovery Efficiency
E	Rotational kinetic energy
Ig_peak	Grid side peak current
E_{Losses}	Energy Losses
$E_{recovery}$	Recoverable energy
$E_{k.e.d.}$	Diminishing Kinetic energy during deceleration
C_d	Skin friction coefficient

ρ	Medium density
R	Radius of motor
L	Cylinder length of the motor
Yi	Experimental value
N	No. of observations
SN_i	Signal to Noise Ratio

List of Figures

List of Tables

List of Appendices

CHAPTER-1

1 Introduction

1.1 General

The first electrical drive was invented 180 years ago. Harry and Ward-Leonard first ever generated idea to regulate the speed of induction motor at the turn of the 19th century. The electrical variable speed drives is persistently being developed to save electrical energy used in industrial applications. The faster growth of power electronics switches have major role in revolution of electrical drives [1].

Electric motor consumes 30-40% power of the world and 70% power used in industries [1][2]. Hence even 1% saving in motion control have huge scope of energy saving. Fig. 1.1 shows different motors utilised in percentage invarious industries.

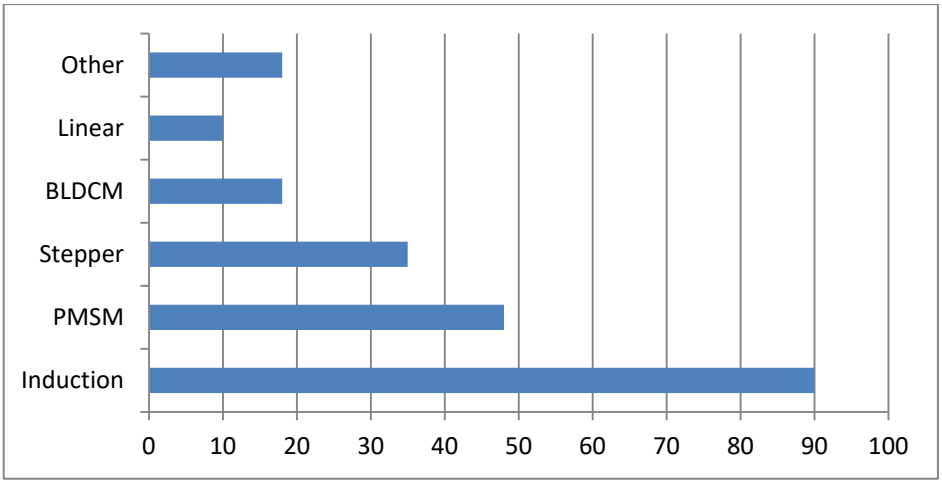

FIGURE 1.1: Motor used in various industries [1]

Induction motor is widely used in industries due to reliability, cost, easy construction and ease of control. Permanent magnet synchronous motors (PMSM), stepper motors and brushless direct current (BLDC) motors are also in keen interest for industries. The

permanent magnets synchronous motors are still more expensive than induction motors. To control speed and torque precisely, recent advancement in variable speed drive technology plays an important role. In addition to process control, the energy saving aspect of variable frequency drives is currently receiving more attention [2].

The aim of this chapter is to explore motivation behind the research work done in this thesis. The chapter contains the main objectives of the research and the thesis organisation.

1.2 Introduction

The electric drives are used for motion control. Nowadays, around 70% of the electric power is consumed by electric drives. During the last four decades, AC drives are become more popular, especially induction motor drives. Due to its robustness, high efficiency, high performance, rugged structure and ease of maintenance it is widely used in industrial application, such as paper miles, robotics, steel miles, servos, transportation system, elevators, machines tools etc.

The Induction motor drives control methods can be divided into two methods, one is scalar and the other is vector control. The general classification of the variable frequency controls is presented in Fig. 1.2 [2],[3]. The scalar control is operates in steady-state and controls the angular speed of current, voltage, and flux linkage in the space vectors. Thus, the scalar control does not operate in the space vector position during a transient state. The vector control, which is based on relations valid for dynamic states, not only angular speed and magnitude but also the instantaneous position of current, voltage, and flux linkage of space vector, are controlled. In the vector control, one of the most popular control methods for induction motor drives is known as Field Oriented Control (FOC). It is presented by F. Blaschke (Direct FOC) and Hasse (Indirect FOC) in the early 1970s, and FOC gives high performance and high efficiency for industrial applications [4]. The DTC was initially introduced in the middle of 1980s, Takahashi Isao and Noguchi Toshihiko proposed a new technique called DTC for the control of induction motor, which gives quick torque response and is highly efficient [5],[6]. This proposed control circuit has the disadvantage of making some drift in extremely low-frequency operation, however, which can be

compensated easily and automatically to minimize the effect of variation of machine constant [5].

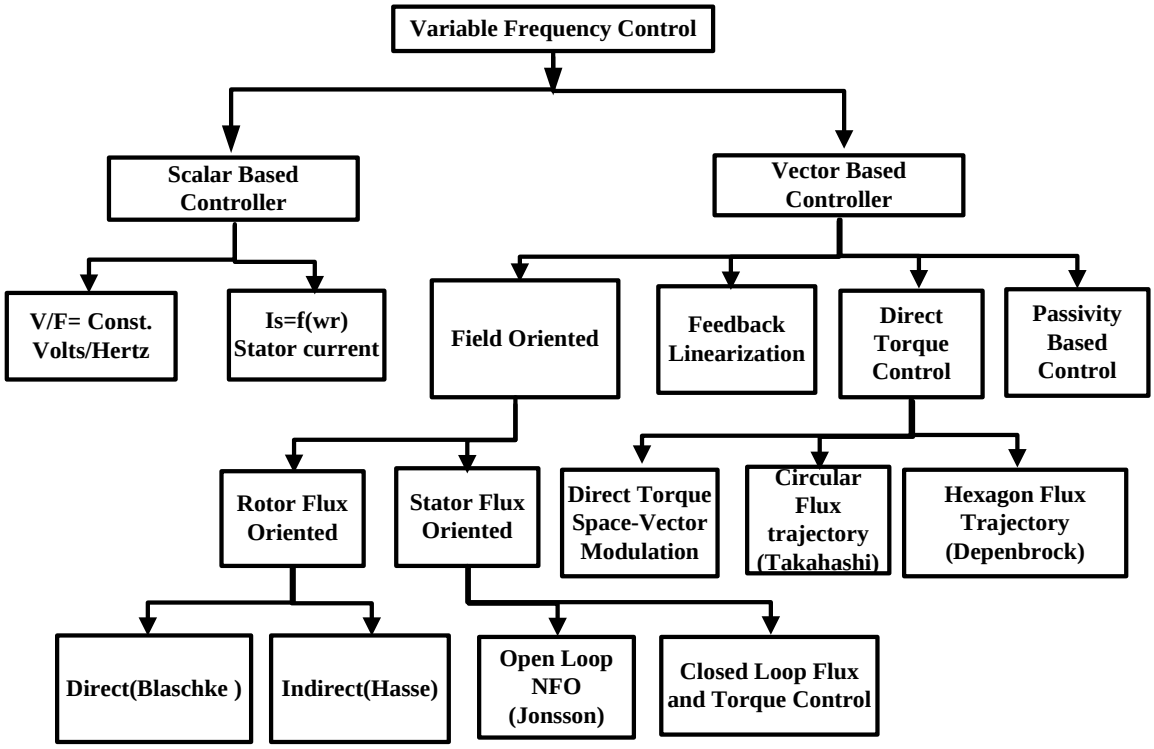

FIGURE 1.2: Classification of induction motor control methods [3].

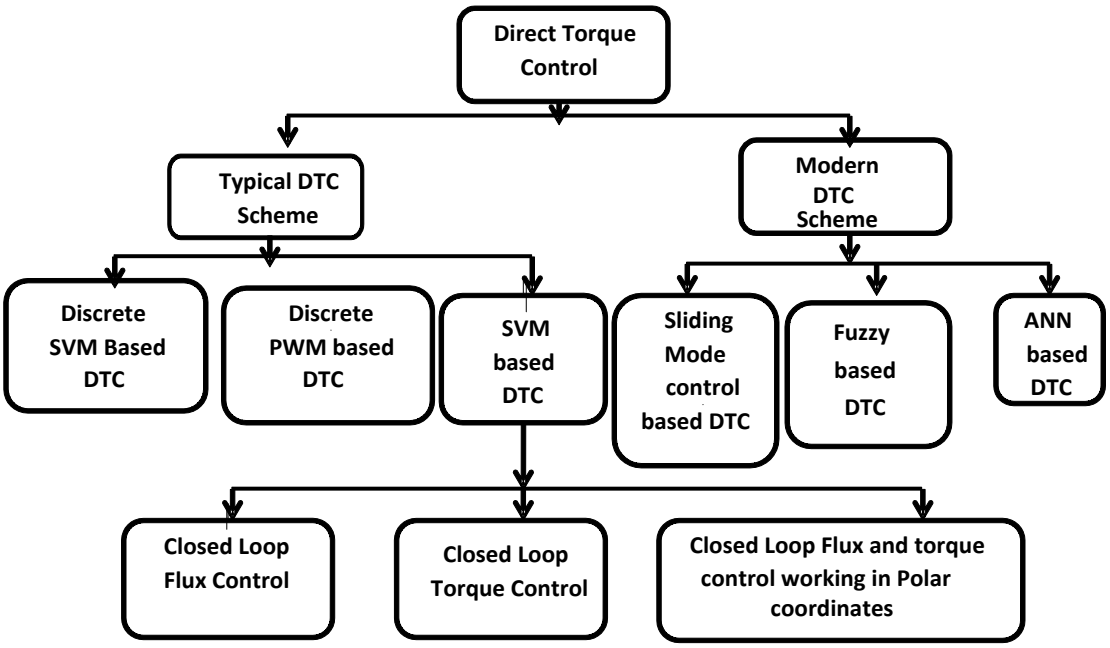

FIGURE 1.3: Advanced classification of Direct Torque Control scheme [7]

In 1986, Depenbrock proposed new “direct self-control (DSC)”, is a simple method of signal processing which gives an excellent dynamic performance to control the torque of an induction motor, in which directly controlled by comparing the time integrals of its line to- line voltages to reference values $+\Psi_{ref}$. This is called “direct self-control” (DSC) [6]. Fig. 1.3 shows different strategies due to improvement in DTC by various researcher using latest technologies incorporated in it [7],[8]. To improve the performance of induction motor many new techniques are available such as GA, ANN, Fuzzy controller, etc, [8].

1.3 Brief description of the Direct Torque Control

The main feature of DTC is a simple structure, good dynamic behaviour, high performance and efficiency. DTC proposed replacement of motor linearization and to decouple via coordinate transformation, by torque and flux hysteresis controllers. This method is referred to as conventional DTC. Fig.1.4. shows a block diagram of the DTC based induction motor drive [5].

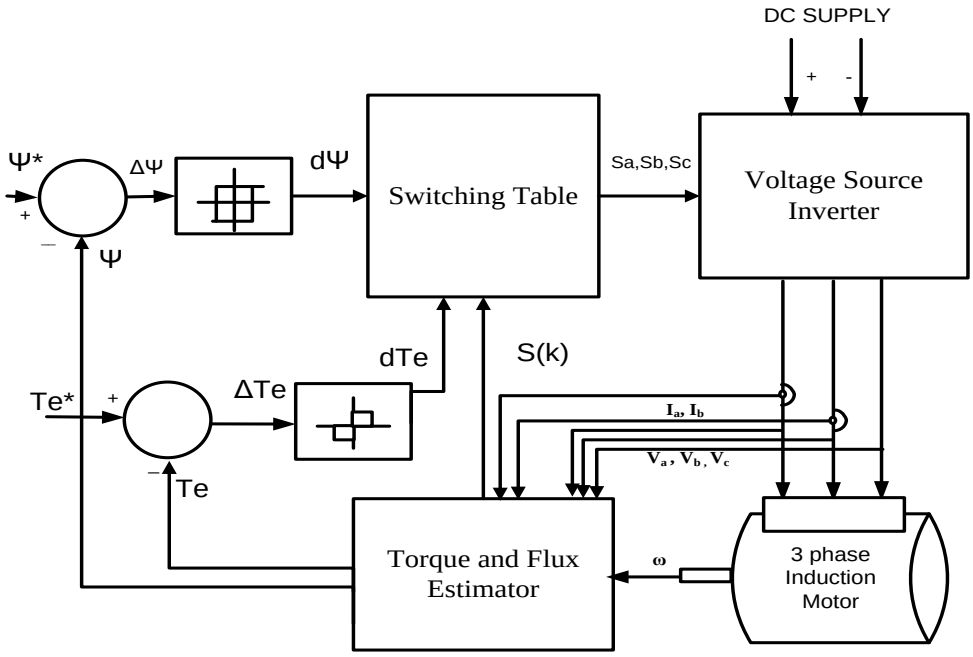

FIGURE 1.4 : Representation of DTC based three phase induction motor drive [5]

DTC scheme is well known for its robustness in control as it is less dependency on machine parameters. DTC does not need the complex field orientation block, speed encoder and the inner current regulation loop. The DTC worked based on comparison method using hysteresis-based controllers. Due to the hysteresis-based operation, the compensation in the torque error may lead to the unpredictable switching frequency as well as high torque ripple which depend on the operating conditions.

Fig. 1.5 shows (a) simplified three phase VSI (b) represents eight possible switches for DTC configurations in three phase two-level VSI, (d) represents a circular trajectory of stator flux. The look-up table is given in Table 1.1 [2],[9].

TABLE 1.1: Lookup Table (Voltage Vector Selection) for DTC [2]

dψ (stator flux error status)	**dTe (Torque Error status)**	**S(1)**	**S(2)**	**S(3)**	**S(4)**	**S(5)**	**S(6)**
1	1	V_2	V_3	V_4	V_5	V_6	V_1
	0	V_0	V_7	V_0	V_7	V_0	V_7
	-1	V_6	V_1	V_2	V3	V_4	V_5
0	1	V_3	V_4	V_5	V_6	V_1	V_2
	0	V_7	V_0	V_7	V_0	V_7	V_0
	-1	V_5	V_6	V_1	V_2	V_3	V_4

In DTC, stationary reference frame is used to find flux vector magnitude and direction in which a-b-c to the d-q transformation is required. In DTC, by applying the switching table of inverter voltage vector to increase or decrease the angle between stator flux and rotor flux hence to control the torque. Fig. 1.4 demonstrates the block diagram of DTC and Fig. 1.5 shows a voltage vector representation for DTC drive [5],[6]. Fig. 1.5 (a) demonstrates the three phase VSI diagram. Fig. 1.5 (b) shows space vectors and sectors, Fig. 1.5(c) shows switching voltage vectors representation and Fig. 1.5 (d) shows circular trajectories of stator flux for DTC drive [5],[6].

The equations to calculate the torque and flux are discussed in [2]. The phase voltages (Va, Vb, Vc) and phase currents (ia, ib, ic) are converted in d-q frame voltages ($V_{qs}{}^{s}$, $V_{ds}{}^{s}$), and currents ($i_{qs}{}^{s}$, $i_{ds}{}^{s}$) using following equations 1.1 to 1.4.

$$V_{qs}{}^{s} = \frac{2}{3}V_a - \frac{1}{3}V_b - \frac{1}{3}V_c \tag{1.1}$$

$$V_{ds}{}^{s} = -\frac{1}{\sqrt{3}}V_b + \frac{1}{\sqrt{3}}V_c \tag{1.2}$$

$$i_{qs}{}^{s} = \frac{2}{3}i_a - \frac{1}{3}i_b - \frac{1}{3}i_c = i_a \tag{1.3}$$

$$i_{ds}{}^{s} = -\frac{1}{\sqrt{3}}i_a - \frac{2}{\sqrt{3}}i_b \tag{1.4}$$

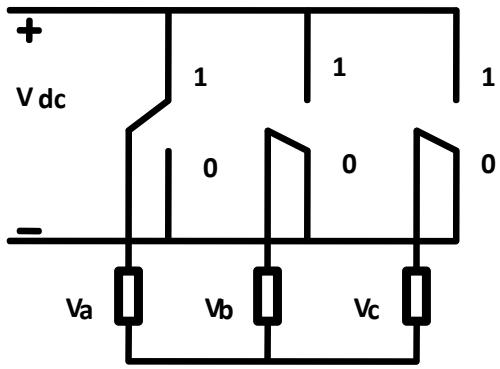

(a) Simplified Diagram of 3 Φ VSI

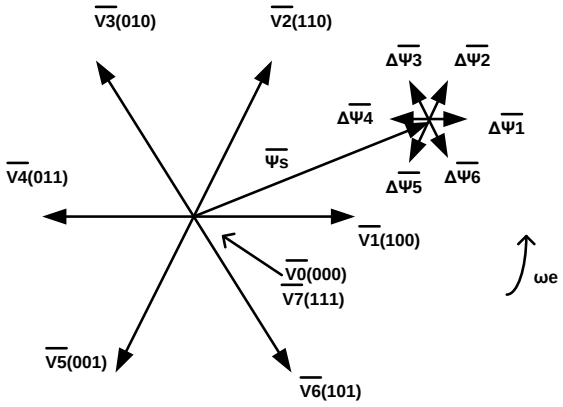

(b) Representation of space voltage vectors

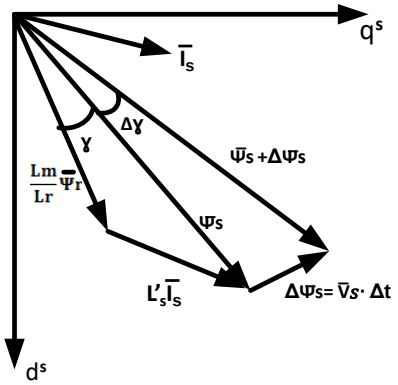

(c) Representation of switching voltage vectors

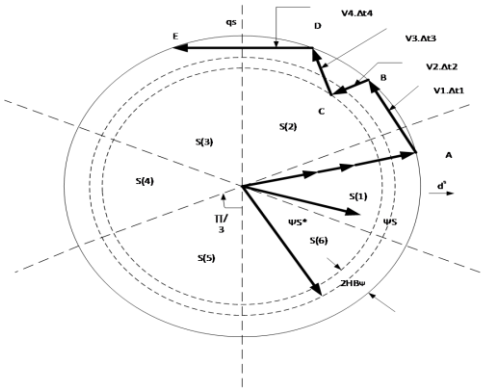

(d) Circular trajectory of stator flux

FIGURE. 1.5: Voltage vector representation for DTC method of induction motor drive

The d axis and q axis stator flux linkages ($\Psi_{ds}{}^{s}, \Psi_{qs}{}^{s}$) are found by equation (1.5) and (1.6) respectively. The effect of stator resistance (R_s) to calculate the flux of d-q axis components is dominant.

$$\Psi_{ds}{}^{s} = \int (V_{ds} - R_s . i_{ds}{}^{s}) dt \tag{1.5}$$

$$\Psi_{qs}{}^{s} = \int (V_{qs} - R_s . i_{qs}{}^{s}) dt \tag{1.6}$$

$$\Psi s = \sqrt{\Psi_{ds}{}^{s2} + \Psi_{qs}{}^{s2}} \tag{1.7}$$

$$\gamma = \tan^{-1}\left(\frac{\Psi_{qs}{}^{s}}{\Psi_{ds}{}^{s}}\right) \tag{1.8}$$

To control flux two level hysteresis comparator is used. Two suitable active voltage vectors are use to control the flux for every sector as shown in Fig. 1.5 d. Output of two level hysteresis comparator is 1 or 0 according to flux error goes positive or negative. The flux error is generated as input of flux hysteresis comparator, by comparing actual stator flux with reference flux value. Three level hysteresis controller is used in torque control unit of DTC. The torque error is generated by comparing actual torque with reference torque value. The output of three level hysteresis torque comparator is 1, 0 or -1. According to Table 1.1, the output of flux control unit and torque control unit status, the suitable voltage vector is selected. Hence fast dynamic control of torque is possible.

γ is the angle between the stator and rotor flux linkage space vectors as expressed in (1.8). By controlling the stator flux using the appropriate switching of stator voltages quickly adjusts the electromagnetic torque (τ). The electromagnetic torque is expressed using equations (1.9) and (1.10).

$$\tau = \frac{3p}{4}(\Psi_{ds}{}^{s} . i_{qs}{}^{s} - \Psi_{qs}{}^{s} . i_{ds}{}^{s}) \tag{1.9}$$

$$\tau = \frac{3p}{4}\left(\frac{Lm}{Ls' . Lr}\right) \Psi s . \Psi r . \sin\gamma \tag{1.10}$$

Electromagnetic torque can be changed by changing the angle between the stator and rotor flux linkage space vectors (γ). Torque pulsations cause noise and vibrations. Torque pulsations caused by supply current ripple, phase current commutation and from machine cogging effect. In electrical machines, torque ripple is due cogging effect, distortion of the sinusoidal distribution of the magnetic flux density in the air gap and unequal permeance in the d and q axis [2]. Torque pulsations become especially noticeable at low frequency

(f_s = 0-5Hz) thus putting the limit on the range of speed control. Low torque harmonics can be damped by stator current PWM. Torque pulsating components with six times of supplied frequency ($6f_s$) are independent of the motor load. The sixth harmonic amplitude is proportional to the square of the flux. Therefore, flux weakening may considerably reduce torque pulsations. For low frequencies (f_s <= 5Hz), the effect of stator resistance voltage drop on the stator voltage becomes remarkable. The increase of the frequency of pulsating torque components may be effectively damped by rotor inertia without causing any fluctuation of its speed [10]. Torque pulsation is produced due to air gap flux at one frequency interacting with rotor MMF at a different frequency. The general torque expression as a function of air-gap flux (Ψ_{rm}), rotor current (i_{1r}) , and the phase angle (δ) between the air gap flux and rotor current.

$$\tau = k\Psi_{rm}.\, i_{1r}.\sin\delta \tag{1.11}$$

6^{th} harmonic torque is produced by the interaction of fundamental flux with the 5th and 7^{th} harmonics currents and vice versa. 6^{th} harmonic torque can be given as

$$\tau_{r6} = k\Psi_{1m}(I_{7r} - I_{5r})\sin 6\omega_e t \tag{1.12}$$

The high frequency pulsating torque component is induced due to PWM control of inverter that produces a ripple current in the phases. This pulsating torque effect is negligible due to enough high inertia of the motor. At low-frequency operation, mechanical resonance may occur, causing severe shaft vibration, fatigue, wearing of gear teeth, instability of the feedback control system[3]. The problem of higher torque ripple is persists in low inertia motor during low speed operation.

1.4 An overview of energy recovery during deceleration of induction motor drive

The basic idea is to improve in energy recovery of DTC based induction motor drive during deceleration of high inertia load. Fig. 1.6 shows speed-torque characteristics for variable frequency drive operation. For variable frequency drive operation, When induction motor commanded to decelerate from higher speed (N) to lower speed (N'), its synchronous speed also transit from Ns to Ns'. Hence, during transition, actual speed of induction motor is N and new synchronous speed Ns', as Ns'< N, hence regenerative action occurs for a short period of time during which energy regeneration is possible.

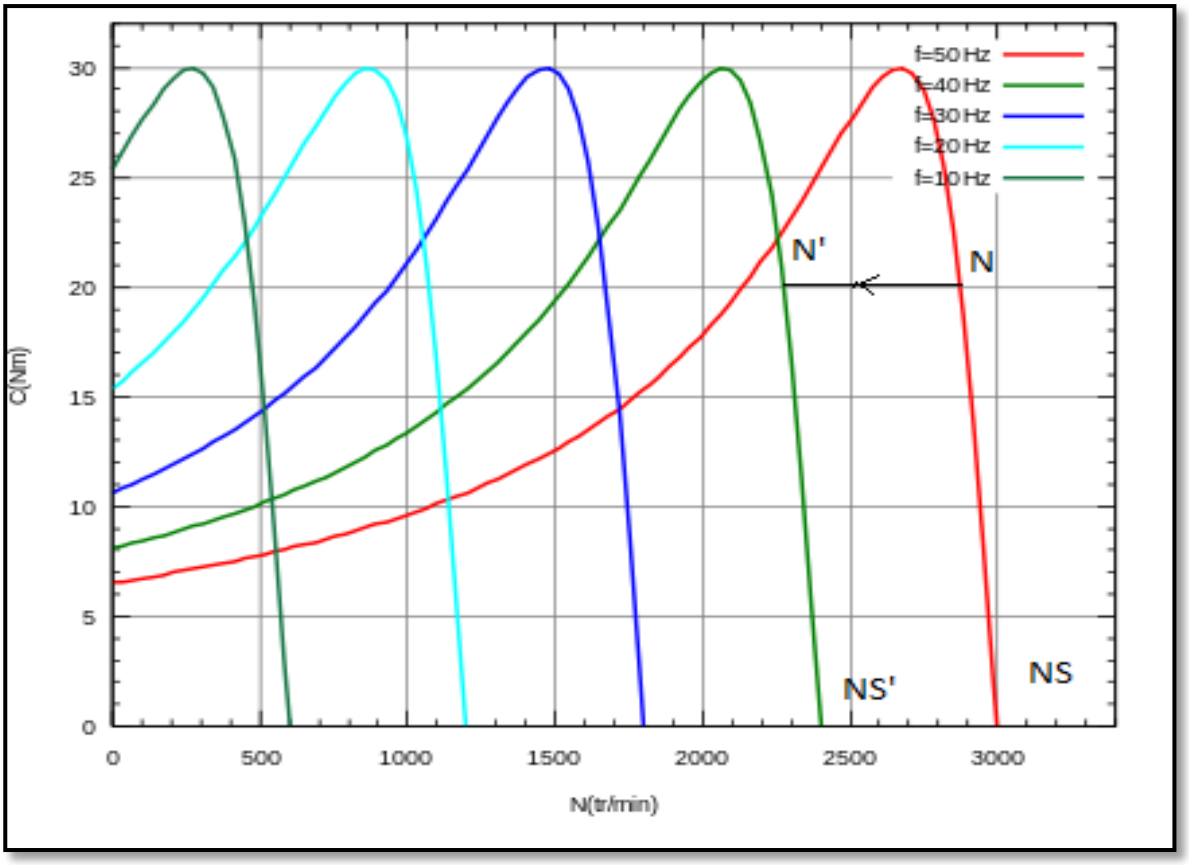

FIGURE 1.6: Speed torque characteristics for variable frequency drive operation [11]

Many researchers have discussed an EV application using DTC based induction motor drive and its capability for an electric vehicle [12][13][14]. Some benefits of DTC as Electrical Vehicle Drive selection like (1) The ability of a wide range of speed variation operations with the maximum ability of torque. (2) DTC is reliable to provide a robust field weakening and support frequent start-stop and acceleration. (3) More extensive speed range [12][13].

S. Harada et al. show that regenerative energy improved up to 16% by optimal deceleration trajectory method [15]. A. Taut et al. developed detection circuit works on point at which recovery occurs. Charging of supercapacitor at constant power topology requires a transfer of power from the power source to the supercapacitor at constant voltage and constant current rate. The supercapacitor voltage is less than 40 % of the maximum and charging current should be lower than 2.5 times the usually required for a reasonable charge. Energy obtains from deceleration is converted to DC and help to store energy in a supercapacitor. It depends on the deceleration time and speed of required deceleration [16]. During the deceleration period, simulation results are shows that the supercapacitor is charged due to high inertia kinetic energy which is recovered from induction motor and load. During acceleration and when a heavy load applied suddenly,

supercapacitor get discharged and helped to the battery to supply motor. In an application like lift, traction, electric vehicle drives, etc. battery or supercapacitor type energy storage device is connected across DC link through DC/DC bidirectional converter.

The study also covered the efficient use of regenerative power of induction motor drives. The main objective of the study is to find energy recovery during deceleration for the DTC based three phase induction motor drive, which in turn increase the efficiency of the system. Conventional variable frequency drive has considerable energy wastage in the form of heat during the braking period due to brake chopper resistor unit. An energy cost-saving approach using regenerative power unit for applications deals with frequent deceleration of large inertia load can be achieved. Various topologies are illustrated for effective utilisation of regenerative power during deceleration of induction motor drive. The simulation results are discussed regarding energy recovery of Direct Torque Control (DTC) drive during regenerative braking mode for three phase induction motor.

During acceleration, the induction motors take power from the AC supply and convert to DC through the diode bridge rectifier circuit. The DC link voltage is maintained to a rated value which is converted to AC voltage by an DTC controlled inverter. The kinetic energy depends on the angular speed of motor and moment of inertia of load and motor. During deceleration, the kinetic energy is fed back through freewheeling diodes works as rectifier circuit, and hence DC bus voltage is increased drastically. In the conventional method, the drive has a dynamic braking resistor unit in which the energy is dissipated as heat, hence efficiency is reduced. The regenerative braking unit allows energy injected back to the source or grid. The resistance bank is replaced by DC/AC converter which fed back this recoverable kinetic energy of the three phase induction motor to the grid during deceleration. Before fed to the grid, a synchronisation condition must be satisfied to achieve it. The appropriate inverter output voltage is obtained using a phase lock loop (PLL) with the grid needed. The vector decouples control strategy, and current control method is applied for regenerative braking. The fed to grid energy recovery system is helpful to industries like text tile, paper, shopping mall lift, escalators, etc.

1.5 An overview of torque ripple reduction strategy of DTC induction motor drive

Industrial applications like Textile and Paper industries demand fast, precise and smooth control. SVPWM DTC based induction motor drive may be helpful to satisfy the requirement of such industries. Torque smoothness is an essential requirement in a wide range of high-performance motion control applications. For example, the quality of the surface finish achievable with metal-working machine tools is directly dependent on the smoothness of the instantaneous torque delivered to the rotary tool-piece. Similarly, the performance specifications of servo motors embedded in equipment ranging from robots to satellite trackers require minimization of all sources of pulsating torque. Even mass-produced consumer products such as electric-assisted power steering demand high levels of torque smoothness to meet user expectations [17]. Space Vector Pulse Width Modulation (SVPWM) DTC technique helps to solve the underlying issues of torque ripple. Constant-switching-frequency DTC-SVM schemes improve the drive performance considerably in terms of reduced torque and flux pulsations, reliable start-up and low-speed operation.

The different methods of torque ripple reduction like Predictive DTC, DTC-SVM schemes, Global Minimum Torque Ripple Design, constant frequency torque controller (CFTC), Single-rate Control Strategy, CSVPWM DTC etc. found in the literature. Conventional DTC has a variable frequency; hence high torque ripple cannot be predicted and not quickly diminished. The space vector pulse width modulation (SVPWM) with DTC is a successful method to reduce the torque ripples as one can predict the torque ripple and hence find a solution. It is found that artificial intelligent techniques (FLC, ANN, etc.) may help to give a better result for torque ripple reduction.

Zhang P.et al. [18] exploit percentage torque ripple considered as present in (1.13). The literature on Torque ripple for DTC drive compared for analysis and survey of different methods to minimize torque ripple is discussed in chapter 2.

$$\%\text{Torque Ripple} = \%\text{TR} = \frac{\text{Te}_{\text{max}} - \text{Te}_{\text{min}}}{\text{Te}_{\text{average}}} \text{X} 100\% \tag{1.13}$$

Based on the steps demonstrated above for carrier space vector pulse width modulation (CSVPWM), the switching of power devices is controlled in a three phase full-bridge voltage source inverter. The main purpose is to inspect the consequence of the different

level of injecting common-mode voltage on the electromagnetic torque ripple. CSVPWM, DTC, Fuzzy speed controller of DTC are compared and analyzed in terms of torque ripple of the three phase induction motor in the next subsection. The third harmonic reference signal is added into sinusoidal fundamental reference signal, which leads to a 15.5% increase in the utilization of dc-link voltage.

From the above results of induction motor torque ripple comparison is carried out. Fuzzy based DTC technique is compared with CSVPWM DTC and conventional DTC. CSVPWM DTC with different Common mode voltages (CMV) are taken during the simulation and compared results. In the third harmonic injection method, it is challenging to add specific third harmonic voltage during the cycle to cycle. In proposed Carrier Space Vector PWM (CSVPWM) this problem is resolved. The torque ripple is significantly reduced. The CSVPWM with 15% CMV, 25% CMV, 35% CMV, Fuzzy DTC simulation torque ripple results presented and compared with conventional DTC.

1.6 Research Motivation

Industries such as paper mill, textile industries needs quick, accurate, smooth control for high-performance motion control applications. Energy recovery during deceleration and braking is equally important for heavy motors used in industries like paper, textile, hoist, crane, lift, escalator, traction vehicle, electric vehicle etc. Electric Drives generally use braking resistors and chopper for rheostatic braking which waste electrical energy in to heat during deceleration and braking. It can be replaced by energy recovery techniques where rapid acceleration/deceleration occurs. In the global scenario, nowadays, electrical vehicles needs more research towards improvement in energy recovery.

The problem is energy wastage due to resistor braking unit utilised in conventional variable frequency induction motor drive. Hence to propose such a method or strategy which recovered power and utilised whenever required, which intern increase efficiency of three phase induction motor drive. For different applications, the best energy recovery method can be find. Many variables play an important role in energy recovery during deceleration. There is a need to investigate the most affecting variable also. For a drive,

important aspect is precise torque resolution and smoothness. It is very essential to reduce torque ripple.

1.7 Objectives of the thesis

The following main two objectives of the thesis are:

1. **Improvement in energy recovery of DTC based induction motor drive during deceleration of load.**
    - Enhancement in energy recovery during deceleration of induction motor based on drive using bidirectional DC/DC converter with the capacitor bank as energy storage.
    - Improvement in energy recovery by regenerative power fed back to the grid using DC/AC converter during deceleration for direct torque control of induction motor.
    - Inspect effect of variables like load torque, initial speed of starting of deceleration, motor power rating and deceleration rate, among that most significant variable responsible for high energy recovery efficiency using Taguchi method.
2. **Analysis of torque ripple of a direct torque control method for induction motor drive during motoring mode.**
    - Comparison of DTC, CSVPWM-DTC, Fuzzy logic controller based DTC technique for analysis of torque ripple reduction for three phase induction motor.

1.8 Thesis Organization

The main contributions of the thesis are discussed in following chapters.

In Chapter 2 describes a literature review to understand energy recovery during deceleration for three phase induction motor. This chapter also describes a literature review on the various methods of torque ripple reduction techniques. Based on the literature review, some significant research gaps have been identified, and the research objectives are set for the research work.

Chapter 3 demonstrated the strategy for energy recovery of a DTC based induction motor drive with DC/DC bidirectional converter and a capacitor storage system. The energy recovery efficiency for 50 HP, 100 HP and 215 HP three phase induction motors is calculated, and it is verify with simulation results.

Chapter 4 presents energy recovery of DTC based induction motor drive using DC/AC converter for energy fed back to the grid, and its talk about simulation results. The energy efficient technique is found and discussed it with proposed block diagram and simulation results. The results with varying load torque, initial speed of deceleration, deceleration rate and motor power rating are discussed.

Chapter 5 discuss effect of variables on energy recovery and losses, also investigate dominant key factors during energy fed back to the supply grid for DTC based induction motor drive.

Chapter 6 details for analysis of torque ripple reduction using various techniques like DTC, CSVPWM-DTC, FLC based DTC.

Chapter 7 Finally, shows the concluding remarks and future scope from the research investigations.

CHAPTER-2

2 Literature Survey

2.1 Introduction

The main focus of this chapter is to analyse different works done in literature on the energy recovery analogy, saving potential and torque ripple reduction in direct torque control based induction motor drive. Induction motor is widely utilised in industry due to its low cost, rugged construction and reliable working. Induction motor is extensively used in fans, pumps, variable frequency drives, paper and pulp industries, textile industries, elevators, tractions, servo, robotics, steel industries, cement mills, etc. Conventionally, induction motor are utilized with constant speed applications and DC motors are used to get speed control but the main limitation of DC motor is the maintenance of commutators and brushes.

Industries drive applications are classified in to constant speed and variable speed drive. Variable speed drives are now well-known for induction motor dynamic speed control [2]. The three modes of operation for induction motor are (1) motoring with $0 < N < Ns$ (i.e., $0< s < 1$), (2) generating with $N > Ns$ ($s < 0$) and (3) braking with $N < 0$ (i.e., $s > 1$) [19]. In the braking mode, the rotor is forced to rotate again stator field. During Plugging, rotor is forced to rotate against the stator field. This can easily possible by reversal of field by changing of phase sequence. The kinetic energy of motor and load has been dissipated in the rotor winding, so motor is likely to overheat and no energy is recovered. The induction machine, which rotates faster than the magnetic field stator, acts as a generator, supplying electrical power back to the supply system. The regenerating mode can be easily activated by lowering the supply frequency with an adjustable speed drive system. It is used as an induction generator connected to the grid.

Variable frequency drive provides facilities with an effective speed control technology with an induction motor. The electrical motor behaves as an electrical generator during regenerative action in deceleration period. Variable frequency drive is aid with braking resistance employed to dissipate the energy in the form the heat cause energy losses. The energy can be saved instead of heat loss. The conversion of kinetic energy into electrical energy during deceleration can be used to charge an energy storage unit or injected into the supply grid. Kinetic energy during deceleration or braking is not fully recovered due to occurrence of various losses such as mechanical, electrical and inverter losses [20].

Fig. 2.1 shows typical acceleration and deceleration in speed curve with torque profile for induction motor. During deceleration, torque goes negative and speed remains positive.

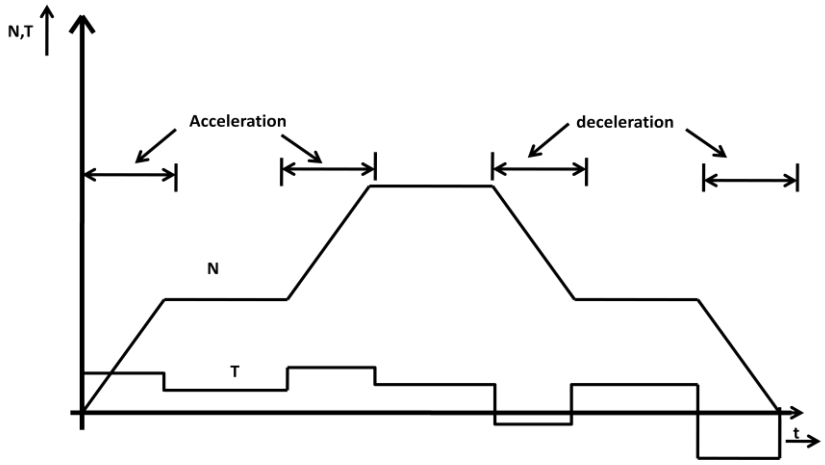

FIGURE 2.1: Speed, torque with respect to time for induction motor drive [2]

$$\frac{d\omega}{dt} = \frac{T_e - T_l}{J_m}, \text{ motoring action} \quad (2.1)$$

$$\frac{d\omega}{dt} = \frac{-T_l}{J_m}, \text{ deceleration} \quad (2.2)$$

Where, T_e = electromagnetic torque developed,

T_l = load torque,

J_m=Total inertia of motor and load.

The equation (2.1) is used during motoring action, where friction is neglected for the induction motor drive. If the power supply is not connected at starting of deceleration, T_e becomes zero, and Load torque remains negative till induction motor halt. The motor

works like an induction generator can be represented by (2.2) during deceleration. The energy can fed back to source or store in the storage device instead of dissipated as heat during deceleration.

The three phase induction motor speed torque characteristics shown in Fig. 2.1.when slip is negative, Rotor speed (ω_m) is greater than synchronous speed (ω_s). During this period motor works as a generator.

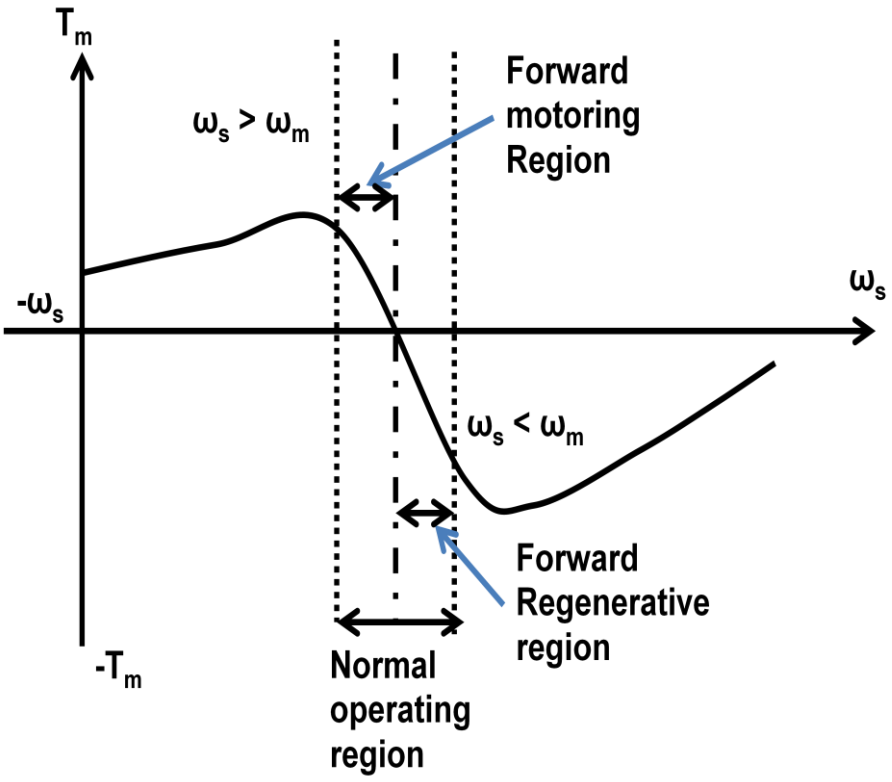

FIGURE 2.2: Speed-torque characteristics for induction motor drive [17]

The three phase induction motor with motoring and regenerative operation modes are shown in Fig. 2.2 [21]. B. Mohan et al. proposed an effective regenerating method of electrical energy by operating induction motor at negative slip region. The energy regeneration is demonstrated during the braking process of an induction motor as applicable in electric vehicles by controlling the supply voltage and frequency [21].

According to load torque and angular velocity direction, the four quadrant operation are demonstrated in Fig. 2.3. The 2^{nd} and 4^{th} quadrants are regenerative region. The three phase induction motor has energy regenerated during forward regenerative and reverse regenerative region.

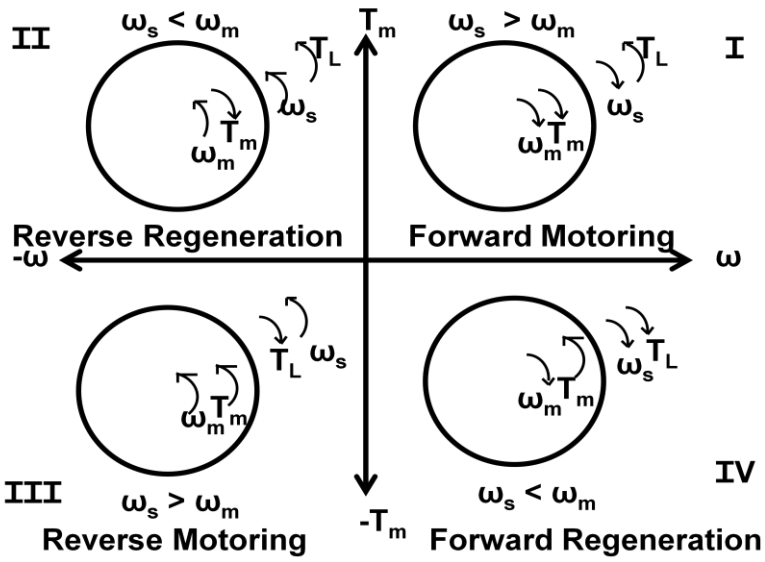

FIGURE 2.3: Four Quadrant operation of induction motor drive [2]

The chapter also discusses torque ripple and its minimization techniques for direct torque control method of induction motor drive. The chapter presents the literature review on the DTC of induction motor drive and latest techniques related to it like DTC using Space Vector Modulation (SVPWM), Carrier SVPWM, Fuzzy PI- DTC, etc. and also strategies for the energy recovery during deceleration and regenerative braking issues related to DTC induction motor drive.

2.2 Energy recovery opportunity of induction motor based DTC drive during deceleration through DC/DC converter to energy storage device

The induction motor (IM) is usually selected for traction and vehicle applications because of its most appropriate torque characteristics. The energy is wasted during traditional mechanical braking can be restored back by regenerative braking. Nowadays, for electric vehicle recovered energy stored in energy storage devices like ultracapacitor or battery. Here DC/DC bi-directional converter is useful to store energy from DC bus to energy storage devices. This section addresses the potential for energy regeneration for AC motor drive and the view of other literature on it.

Bhim Singh et al. studied the behaviour of DTC based induction motor for an EV through simulation. For electric vehicle energy recovery using energy storage devices like

ultracapacitor and battery are also discussed. Here, bidirectional DC to DC converter is useful to store energy from DC bus to energy storage devices. The starting, acceleration, deceleration and braking features of the EV drive are simulated and presented in detail. It allows precise and quick control of the induction motor flux and torque. In this paper, the behaviour of DTC based induction motor for an EV is studied through simulation using MATLAB^{TM}. The proposed scheme is capable of providing four quadrants operation along with regenerative braking with partial recovery of kinetic energy to charge the battery and thereby improving the overall efficiency of the system [13].

X. Yan et al. [14] discussed Brushless DC Motor with PWM strategy as suggested power topology in Fig.2.4. Ultra capacitor (UC) is used as charging and discharging device during acceleration and deceleration period of induction motor. Regenerative energy is improved about 4% in simulation with same braking distance and about 11% improvement due to optimization of velocity trajectory and distribution ratio. The bidirectional DC/DC converter is utilized for energy recovery. The working of buck boost topology is discussed. During acceleration, capacitor bank (UC) and battery need to fed to DC link using boost converter. During the transient period and suddenly increased load transients are supplied by UC. During deceleration of motor, DC link voltage increases, so recovery of energy possible. Here, the buck converter is used to charge capacitor bank. Energy recovery is possible frequently in electric traction, lift, textile mills, paper mills etc [14].

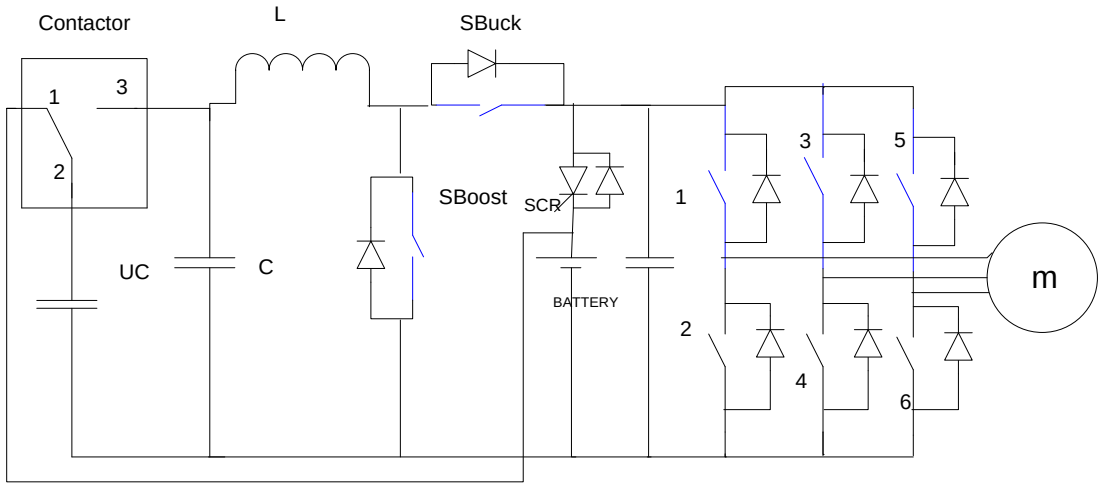

FIGURE 2.4 : Energy recovery using bidirectional DC/DC converter

S. Harada et al. reported regenerative energy can be improved up to 16% by optimal deceleration trajectory method [15]. A. Taut et al. [16] discussed energy recovery in tank capacitor during deceleration. Energy can be stored to supercapacitor bank by buck or

boost configuration using constant power charging method. Energy obtained during deceleration is rectified and stored in capacitor. The DC link voltage increases or decreases according to the duration of deceleration and speed of deceleration. Bidirectional buck-boost converter used for energy recovery during braking and deceleration [16].

S.K. Yadav et al. [20] discussed benefits of supercapacitor like fast charging, discharging capability, high capacitance, high power density, high efficiency, long life span (10 to 15 years), lighter in weight. The disadvantage are high cost, low voltage capacity so several capacitors need to be connect to get higher voltage, which lead to reduced capacitance value [18].

I. Karatzaferis et al. [22] developed new control algorithm for energy recovery purpose for universal converter. Improvement observed in energy consumption due to energy recovery 9% under light load operation, whereas 2.7% improvement under heavy load operation.. During regenerative braking action losses like mechanical losses, electrical losses at the motor, inverter losses, and the bidirectional converter loss occurs which is subtracted from kinetic energy available for recovery [22].

Z. Raud et al. find that the DTC provides great possibility of saving energy due to stable regenerative current, while the voltage frequency control (VFC) have current oscillates heavily, resulting in very less energy savings [23]. V. Vodovozov et al. [24] represented that average recovery energy 20 to 30 percent in energy storage devices of electric vehicles. The maximum efficiency of the recovered energy in the storage unit during deceleration found in literature is about 20 % to 35% [22],[23],[24]. Theoretical problems related to the use of regenerative braking systems in two-axle vehicles have been identified [25].

L. Liu et al. [26] demonstrated a 5.5-kW PMSM drive system. Module providing peak power during acceleration and absorbing regenerative power during deceleration, which improves the energy efficiency of the motor drive system and reduces the size of the energy source. Speed trajectory at one simplified driving cycle is simulated. The corresponding power flow between the energy source, the energy storage, and the electric motor is described [26].

Y. Fan et al. [27] presented an improved control scheme of a new self-decelerating permanent-magnet (SDPM) in-wheel motor, the direct torque control (DTC) method is adopted flux linkage adaptive approach and SVPWM technique. All results demonstrate

that the improved DTC scheme for the new SDPM in-wheel motor has the preponderant characteristics of fast response, low torque and flux ripple, good current waveforms, strong robustness and small reactive current component [27].

A. K. Kaviani et al. [28] obtained analytical approach for the management of regenerative energies in multiaxis servo-motor-drives, which can operate in parallel packaging lines, is presented in this paper. This energy management is achieved through a proper time-coordination with the speed commands of multi axis drives. Moreover, the proposed approach significantly limits the peak value of the ac input A set of closed-form formulas is developed for different acceleration–deceleration time ratios, where motor losses are neglected [28].

S.D. Cairano et al. [29] considered the speed control of a spark ignition engine during vehicle deceleration. The engine speed during vehicle decelerations needs to be precisely controlled by feedback control. It is needed to coordinate airflow and spark timing and enforce several constraints, including engine stall avoidance, combustion stability, and actuator limits. Hence a predictive controller is developed that control airflow and spark to track the reference signal for engine speed while enforcing constraints and synthesize it in the form of a feedback law. The controller is evaluated in simulations and in a vehicle, it is shown to achieve a responsive and consistent deceleration and the potential for reducing fuel consumption [29].

M. Saleh et al. [30] developed direct current (DC) microgrid laboratory testbed. Management of Energy resources, energy storage system with design steps, requirements, and results are discussed. The control scheme of DC/DC bidirectional converter was tested and validated. The battery side voltage set to 250 V and the DC bus side was set to 400 V with a 100 ohms DC load parallel to validate the prototype [30]. The buck-boost bidirectional converter is controlled by different control strategy [30]. S. Kim et. al also discussed the control strategy for bidirectional converter [31].

F.J.T.E. Ferreira et al. [32] found 174.6€ per year of annual saving for 200 kW, 2/4 pole induction motor by energy recovery during deceleration. The outcome is determined by pole amplitude modulation [PAM] method changing synchronous speed half, by change 2 poles to 4 poles, found 70kJ energy recovery in each stop, considered 15 stops per hour,6000 hours/ year operating time [32].

Direct torque control for BLDC motor is projected to regenerate electrical energy from the kinetic energy and bringing it back to the batteries. S. Geraeea et al. [33] calculated the

state of charge of the battery in common direct torque control against the modified one shows 0.6% improvement through 0.9 s simulation time [33].

K. Itani et al. [34] reported results of energy recovery efficiency varying observed 3.7% for high friction road type, 11.2% for medium friction road for 60 kW PMSM [34].

To find possibilities of energy saving from electric braking in the transportation vehicle, L.H. Bjornsson et al. [35] found recoverable energy ($E_{recoverable}/E_{traction}$) = 26% , reusable energy ($E_{reuse}/E_{traction}$) = 17%. Recoverable energy is the energy fed back out of available inertia recovery energy to the battery after losses of air drag and rolling resistance. Reusable energy means again reutilise for the fed to motor after subtracting losses of inverter and other losses. Evaluating the possible energy savings from regenerative braking energy is a key to understand the energy-efficiency progress in transportation. A simple car model and individual drive cycles are collected from the real-world driving scenario, to estimate energy loss through braking and the corresponding regeneration potential for privately driven cars in Sweden [35].

For Direct torque control and direct vector control strategy, N. Apostolidou et al. [36] found even though variation of load from 0.66% to 67 % of nominal torque value of 1355 Nm. for different slope condition of road, and high load variation, with constant speed, DTC and Direct Vector Control method are more effective than others [36].

K.Y. Lin et al. [37] analysed two-way inverter system for energy consumption and regenerative energy of elevator drive. It is demonstrated regenerative energy ratio for different cases for load. The average rate of energy-saving is about 23.1%. A. Pyper et al. [38] evaluated freight trains that energy savings between 10% and 24% by flywheel energy storage system during regenerative braking. S. Heydari [39] found recaptured energy improvement increases by 25.95% through regenerative braking using electric vehicle motor performance lookup table.

High inertia load such as electric vehicles, winders, centrifuges, pumps, grinders are more difficult to accelerate and decelerate. The total mass moment of inertia referred to as the motor shaft can be compounded to calculate kinetic energy of the drive [19].

The literatures discussed in this section are on energy recovery performance and strategies using DC/DC converter for induction motor DTC drive. Typically, the motor braking energy is dissipated in a dynamic braking resistor in the DC link. It works as a pulsed resistance to dissipate energy and protects the DC capacitor against overvoltage during motor braking. Rapid speed reduction results in a negative slip command occur in speed

control of motor, and the motor goes into regenerative braking. Hence, the regenerated energy can be stored in the energy storage devices like a capacitor bank, battery, etc through DC/DC converter.

2.3 Energy recovery opportunity for direct torque control based induction motor by regenerative power fed back to the grid through DC/AC converter during deceleration

In industry, the variable frequency drives for three phase induction motor are commonly utilized. The mechanical power of induction motor is evaluated by the motor speed and torque multiplication. During the deceleration period, the torque goes negative and speed remains positive. Hence the negative mechanical power occurs, which cause DC link voltage rise. Generally, the dynamic braking resistor unit utilises to control the DC bus overvoltage by introducing resistive losses. A regenerative braking unit may easily mount externally by replacing the dynamic brake resistor unit to fed back recovered energy to the grid. In the regenerative braking unit, DC/AC converter is utilized to fed back energy from DC bus to the main grid. Different strategies are discussed to fed power to the grid supply with control strategy.

N.R. Raju et al. [40] discussed different SCR based regenerative converter and proposed SCR based front end rectifier, which is activated when dc bus voltage rise is more than 15%. The main drawback of the method is to increase harmonic content in line current. Fig. 2.5 shows various topologies for induction motor drive for energy fed to the grid during regenerative braking. The inverting SCR bridge connected to the dc bus rails as Fig. 2.5 (a) transfers energy from the dc link to the mains during regeneration. The SCR rectifier, Fig. 2.5 (c), with reversing bridge works same as when two middle switches operated. The bridge connected to the center-tap provides improved commutation to the inverting bridge as shown in Fig. 2.5 (b). In addition, it can be used to boost the dc bus during input voltage sags. The PWM rectifier, shown in Fig. 2.2 (d), provides bidirectional power flow in addition to its other merits, such as low input harmonics [40].

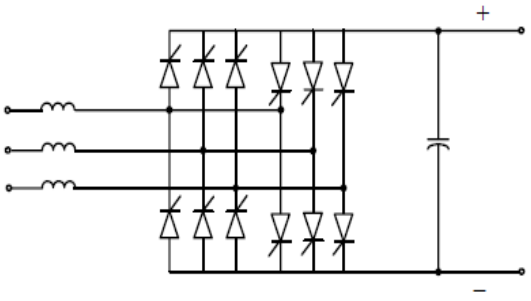

Fig. 2.5 (a) Dual SCR bridge

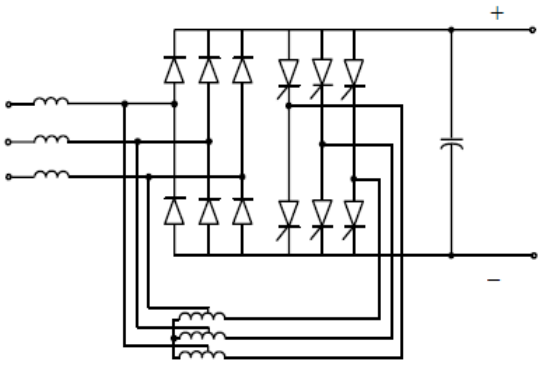

Fig 2.5 (b) Auto transformer connected SCR Bridge

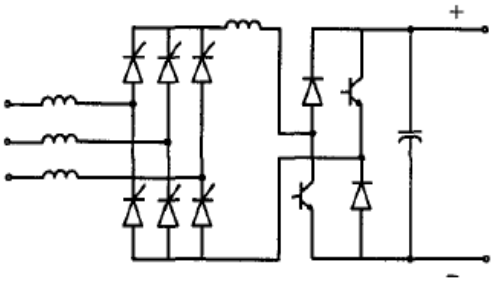

Fig 2.5 (c) SCR Rectifier with Reversing Bridge

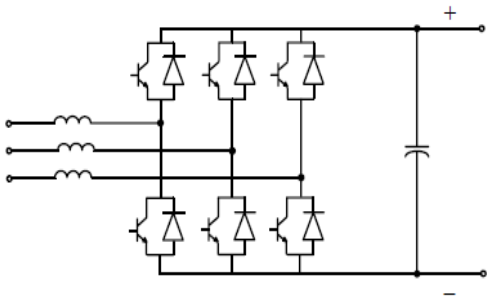

Fig 2.5 (d) PWM Rectifier Front End Converter

FIGURE 2.5 : Conventional topology for energy recovery fed back to grid power supply

During acceleration, the induction motors take power from the AC supply and convert to DC through the diode bridge rectifier circuit. The DC link voltage is maintained to a rated

value which is converted to AC voltage by an inverter. The kinetic energy depends on the angular speed of motor and moment of inertia of load and motor. During deceleration, the kinetic energy is fed back through freewheeling diodes works as rectifier circuit and hence DC bus voltage is increased drastically. In the conventional method, the drive has a dynamic braking resistor unit in which the energy is dissipated as heat, hence efficiency is reduced. The regenerative braking unit allows energy injected back to the source or grid. The resistance bank is replaced by DC/AC converter which fed back this recoverable kinetic energy of the three phase induction motor to the grid during deceleration. Before fed to the grid, a synchronisation condition must be satisfied to achieve it. The appropriate inverter output voltage is obtained using a phase lock loop (PLL) with the grid needed. The vector decouples control strategy and current control method is applied for regenerative braking. An application like lift, traction, electric vehicle drives etc. battery or supercapacitor type energy storage device needs to be connected across DC link through DC/DC bidirectional converter.

C. L. Chua et al. [41] found that the electric vehicle drive dynamic testing system simulates the full-range speed and torque output to save 65~70% energy. The inverter drives the three phase induction motor with the torque and speed control, and this three phase induction motor operates in regenerative braking mode to further feedback the power to the utility system through the power regenerative inverter with a unit power factor and low harmonics sine wave [41].

A. T. Almeida et al. [42] elaborated variable speed drive with energy recovery can be reduced consumed energy 19 % compared to conventional system in lift. The new technology allows braking energy injected back to the source or grid. Different cases for lift are discussed for energy saving during tracking of motor. Inverter adjusting a frequency such that below the motor actual stator frequency, motor wheel act like a generator, which help in maintaining DC bus voltage level during deceleration [42].

K. Inoue et al. [43] found new design methodology of optimal torque and the power generation during deceleration. It occurs if power generated is larger than the interior loss of motor. A Mohamed et al. [44] discussed bidirectional rectifier SPWM based technique to control bidirectional power using dual converter has been designed and implemented to connect with the grid. Vector decoupling current control of grid-connected inverter is discussed. A. Maiti et al. [45] shows how the PV module output is to be connected to DC link of inverter connected to the grid. Initially the PV module is connected with the boost

converter to charge battery. During the connection to grid inverter synchronisation results are shown. The bidirectional converter output current and voltage of grid for operation of rectification and inversion are discussed.

The different topologies for regenerative braking drives are anti-parallel thyristors bridge, six pulses external regenerative braking unit, matrix converter drive, front end converter drive, external regenerative converter used to recover energy and fed to the main grid [46] [47]. The choice of topology depends on cost-saving ability, low input current harmonics, initial cost payback period, number of motor connections, power factor improvement and additional space required compared to a conventional drive.

In the quadratic load like fan, pump etc. has fast natural deceleration between 100% to 50% of nominal speed during natural braking. The constant torque load like crane, elevator, lift, conveyer etc. has constant natural deceleration. If load release at starting of the braking, the kinetic energy remains unchanged but natural braking effect is small. The mechanical power depends on torque and speed during braking. This power is fed back to the grid during electric braking typically shows that 25 % of kinetic energy conserved for 90-kilowatt motor during speed restoration from 1000 rpm to rest. The calculation shows occasional braking cannot cover the cost of investment of regenerative unit but frequent braking in case of crane and centrifuge applications energy-saving and cost-effectiveness is found [47].

A grid connected front end converter proposed and control strategy of it is developed. The current control strategy used for grid side converter. The main part of control strategy is to get I_d and I_q components from the reference active and reactive power which will decide flow of current from the converter [48].

A. Parra et al. [49] demonstrated energy performance improvement by decrease energy consumption up to 2%, using a nonlinear model predictive control (NMPC) [49].

In industrial motor, during acceleration power given to motor by AC supply and is converted to DC through diode rectifier circuit. The DC link voltage is maintained to 600 V and is converted to AC voltage by inverter which is controlled using direct torque control method. During deceleration, the motor inertia kinetic energy is restored or feedback through freewheeling diodes of inverter which is works as rectifier circuit and hence, DC bus voltage is increased drastically to enough voltage level. Conventional

drives have resistance braking unit in which energy is dissipated in to heat, hence efficiency is decreased. Now if resistance bank is replaced by DC/AC converter which is fed back kinetic energy to grid during deceleration for short period of time. Prior to fed to the supply grid, synchronisation of the output inverter voltage with the grid needed. PQ theory for control strategy is applied for inverter to fed back power to supply grid. The mechanical power depends on torque and speed at braking. After the accelerating period during the deceleration the negative torque of induction motor is generated. Due to the negative power occurs, it is observed that DC link voltage becomes high. The energy recovery during deceleration of induction motor for the industry based induction motor drive is discussed in the thesis.

The industrial drives have greater chance to improve energy recovery performance as directly connected to grid. Hence Energy storage device need not to incorporate for energy recovery and fed power back to supply grid using DC/AC converter during deceleration of DTC based induction motor drive. The induction motor used for the crane has a motor size of 10 kW to 600 kW (13 HP to 804 HP) for mines and steel plants [50]. Different hoist motors used range from 1 to 465 HP according to load capacity [51]. High-performance AC drives available for the textile mill have ranged from 0.25 HP to 30 HP [52]. Hence to accommodate all range of motor used for different applications in industries 5.4 HP, 50 HP, 100 HP and 215 HP induction motor are selected to study and analyse for energy recovery induction motor drive .

2.4 Overview on literatures of torque ripple reduction for DTC of induction motor drive

The conventional DTC has some drawbacks, such as, variable switching frequency, high torque and flux ripples, problem during starting and low speed operating conditions, flux and current distortion caused by stator flux vector changing with the sector position [44], and the speed of induction motor is changing under transient and dynamic state operating condition.

The electromagnetic torque is expressed in terms of stator and rotor fluxes as below equation (2.3).

$$T = \frac{3}{2}.\frac{p}{2}.\frac{L_m}{\sigma.L_s.L_r}\overline{\varphi}_s \times \overline{\varphi}_r \qquad (2.3)$$

Here, p is no of poles, Ls, Lr are the stator and rotor Inductance respectively, Lm is the mutual inductance, $\overline{\varphi}_s$ = stator flux linkage, $\overline{\varphi}_r$ = rotor flux linkage.

Various strategies to minimize torque ripple such as Prediction scheme, PI and Fuzzy logic controller, Global minimum torque ripple strategy, CFTC Technique, optimal switching instant technique for torque ripple reduction and a duty cycle control scheme for DTC has been reviewed and compared. The main problem with DTC is the drift of the stator resistance, which results in the stator flux estimation error. DTC strategy will continue to play a strategic role in the development of high performance motion-sensorless ac drives.

Several methods had been proposed by researchers to overcome the torque ripple problems, like CFTC [9], dithering technique, controlled duty ratio cycle technique [53], space vector modulation (DTC-SVM) based DTC [54][55], predictive control[56], global minimum DTC [57],carrier SVPWM [58], FLC based DTC [59], DTC with harmonic elimination method [60].

Giuseppe S. Buja et al. [3] reviewed various DTC strategies for PWM inverter-fed AC motor drives and main features of DTC are summarized. DTC is well suited for traction and vehicle drives. A variety of techniques, like switching-table- based hysteresis DTC, direct self control, constant-switching-frequency DTC with space-vector modulation (DTC-SVM) has been reviewed. The trends in the DTC- SVM techniques based on neuro-fuzzy logic controllers are discussed. Classification for induction motor control method is discussed and main features of DTC are summarized [3].

In order to overcome torque ripple problem, T. Ramesh et al. [4] proposed DTC with PI and fuzzy logic controller. The PI controller is used for speed control in the speed regulator loop where as the fuzzy logic controller is used for stator flux and torque ripple reduction in the torque control loop. The effectiveness, validity, and performance of DTC of induction motor drives using both conventional and proposed controllers are analyzed. It is shown that low stator flux ripple and torque ripples, good speed regulator of induction

motor drives with this technique. In FLC based DTC a fuzzy control rule look-up table is designed from the performance of torque response of the DTC of induction motor drives. According to the torque error and change in torque error, the proportional gain values are adjusted using look-up table [4].

A. Jidin et al. [9] used constant switching frequency and reduced torque ripple in DTC by replacing the torque hysteresis controller with CFTC. By replacing the torque hysteresis controller with the CFTC in the basic DTC structure, significant reduction of output torque ripple can be established with the proper PI-controller gains and selection of triangular frequency in CFTC. The torque ripple observed in conventional DTC is 19.4% and CFTC method improved it to 11% [9].

D. Telford et al. [53] presented a simple duty-cycle control scheme for DTC of an induction motor. The scheme reduces torque ripple particularly at low speeds, controls the average output torque, and reduces the variation in switching frequency. The scheme has also been shown to effectively control the mean of the output torque and to limit the switching frequency variation. The torque response of the machine checked and compared during a series of torque reversals of ±10 Nm with and without the torque-ripple reduction scheme. During the torque reversal, the machine is accelerated from -70 to +70rad/s. This shows that, with the duty-cycle control scheme, the torque ripple has been significantly reduced when compared to the conventional DTC scheme, particularly at low speed [53].

T. G. Habetler et al. [54] proposed a direct torque control method of induction machine based on predictive, dead beat control of the torque and flux. Here the change in torque and flux, over the switching period is calculated by estimating the synchronous speed and the voltage behind the transient reactance and the stator voltage[54].

S. N. Pandya et al. [55] mainly focused to solve two major problems associated with conventional DTC drive are electromagnetic torque ripple and variable switching frequency. At load torque of 10 N-m, torque ripple found in the conventional and SVPWM DTC based induction motor drives are 5 N-m and 2 N-m respectively. The drastic reduction in torque ripple has been achieved in SVPWM DTC based induction motor drive using proposed technique is due to proper tuning of the gain parameters of torque and flux controllers. The torque ripple observed in conventional DTC is 22.72% and SVPWM method improved it to 9 % [55].

Jef beerten et al. [56] presented the diminishing effect of the prediction scheme on the torque and flux ripples in a direct torque control (DTC) induction motor drive. The prediction scheme has low computational complexity and low parameter sensitivity. The prediction scheme can easily be extended to compensate for multiple time delays when the sampling frequency is raised but the computation time remains unchanged. The prediction scheme uses incremental changes in stator flux magnitude, stator flux angle, and electromagnetic torque, which are stored in memories and used as a prediction in order to compensate for the time delay caused by the data processing. The scheme can easily be extended to raise the sampling frequency while maintaining the same computation time. The new multiple predictions, further diminishes the ripples when the data processing time forms a restrictive parameter. It demonstrates the significant reduction of both torque and flux ripples resulting from the prediction scheme. The torque ripple observed in conventional DTC is 45% and extended predictive method improved it to 14.5 % [56].

Kuo-Kai Shyu et al. [57] proposed a simple and effective method to reduce the torque ripple for direct torque control (DTC) of Induction motor drives. The proposed DTC provides a global minimum torque ripple, which satisfies the root-mean-square (rms) criteria of torque ripple. The proposed global minimum torque ripple DTC is a two-step design. The first step drives the torque error to zero at the end of the control period. The second step reduces the torque bias and rms ripple by modifying the asymmetry switching patterns of the applied voltage vectors of the first step in to symmetry ones. Furthermore, the related current ripple is also reduced. The main problem left here is the drift of the stator resistance, which results in the stator flux estimation error. The torque ripple observed in conventional DTC is 8.38% and global minimum DTC method improved it to 11% [57]. In CSVPWM DTC based induction motor drives [58] torque ripple reduction up to 35% of that measured with conventional DTC.

Rasoul Rahmani et. al. [59] discussed two different control methods to select the appropriate output voltage vector for reducing the torque and flux error to zero. The first is based on the conventional DTC scheme using a pair of hysteresis comparators and look up table to select the output voltage vector for controlling the torque and flux. The second is based on a new fuzzy logic controller using Sugeno inference method to select the output voltage vector to replace the hysteresis comparators and lookup table in the conventional DTC. The simulation results also verified using a fuzzy controller instead of hysteresis

controller resulted in reduction in the flux and torque ripples significantly. The flux ripples reduces the THD of the stator current is below 4 % [59].

T.H. Atyia et al. [60] compare induction motor performance for torque ripple with DTC, DTC with Harmonic elimination and Matrix Convertor. Simulation results are analyzed, evaluated, and compared to each other.

Jun-Koo Kang et al. [61] proposed to find an optimal switching instant during one switching cycle is calculated for T.R.R. which is derived from RMS torque ripple equation. The proposed scheme provides combining a low torque ripple characteristic in the steady state and the conventional fast torque dynamic characteristic. It also improves the torque control characteristic especially in the low speed region. In the torque ripple minimization algorithm, the optimal switching instant is calculated per every switching cycle based on instantaneous torque slope equations [61]. The torque ripple observed in conventional DTC is 20% and proposed method improved it to 5%.

Shrivastava et al. [62] is found torque ripple reduction up to 30% of that observed with conventional DTC using SVPWM DTC [62]. K. K. Chouhan et al. used CFTC method to reduce torque ripple up to 23% [63]. The torque ripple is minimized up to 80% for T2NFS controller in the steady-state compared to PI controller [64]. A. A. Ahmed et al. proposed continuous control set model predictive control (CCS-MPC) DTC has good dynamic performance overall speed with minimal torque and current ripples and reduced torque ripple up to 8% [65]. Y. Cho et al. proposed predictive torque control (PTC) DTC which has reduced torque ripple up to 25% [66].

Kazmierkowski et al. [67] reviewed Direct Torque Control (DTC) strategies for PWM inverter-fed AC motor drives and main features of DTC can be summarized . It is represented that constant switching frequency DTC-SVM schemes improves the drive performance in terms of reduced torque and flux ripple , reliable start up and low speed operation, well-defined harmonic spectrum and radiated noise. DTC is well suited for traction and vehicle drives [67].

D. Casadei et al. [68]proposed ST-DTC scheme for multilevel and multiphase converters and checked simulation results. In basic ST-DTC schemes, voltage vectors are usually employed to compensate flux and torque errors. Using the DSVM technique, with three equal time intervals, 18 virtual vectors and a null vector can be used. The principles of

ST-DTC schemes, for multilevel inverters and multiphase drives, have been analyzed, in which subdividing the switching period in three equal time intervals leads to a substantial reduction of torque and current ripple [68].

S. V. Jadhav [69] presented the design of DTC Induction motor drive that incorporates ANN based controller. The control algorithms are employed to improve control performance, and to reduce torque and flux ripple. It is proposed that ANN based SVM-DTC is less complex, requires a single ANN controller for decoupled torque and flux control, and improves the performance [69].

S. Gdaim et al. [70] reported the sampling period and the execution time for FPGA based DTC. This is principally due to the fast computation process ensured by the high computation capabilities of FPGAs. The high computation speed is necessary for the system to be able to acquire the currents in the same sample period in which it derives the command signal. S. Gdaim et al. shows the control algorithm execution needs 57 clock cycles, meaning at 100-MHz clock rate, the total computing time of DTFC is equal to 0.57 μs. By adding the (A/D) conversion time (T_{adc}), total execution time (t_{ex}) equals 2.77 μs which shows more than the sampling period is very big compared with the execution time [70].

F.D.R Figueroa et al. [71] proposed DTC is used to facilitate the control of the induction machine. Speed control is based on non-interactive PID control theory and Mamdani fuzzy systems. The optimizations based on genetic algorithms (GA) proved to effectively optimize the fuzzy controllers. It can be seen that the GA successfully improved the response of the controller, making the response of the machine faster [71].

J. Yuan et al. [72] found a problem of high torque ripple and harmonics in conventional DTC. For solving this problem, a model which is a combination of space vector modulation and a three-level inverter is proposed. A 2-level DTC and a 3-level SVM-DTC are modelled and simulated. The simulation results show that 3-level DTC can reduce torque ripples and harmonics effectively. The 3-level DTC has a good performance of improving torque ripples, and it seen that the ripple of 2-level is about 20 % and the torque ripple of 3-level is only 5% [72].

R. Sadhwani et al. [73] represented simulation on three level inverters are preferred to reduce the voltage stress on switches in medium voltage drive applications and to increase

the power handling capability of the converters. The problem of DC-link voltage balancing between the capacitors is one of the major concern of three level inverter. A comparative study of three control methods, namely: scalar control, IFOC and DTC fed by three level inverter is presented. the response time is reported for DTC is 7 ms, for IFOC is 20 ms and for scalar control is 100ms . SVPWM is one of the solution for reducing the unbalanced capacitor voltages by proper selection of switching vectors. The problem of neutral point unbalancing in three level inverter is also solved using vectors redundancy logic in SVPWM technique [73].

D. Mohan [74] proposed a simple Duty cycle-DTC based three level inverter method which is less dependent on machine parameters. For an interior permanent magnet synchronous motors (IPMSM), the switching table and the voltage vector selection criteria is used for the D-DTC strategy. The proposed method reduces the torque ripples significantly and improves the flux responses in conventional 3L-DTC, at the cost of a minimal increase in average switching frequency. Torque ripple reduction is achieved through the application of more than one voltage vector per switching cycle [74].

SVPWM-based multilevel inverters used in electric vehicles, grid interfacing, motor controls. K. C. Jana [75] presented a generalised online switching scheme for a SVPWM-based multilevel inverter. The proposed generalised SVPWM switching algorithm has been implemented at a high sampling rate of 40 μs using a DS1104-based digital controller. SVPWM-based generalised switching scheme tested experimentally on 1.5 HP induction motor for a five-level cascaded 3-phase inverter [75].

Hassan khan et al. [76] proposed a general SVPWM algorithm for three-level based on standard two-level SVPWM. Torque Ripple in classical DTC is Torque Ripple 14 Nm reported whereas DTC-SVM with two-level inverter has 7.4 Nm. Torque Ripple in DTC-SVM with three-level inverter 3.5 Nm [76].

J C Trounce et al. [77] represented the control schemes that operate at a fixed switching frequency, an inverter switching frequency of 10 kHz was used. For the standard DTC simulations, torque and flux hysteresis bands of 1 Nm and 0.0016 Wb respectively. A minimum vector hold time of 25 ms was chosen to simulate the time required to sample currents and voltages, and calculate the new vector. DTC using SVM has significantly reduced steady state torque ripple, than FOC which also uses SVM. FOC and SVM-DTC show very low switching ripple, but DTC has comparatively high current distortion [77].

DTC have variable frequency hence high torque ripple cannot predicted and not easily diminished. Various techniques are discussed to reduce torque ripple for conventional DTC. The incorporation of space vector modulation (SVM) with DTC has shown to be an effective method to lower the torque ripples as one can predict the torque ripple and hence find solution. Enough literature is available to deal with torque ripple reduction for three phase induction motor DTC drive. It is found that extensive research on artificial intelligence techniques (FLC, ANN, etc.) to conferred better results for torque ripple reduction.

2.5 Problem Definition

Direct Torque Control (DTC) method is one of the most outstanding and proficient control techniques of the induction motor. The foremost drawback of DTC induction motor drive is high torque pulsation and variable frequency of inverter switching. The challenging problems in the DTC based induction motor drive are energy recovery enhancement during deceleration for applications deals with frequent deceleration of large inertia load and torque ripple reduction for induction motor drive.

For precise torque resolution and smoothness, it is very important to reduce torque ripple. To study and analyse different strategy to reduce torque ripple and among them to investigate the best method to reduce torque ripple of DTC based induction motor drive. The problem of energy wastage is due to resistor braking unit utilised in conventional variable frequency induction motor drive. Hence to propose such a method or strategy which recovered power and utilised whenever required, which intern increase efficiency of three phase DTC based induction motor drive. Many variables play an important role in energy recovery among them most affecting variable needs to be investigated.

The problem definition is given below.

“Investigate suitable energy recovery techniques to replace conventional braking resistor unit and explore the impact of different variables for energy recovery efficiency. Study the most significant variable that affects energy recovery efficiency. Analyse different strategies to deal with the reduction of torque ripple for direct torque control based induction motor drive.”

2.6 Research Gap

As per the brief description shown in the above literature review, the following research gap has been identified.

- Various technologies regarding the energy recovery for DTC based induction motor drive are to be explored to energy recovery efficiency.
- The solutions available for energy recovery in literature need to be explored in detail for a bidirectional converter with energy storage system.
- Energy recovery using grid fed by DC/AC converter need to be investigated with change in variables in detail.
- In the energy recovery process during deceleration and braking, different variables like load torque, deceleration rate, power rating of motor, initial speed during starting of deceleration plays an important role. Influence of these variables need to be explored.
- In most of the reported work, energy losses have not been studied in detail during deceleration. Hence it needs to be explored.
- Conventional DTC based induction motor drive has torque ripple between 17% to 45% observed for different power rating of the motor due to hysteresis controller. The torque ripple reduction techniques like fuzzy based PI controller for DTC and CSVPWM need to be explored.

In the next chapter, energy recovery during deceleration of induction motor based on DTC drive by capacitor bank as energy storage is discussed.

CHAPTER-3

3 Enhancement in energy recovery during deceleration of induction motor based on DTC drive by capacitor bank as energy storage

3.1 Introduction

This chapter represents the development of DTC drives with energy recovery enhancement for induction motor drive. Different strategies are discussed in literature for three phase induction motor with variable frequency drive with energy recovery during braking. N. Apostolidou et al. [36] showed that energy savings up to 24% of typical energy consumption using storage unit would result from direct torque control (DTC) topology. The topology for energy recovery has been discussed. It is observed that significant energy savings potential during deceleration exist in three phase induction motor DTC drive. Bjornsson et al. [35] demonstrated that in applications where energy is rapidly accelerated and decelerated, there is sufficient energy recovery by deceleration. Electrical Drives that use braking resistors have good scope for energy recovery by using regenerative braking. Literature is available in which energy savings from brake, energy regeneration discussed for transportation electric vehicle [35]. K. Itani et al. [34] find that energy recovery efficiency is about 11.2 % for the electrical drive motors of 60 kW PMSM [34]. In this chapter, results are obtained for bidirectional DC/DC converter with capacitor bank as energy storage system for energy recovery enhancement during deceleration of the induction motor. The basic idea is to improve in energy recovery of DTC based induction motor drive during deceleration for high inertia load such as electric vehicles, winders, centrifuges, pumps, grinders, etc.

3.2 Energy recovery equations

Following formulae helps to understand the behaviour of energy recovery of induction motor drive [19][78] .

Let, a motor with the rotor inertia of J_m that drives a load with the moment of inertia J_L through the transmission of gear ratio N.

The kinetic energy K_L of the load rotating with angular velocity ($\omega_{L)}$ can be given by (3.1)

$$K_L = \frac{J_L \omega_L^2}{2} \tag{3.1}$$

While the motor kinetic energy (K_m) and whose rotor velocity is ω_m,

$$K_m = \frac{J_m \omega_m^2}{2} \tag{3.2}$$

The total kinetic energy can be expressed as

$$K_T = [(\frac{\omega_L^2}{\omega_m^2})J_L + J_m]\frac{\omega_m^2}{2} \tag{3.3}$$

(3.4)

$$K_T = J.\frac{\omega_m^2}{2}$$

Where, $J = [(\frac{\omega_L^2}{\omega_m^2}) * J_L + J_m]$

The difference between the motor torque T_m and Load torque T_l , is dynamic torque T_d

$$T_d = T_m - T_l = \frac{J.d\omega_L}{dt} \tag{3.5}$$

Hence, from the above equation, high moment of inertia makes a sluggish response and so that high dynamic torque required for fast deceleration and acceleration.

Kinetic energy during acceleration

$$E = -J.\omega^2 \int_{S_1}^{S_2} \frac{T_m}{T_m - T_l} s.ds \tag{3.6}$$

Here, S_1= starting slip, final slip=S_2, J = Total moment of inertia of machine with load, Tm =Motor electromagnetic Torque, T_L = Load torque, ω_s = synchronous angular speed, ω = angular velocity, N_s = synchronous speed.

Assume, $T_L = 0$, and the motor is with starting slip $S_1 = 1$, reach to full speed at slip $S_2 = 0$,

$$E = \frac{1}{2} J.{\omega_s}^2 = \frac{J \times [N_s(\text{in rpm})]^2}{182.4} \quad (3.7)$$

During reverse rotation braking $S_1 = 2$ and $S_2 = 1$.

$$E = -J.\omega^2 \int_{S1}^{S2} \frac{T_m}{T_m - T_l} s.ds = -3(\frac{1}{2} J.\omega^2) \quad (3.8)$$

During regenerative braking,

Consider application for which the speed is to be reduced from twice synchronous speed to synchronous speed.

During braking action, initial slip is -1 and final slip settles to zero. $S_1 = -1$ and $S_2 = 0$.

$$E = -J.\omega^2 \int_{S_1}^{S_2} \frac{T_m}{T_m - T_l} s.ds = (\frac{1}{2} J.\omega^2) \quad (3.9)$$

3.3 Strategy for energy regeneration

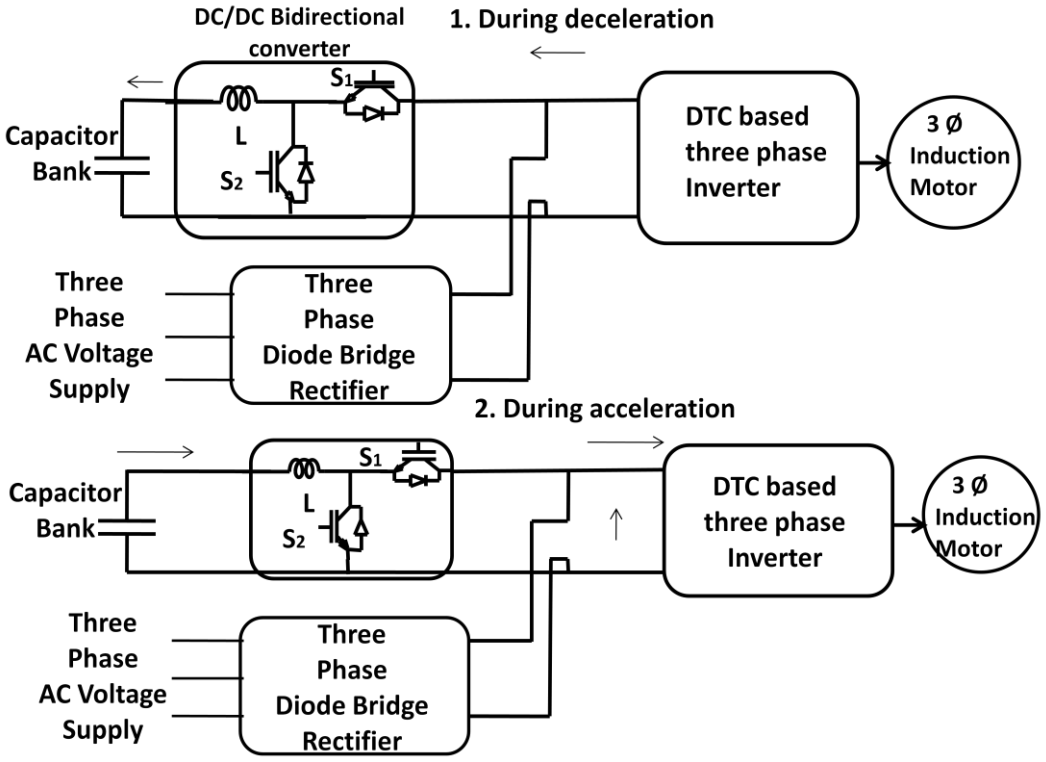

FIGURE 3.1: Block diagram for energy recovery for DTC based induction motor drive

The bidirectional DC/DC converter is proposed long back by Xinxiang Yan et al. for energy recovery [14]. Fig. 3.1 shows suggested power topology for DTC based three

phase induction motor drive is simulated using MATLAB^{TM}/ SIMULINK^{TM}. During deceleration, bidirectional converter works buck converter for charging of capacitor bank. During acceleration, bidirectional converter works as boost converter. Bidirectional buck-boost converter utilised for charging, discharging of energy storage device. The bidirectional converter is discussed with its control strategy by M. Saleh et al. [30]. Here, the inner current control outer voltage control strategy is utilized. During the transient period and suddenly increased load transients are supplied by a capacitor bank. During acceleration, capacitor bank need to supply power to DC link using boost converter. During deceleration of the motor, DC link voltage increases. Energy obtains from deceleration is rectified and stored in a energy storage devices like supercapacitor, capacitor bank or battery etc. The buck converter is used to charge capacitor bank during deceleration. Energy recovery is possible in applications such as electric traction, lift, textile mills, paper mills, electric vehicles etc.

3.4 Simulation results and discussion

In this section, the main focus is to investigate the energy recovery strategy for a direct torque control based induction motor drive. Fig. 3.2 shows suggested power topology for DTC based three phase induction motor drive is simulated using MATLAB^{TM}/ SIMULINK^{TM}. The proposed block diagram for energy recovery shown in Fig. 3.2, consists of direct torque control based induction motor drive, DC/DC bidirectional converter with current control strategy, and capacitor bank as energy storage unit. Fig. 3.3 shows the control strategy to operate DC/DC bidirectional converter under buck or boost mode. Simulation is prepared for the proposed strategy. Capacitor storage bank (C_t) is supplies energy during acceleration of induction motor through DC link using boost converter. During the transient period and when load increase suddenly, capacitor storage bank (C_t) is supplied energy. During deceleration of the motor and load, the DC link voltage increases which can be tracked by continuous monitoring it, so energy can be trapped using bidirectional converter to capacitor bank storage unit.

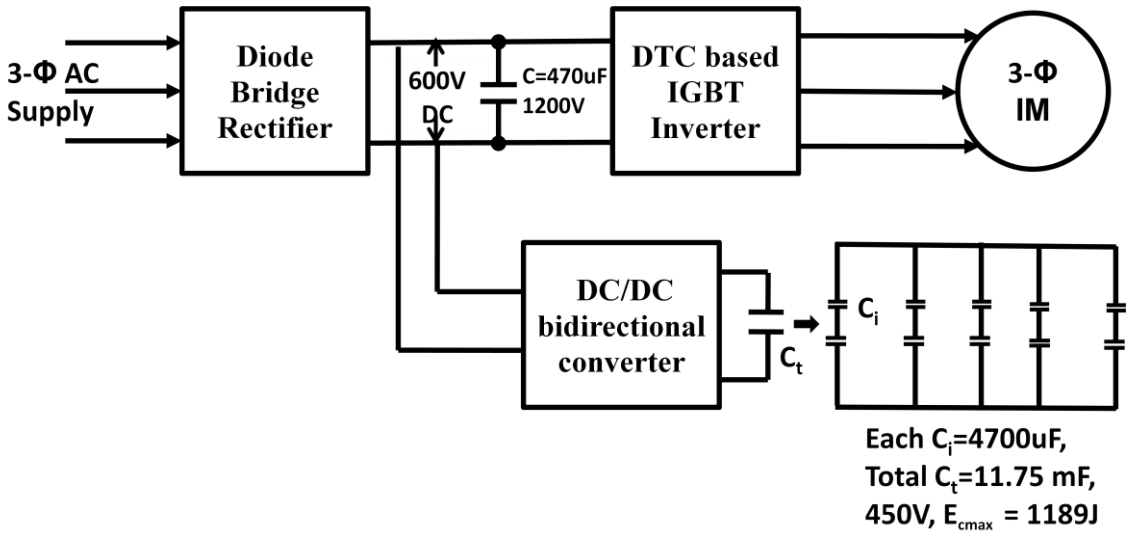

FIGURE 3.2: Block diagram for energy recovery for 5.4 HP DTC based induction motor drive

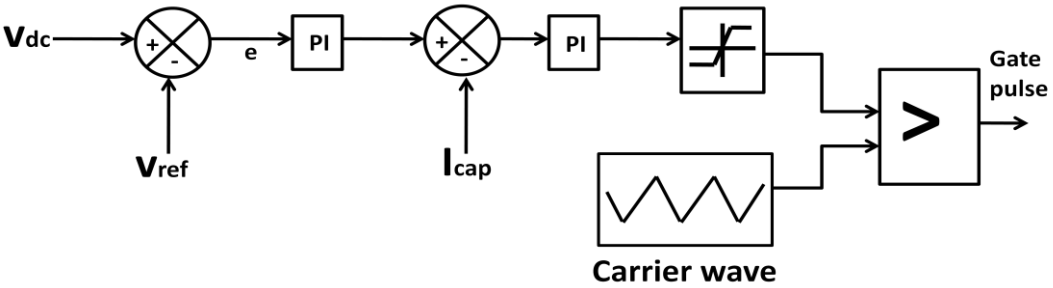

FIGURE 3.3: Control strategy for DC/DC bidirectional converter for energy recovery for DTC based induction motor drive

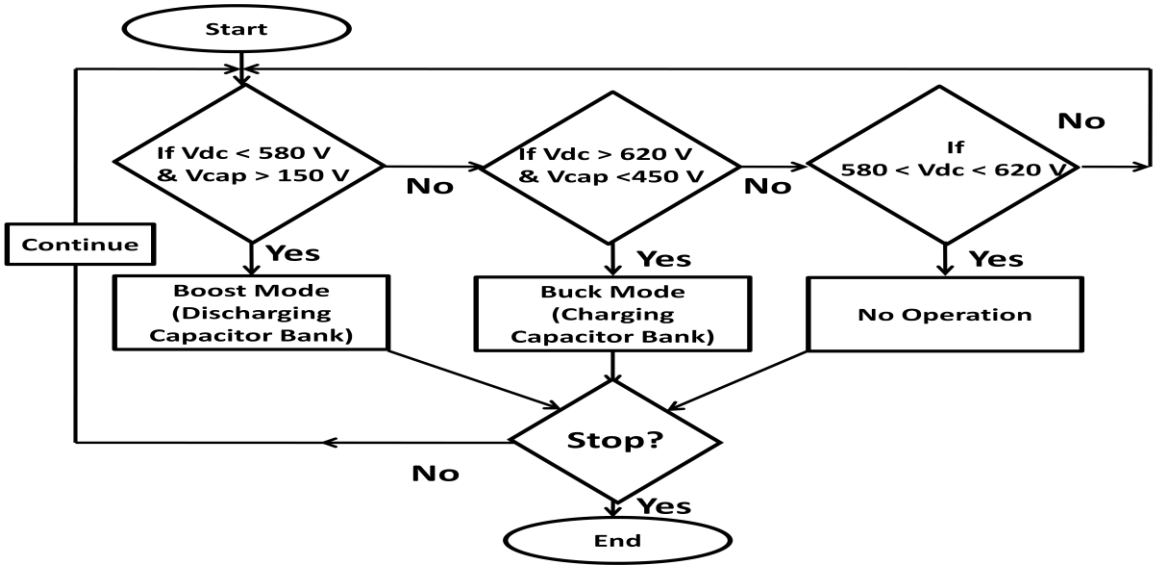

FIGURE 3.4: Flow chart for selection of Buck / Boost operation for Bidirectional DC/DC Converter

Fig. 3.4 shows a flowchart illustrate working of the bidirectional converter. The DC bus voltage and DC voltage of the capacitor bank is to be sensed based on which the following action occurs. Here, rated voltage across the capacitor is assumed to be 450 V.

$V_{cap} > 150$ V, $V_{dc} < 580$ V, Boost action, capacitor bank discharge.

$V_{cap} < 450$ V, $V_{dc} > 620$ V, Buck action, capacitor bank charge

Table 3.1 shows machine parameters and Table 3.2 shows operating condition for DTC based energy recovery drive for induction motor. Fig. 3.5 represents rotor speed in rpm under different operating condition. The rated speed of 5 HP induction motor is 1440 rpm and rated torque is 27 Nm. Electromagnetic torque of 10 Nm constantly applied to the induction motor.

TABLE 3.1: Three phase 5.4 HP induction motor parameters

Parameters	**Ratings**
Rated Power	5.4 HP
Frequency	50 Hz
Rated Voltage	400 V
Rated Speed	1440 RPM
Pole pairs	2
Stator resistance	1.405 Ω
Rotor resistance	1.395 Ω
Stator leakage inductance	5.83 mH
Rotor leakage inductance	5.83 mH
Mutual inductance	0.1722 H
Rotor Inertia (J)	0.0131 kg.m^2
Friction factor(F)	0.002985 Nms

TABLE 3.2: Operating condition for DTC based energy recovery drive for induction motor

Sr. No	Time (S)	Speed (rpm)	Acceleration rate rpm/s	Load torque
1	0	500	500	Load torque = 10 Nm constantly applied during entire simulation
2	3	1440	940	
3	5	0	-11520	
4	7	1440	11520	

The reference speed of the motor is changed to 500 rpm at time t = 0 sec, 1440 rpm at t = 3 sec, 0 rpm at t = 5 sec and 1400 rpm at t = 7 sec. Electromagnetic torque is observed in Fig. 3.6. During acceleration at 8 sec, the torque requirement increases up to 30 Nm. Capacitor bank (C_t) discharged which can be observed by negative current flowing through it during acceleration period as demonstrated in Fig. 3.7. As shown in Fig. 3.8

bidirectional converter operate in boost mode provided voltage across storage capacitor (C_t) above 150 V, hence it supplies energy during acceleration period. During this period, the DC link voltage falls below 580 V as shown in Fig. 3.10. Bidirectional converter works on buck PWM for switch S_1 on during deceleration and boost PWM for switch S_2 on during acceleration. The Fig. 3.12 shows the buck and boost operation PWM pulses, which is generated by control strategy discussed in Fig. 3.3.

During deceleration at t = 5 sec, the negative torque -8.5 Nm observed. Capacitor bank (C_t) charged which can be observed by positive capacitor current flowing through it during deceleration period and voltage across the capacitor bank (C_t) increases from 31.4 V to 118 V as represented in Fig. 3.7. As shown in Fig. 3.3 bidirectional converter operate in buck mode provided voltage across storage capacitor (C_t) below 450 V, hence it store energy during deceleration period. The DC link voltage rises from 583 V to 627.5 V during deceleration as shown in Fig. 3.10 which is to be maintained at 600 V ± 3.3%. Fig. 3.8 and Fig 3.9 show capacitor voltage and capacitor current with respect to time. Energy recovered in the storage capacitor (C_t) during deceleration cycle. At time t = 5 second, it is $E = V \times i \times t$. It can be calculated using graphical method, by finding area under curve. Energy recovery found 75.89 J is calculated by trapezoid strip integration method of power curve shown in Fig. 3.11. Each strip of 10 microseconds is taken for integration. The Recoverable Kinetic energy $= \frac{1}{2} J\omega^2$ = 0.5× (0.0694+0.0131) ×$(150.72)^2$ = 937.05 J, Where the Load inertia is 0.0694 kg.m^2 and motor inertia is 0.0131 kg.m^2. Hence, Energy recovered is 8.09% which is calculated by trapezoid strip integration method for area under curve per deceleration. The energy-saving depends on deceleration cycle and the inertia of the load. During deceleration, the applications like grinders with flywheels, sheet saws driven by high-inertia wheels, centrifuges, and flywheel presses etc. may have a great opportunity of energy saving through regeneration.

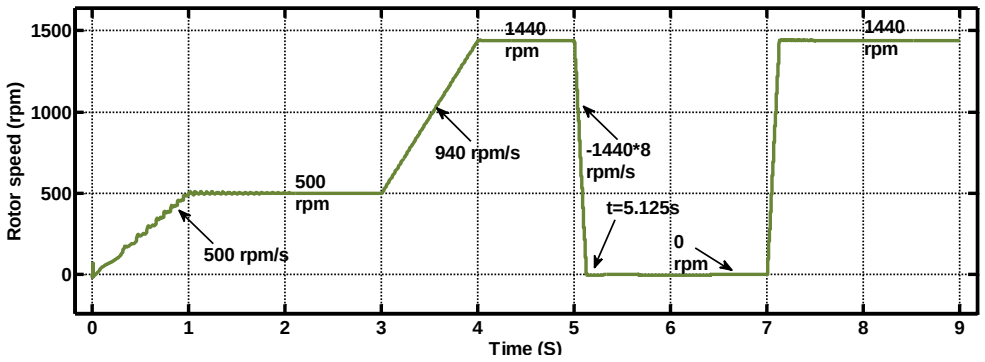

FIGURE 3.5: Rotor speed (rpm) with respect to time (sec)

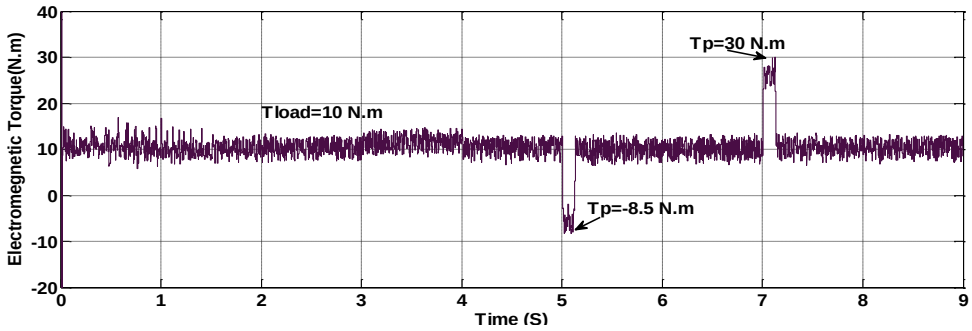

FIGURE 3.6: Electromagnetic torque (Nm) with time (sec)

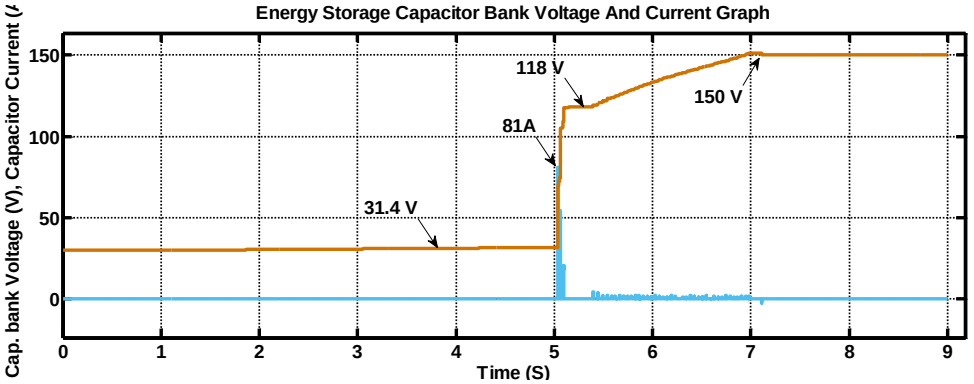

FIGURE 3.7: Capacitor voltage (as energy storage device) shown as upper trace and capacitor current with respect to time (sec) shown as lower trace

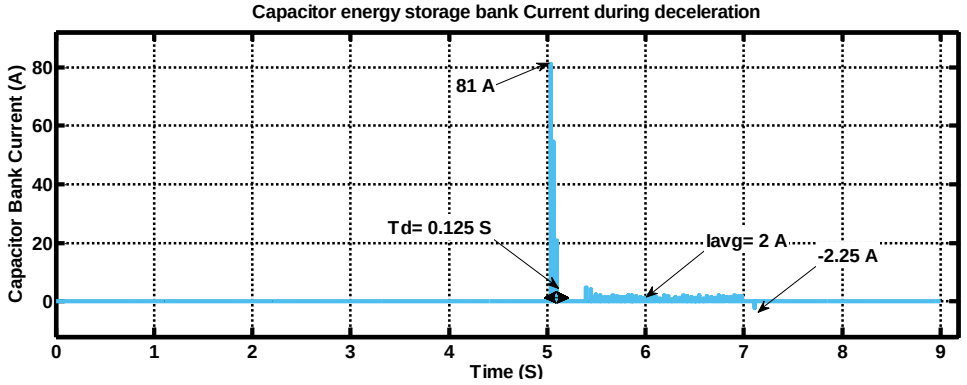

FIGURE 3.8: Current of capacitor bank (I_{cap}) with respect to time (sec)

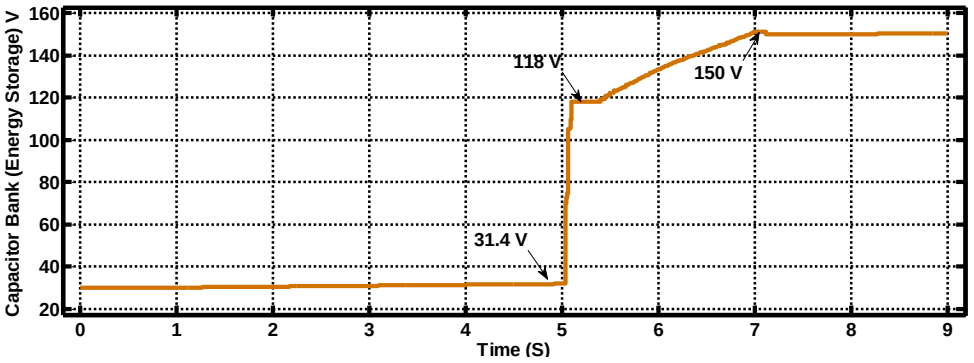

FIGURE 3.9: Capacitor bank voltage (as energy storage device) with respect to time (sec)

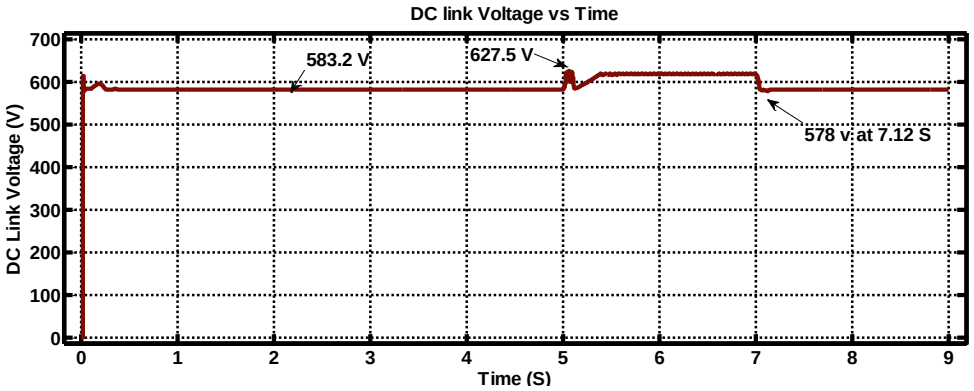

FIGURE 3.10: DC link voltage with respect to time (sec)

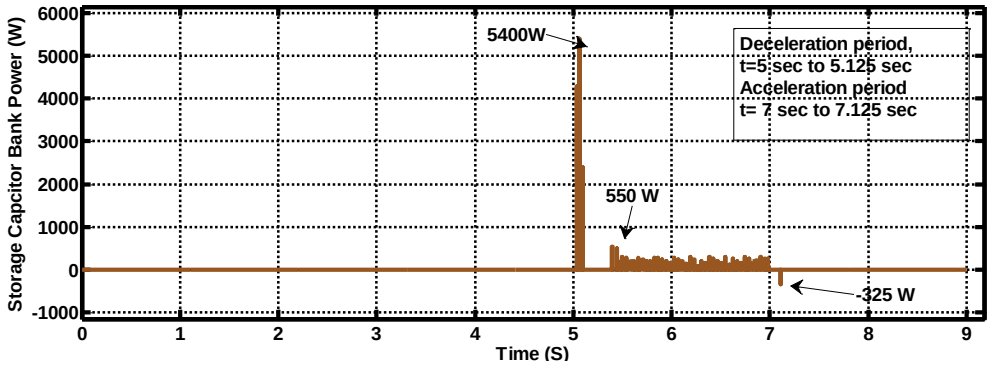

FIGURE 3.11: Energy storage capacitor bank power (w) with respect to time (sec)

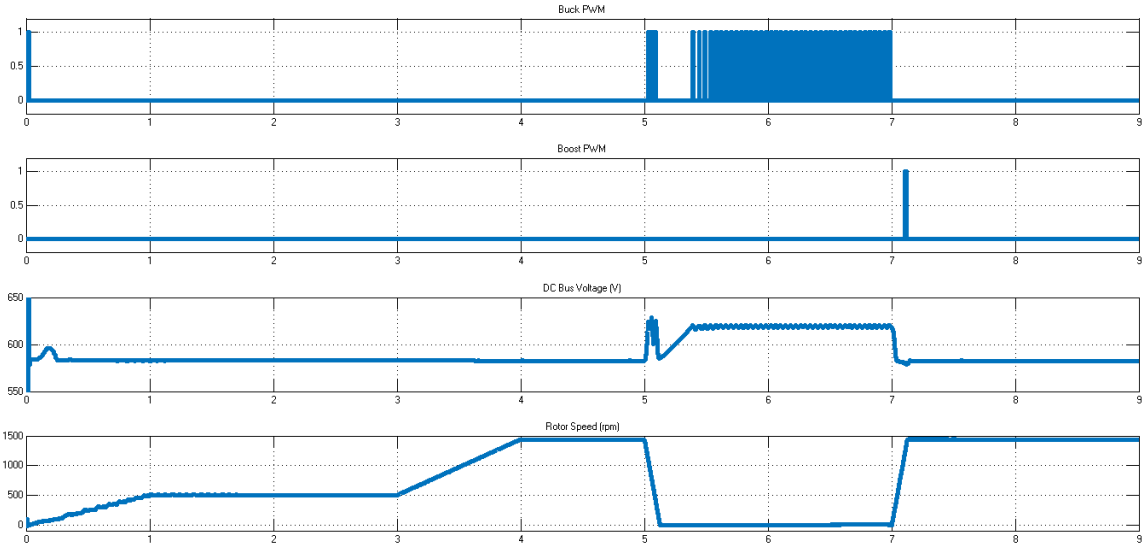

FIGURE 3.12: Bidirectional converter-buck PWM during deceleration (upper trace) and boost PWM (2nd trace) with DC bus voltage (3rd trace) and rotor speed (rpm) (lower trace)

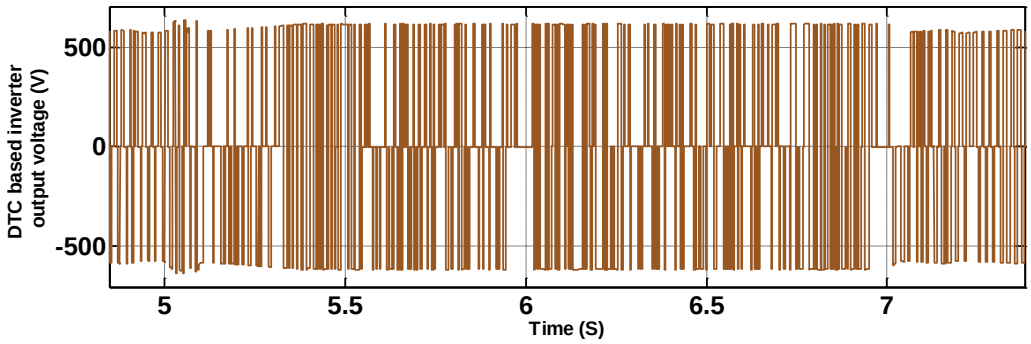

FIGURE 3.13: DTC based inverter output line voltage (V)

Fig. 3.10 shows DC link voltage as input voltage of DTC based inverter where as Fig. 3.13 observed output voltage of DTC based inverter. Fig. 3.14 is the voltage across inductor (4.5 mH) of DC/DC bidirectional converter. At 5 sec, voltage developed across inductor due to deceleration. The current passing through inductor is same as passing through capacitor bank as shown in Fig 3.8. The discontinuous mode of operation observed for converter as given in Fig. 3.15. It is enlarged view of Fig 3.8. The buck action is continued as per flowchart discussed in Fig 3.4, till 7 sec as higher voltage observed than 620 V at DC Link. The current passing through the inductor is equivalent as shown in Fig. 3.8 as inductor is connected in series with capacitor bank.

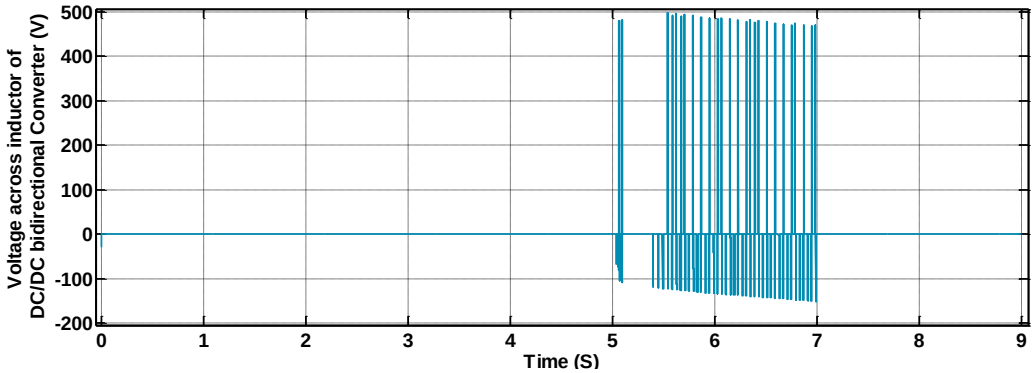

FIGURE 3.14 : Voltage across inductor of DC/DC bidirectional converter

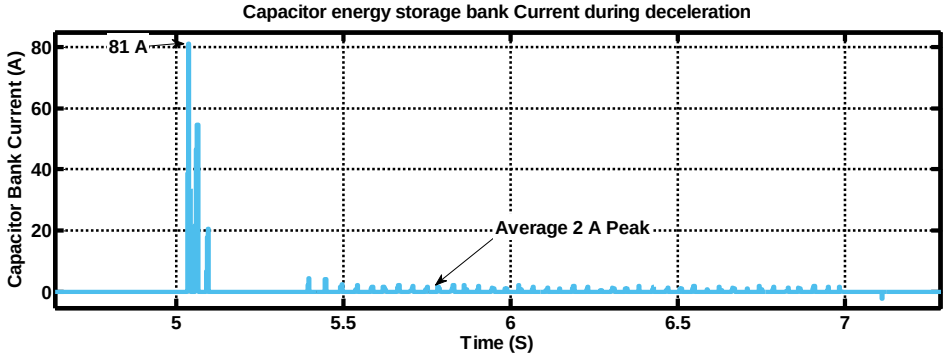

FIGURE 3.15 : Discontinuous mode of current passing through inductor (L) of DC/DC bidirectional converter (shown enlarged view of Fig. 3.8)

3.5 Energy calculation by trapezoidal strip integration method

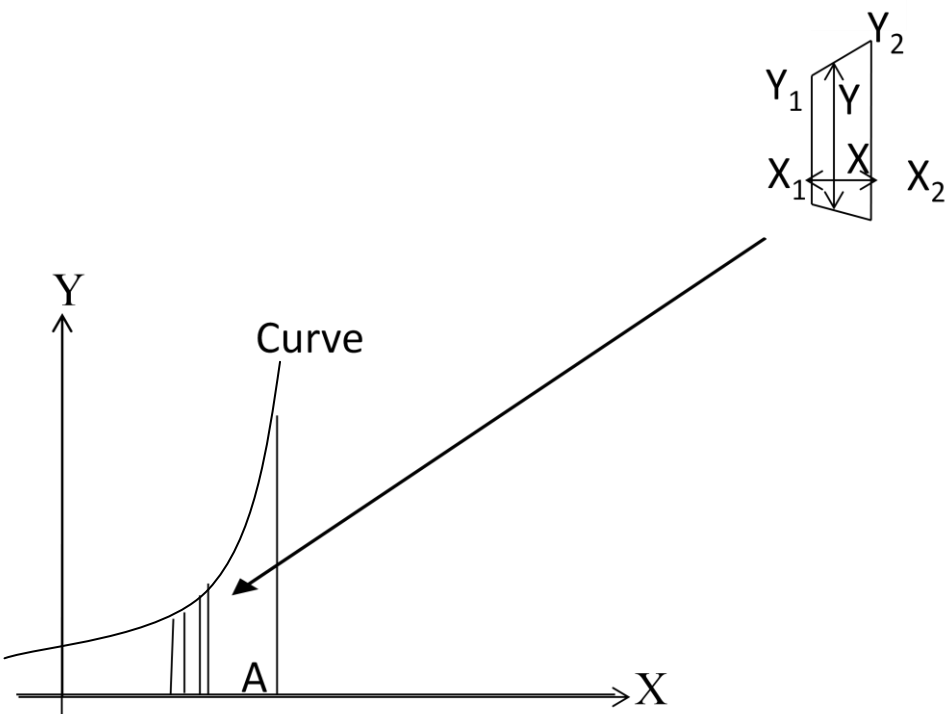

FIGURE 3.16 : Strip Integration method

The energy recovery found by $E = V \times I \times t$ using triangle area does not give accurate result because assumed average voltage and current pass through capacitor during transient recovery. The graphical trapezoidal strip integration method as shown in Fig. 3.16 is quite accurate to find area under the curve. The trapezoidal strip has two sides of Y_1 and Y_2 height. The distance between two strips shows small time period (dt). The area found by multiplication of trapezoidal strip height and the distance between two strips is shows energy. The Table 3.3 shows energy (J) found using trapezoidal strip integration method.

The proposed strategy for energy recovery has a significant energy savings potential during deceleration of three phase induction motor DTC drive. The energy recovery is calculated from power graph illustrated in Fig. 3.11. The Energy recovery is 8.09% during each deceleration from 1440 rpm to 0 rpm for above case which is remarkable for same

rating motor without using supercapacitor bank. Different deceleration time period (T_d) is simulated to check the energy recovery efficiency is tabulated in Table 3.4.

TABLE 3.3: Energy (J) found by trapezoidal strip integration method

Time	Power (watt)	dt =A= X Strip $=t_2-t_1$ (sec)	B=Y strip $=(Y_1+Y_2)/2$ (watt)	Energy = Each Strip Area =A*B (joule)
5	0.163932	1E-05	0.163914	1.63914E-06
5.00001	0.163895	1E-05	0.163877	1.63877E-06
5.00002	0.163859	1E-05	0.16384	1.6384E-06
5.00003	0.163822	1E-05	0.163803	1.63803E-06
5.00004	0.163784	1E-05	0.163764	1.63764E-06
5.00005	0.163745	1E-05	0.163725	1.63725E-06
5.00006	0.163705	1E-05	0.163684	1.63684E-06
5.00007	0.163664	1E-05	0.163643	1.63643E-06
5.00008	0.163622	1E-05	0.163601	1.63601E-06
5.00009	0.163579	1E-05	0.163577	1.63577E-06
:	:	:	:	:
:	:	:	:	
5.03411	1801.456	1E-05	1800.404	0.018004038
5.03412	1799.351	1E-05	1798.292	0.017982916
5.03413	1797.232	1E-05	1796.165	0.017961646
5.03414	1795.098	1E-05	1794.023	0.017940231
5.03415	1792.949	1E-05	1791.867	0.017918669
5.03416	1790.785	1E-05	1789.696	0.017896962
5.03417	1788.607	1E-05	1787.511	0.017875109
5.03418	1786.415	1E-05	1810.983	0.018109831
5.03419	1835.551	1E-05	1860.14	0.018601397
5.0342	1884.728	1E-05	1883.693	0.018836935
5.03421	1882.659	1E-05	1881.617	0.01881617
:	:	:	:	:
:	:	:	:	:
5.20576	0.423456	1E-05	0.423385	4.23385E-06
5.20577	0.423313	1E-05	0.423238	4.23238E-06
5.20578	0.423162	1E-05	0.423082	4.23082E-06
5.20579	0.423002	1E-05	0.423005	4.23005E-06
5.2058	0.423009	1E-05	0.423012	4.23012E-06
5.20581	0.423015	1E-05	0.423014	4.23014E-06
5.20582	0.423012	1E-05	0.423007	4.23007E-06
5.20583	0.423001	1E-05	0.423078	4.23078E-06
5.20584	0.423155	1E-05	0.423229	4.23229E-06
5.20585	0.423303	1E-05	0.423319	4.23319E-06
5.20586	0.423334	1E-05	0.423348	4.23348E-06
5.20587	0.423362	1E-05	0.423371	4.23371E-06
			Total Recovered Energy (J)	75.89022616
			Recoverable Kinetic energy $(\frac{1}{2}J\omega^2)$	937.05 J
			Energy recovered (%)	8.0992771

TABLE 3.4: Effect of variation in time period of deceleration (T_d) on energy recovery for DTC based three phase induction motor (5.4 HP) drive

Sr. No.	Deceleration time T_d (ms)	Increase in voltage of storage capacitor bank (V_c) during deceleration period	Peak charging current I_{peak} (A) of Storage capacitor bank during deceleration period	Energy recovery by strip integration method (J)	Recoverable Rotational kinetic energy (J)	% Energy recovery during deceleration
1	125	86.6	81	75.89	937.05	8.09
2	62.5	150	41.25	187.41	937.05	20
3	50	145	73.1	250	937.05	26.68

The effect of deceleration time period on energy recovery for DTC based three phase induction motor drive is checked and found good scope to analyse effect of different variables on energy recovery of DTC based three phase induction motor drive. Further, effect of different variables on energy recovery is discussed in chapter 5.

3.6 Chapter Conclusion

- In this chapter, energy regeneration during deceleration of the direct torque control drive for the induction motor is discussed.
- Energy regeneration during deceleration of DTC based induction motor drive with capacitor bank as an energy storage device is simulated.
- Table 3.4 shows remarkable kinetic energy is recovered in energy storage device with different deceleration rate.
- Energy recovery enhancement is done using proposed method about 8.09% to 26.68%.
- The suggested strategy for energy recovery has a significant energy saving potential during deceleration of DTC based induction motor drive.

In the next chapter, energy recovery by regenerative power fed back to the grid using DC/AC converter during deceleration of DTC based induction motor is discussed.

CHAPTER-4

4 Improvement in energy recovery by regenerative power fed back to the grid using DC/AC converter during deceleration of DTC based induction motor

4.1 Introduction

A detailed study concerning the use of energy recovery using DC/AC converter with DTC based three phase induction motor drive during deceleration is done. Energy recovery during deceleration of DTC based induction motor drive using DC/AC converter connected to grid has been simulated. The role of the DC/AC converter is to return back the energy to the power supply network in this circuit during deceleration or braking. The main advantage is to use braking energy instead of being wasted as heat in braking resistor. The considerable amount of energy saving can be obtained when the kinetic energy recovered during deceleration. A study on energy recovery using DC/AC converter gives maximum energy recovery, depends on several parameters like the moment of inertia, speed profile of the application, deceleration duration, deceleration rate, load and motor power rating etc.

4.2 Types of energy recovery strategies for grid connected DTC induction motor drive

Regenerative energy fed drive technologies have a benefit function that kinetic energy can be recover during deceleration and braking by given back to supply grid. Instead of wasting energy as a heat in the resistor, regenerative operation provides energy saving. Additional cooling arrangement for high power drive due to waste heat during resistor braking is not required. One strategy is to use energy storage units like supercapacitor, lithium battery or flywheel at site to absorb the surplus regenerated energy and regulate DC voltage. However, some drawbacks of energy storage system are bigger space requirements, higher cost, shorter service life and more safety constraints. Different energy recovery strategies are discussed for a grid connected direct torque control method of induction motor drive. The different topologies for regenerative braking drives are anti-parallel thyristors bridge, six pulses external regenerative braking unit, matrix converter drive, front end converter drive, etc [46][47]. The choice of topology depends on cost-saving ability, low input current harmonics, initial cost payback period, number of motor connections, power factor improvement and additional space required compared to a conventional drive. Fig.4.1. represents block diagrams for different topologies for induction motor drive for energy fed to the grid during regenerative braking. Anti-parallel thyristors bridge is conventionally used, has low cost than IGBT based front end converter. The disadvantage of anti-parallel thyristors bridge is that the total harmonic distortion (THD) is higher than IGBT based front end converter and regenerative braking unit. The IGBT based front end converter for induction motor drive has more reliable operation than anti-parallel thyristors bridge. Matrix topology uses more number of switches, less THD than anti-parallel thyristors bridge. It can allow braking energy return back to supply line to any output phase but its braking capability fails during main supply failure.

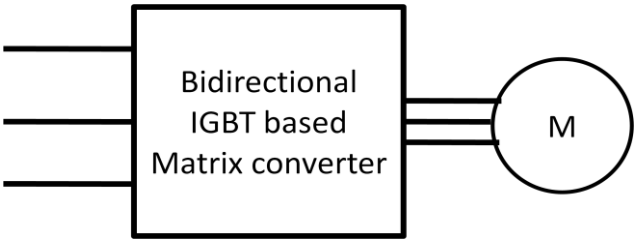

Fig.4.1 (a) Matrix converter fed induction motor drive

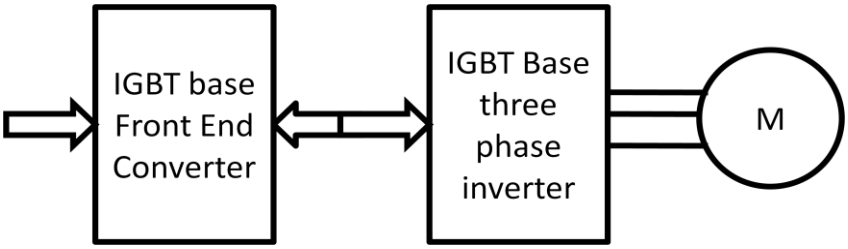

Fig.4.1 (b) IGBT base front end converter drive

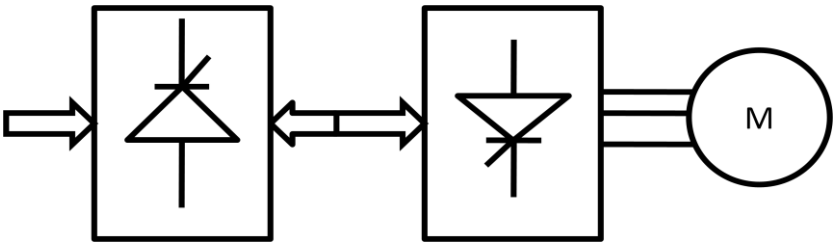

Fig.4.1 (c) Anti-parallel thyristor unit

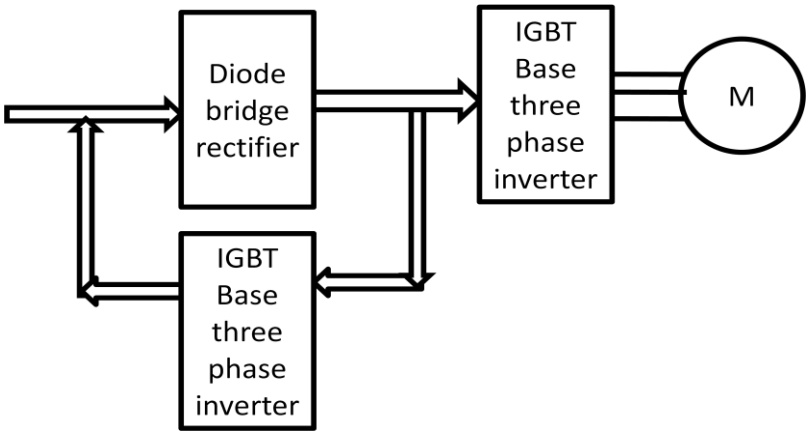

Fig. 4.1 (d) Regenerative braking unit for induction motor drive

FIGURE 4.1: Various topologies for induction motor drive for regenerative energy fed to supply grid during deceleration

4.3 Block Diagram of DTC scheme for induction motor drive with regenerative braking unit

The schematic diagram of the DTC based induction motor drive with the regenerative braking unit is shown in Fig. 4.2.

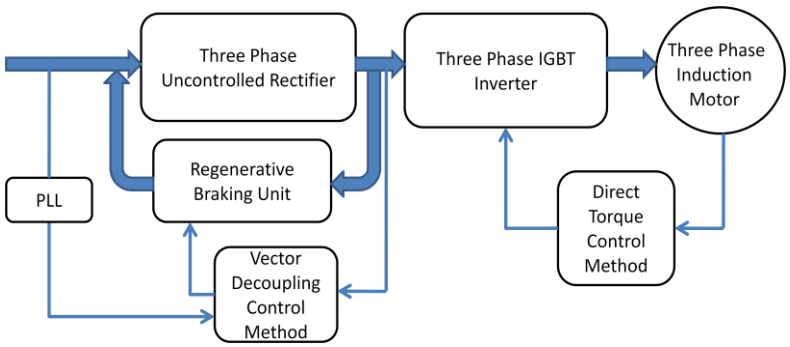

FIGURE 4.2: Outline schematic diagram of three phase induction motor DTC drive with regenerative braking unit

The flowchart shown in Fig. 4.3 display the working of the regenerative braking unit when DC bus voltage is above threshold value. Under normal condition, DC link voltage should remain constant to 600 V. However, it suddenly increases if load decreased or brake applied. Increase DC bus voltage during deceleration can be limited by braking resistor heat dissipation. However, the present work shows the recovery of energy during deceleration along with DC bus voltage control using regenerative braking in DTC based induction motor drive.

The block diagram of the DTC based induction motor drive with the regenerative braking unit is shown in Fig. 4.4 and the control scheme for regenerative braking is shown in Fig. 4.6.

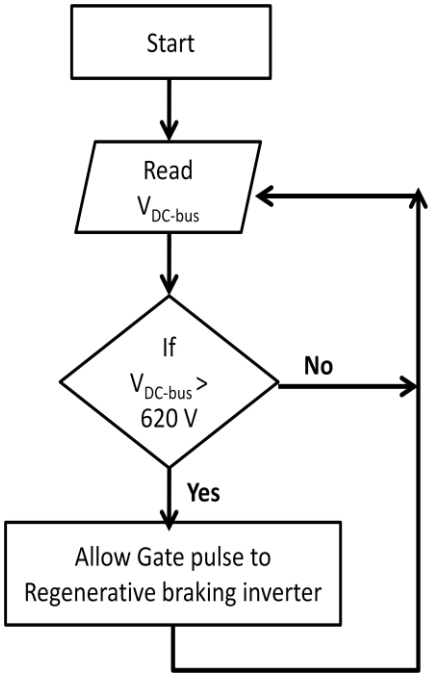

FIGURE 4.3: Flowchart for regenerative braking inverter

Grid-connected DC/AC converters are controlled with vector decoupled control method. It consists of outer dc link voltage control loop and inner current control loop. Here, three phase IGBT based DC/AC converter which is connected directly to grid is controlled with sinusoidal pulse width modulation (SPWM) signal. The phase locked loop (PLL) is used to establish synchronization between generated inverter output and the grid supply. The simulation performance of the proposed control algorithm for three phase grid connected DC/AC converter found satisfactory during deceleration period of DTC based induction motor drive.

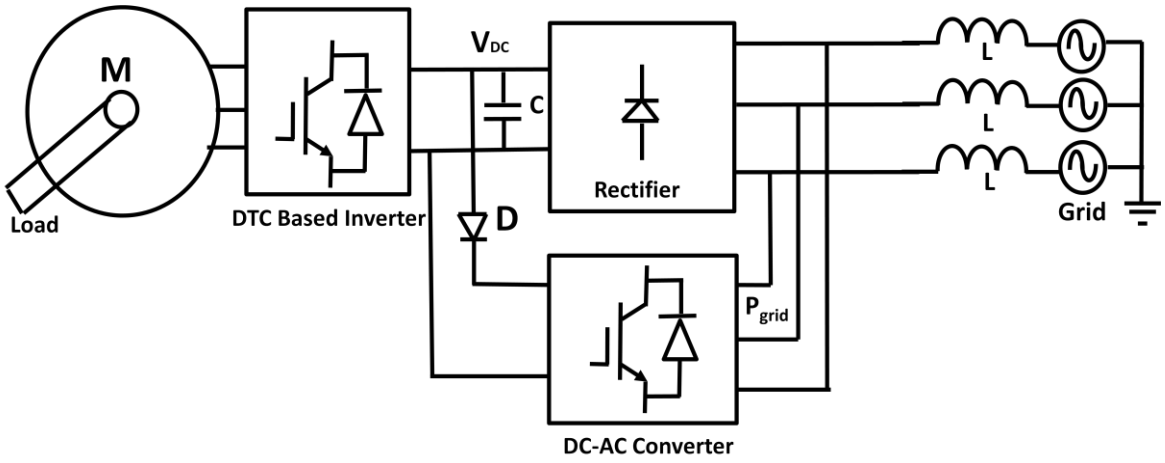

FIGURE 4.4: Block Diagram of DTC based three phase induction motor drive with a regenerative braking unit (DC/AC Converter)

4.4 Energy recovery equation

During motoring action of the induction motor own can write,

$$\frac{d\omega}{dt} = \frac{T_e - T_l}{J} \qquad (4.1)$$

Where, T_e = electromagnetic torque and T_l = load torque, assume friction is zero.

If suddenly brake command is applied to the motor drive, assuming high inertia of the load and rotor itself, assuming of the load and rotor itself have high inertia for high power motor, negative electromagnetic torque (T_e) is developed which can be given as (4.2). Due to negative torque (T_e) fast deceleration and quick braking occurs.

$$\frac{d\omega}{dt} = \frac{(-T_e - T_l)}{J} \qquad (4.2)$$

Assume supply cutoff for drive (4.1), hence electromagnetic torque (T_e) is zero, and natural deceleration occurs with deceleration rate can be given as in (4.3)

$$\frac{d\omega}{dt} = -\frac{(T_l)}{J} \qquad (4.3)$$

Energy stored in inertia need to be dissipated in form of heat energy in resistor conventionally, machine take longer time to decelerate and come to halt. Using regenerative braking drive unit in drive, instead of dissipating the kinetic energy, it can be recovered and fed back to the source.

The relationship between mechanical power (P_m), deceleration time and the energy equation for three phase induction motor is discussed [78].

$$P_m = T_m . \omega \text{ watt} \qquad (4.4)$$

$$P_m = \frac{(T_m . 2 . \pi . N)}{60} \text{ watt, N} = \text{speed in rpm} \qquad (4.5)$$

The mechanical power (P_m) for the motor (P_e) is shown in (4.4) - (4.5). The motor torque (T_m) require to provide friction and inertial load along with acceleration.

$$T_m = -(J . \alpha + \beta . \omega + T_l) \qquad (4.6)$$

If the load inertia is J kg.m^2, the load torque is T_l Nm and the load is driven with N_1 (rpm) at time t_1(sec), the motor torque is taken during deceleration as zero and the final speed N_2 (rpm) is zero at time t_2 (sec). To find braking time, assume zero friction value.

$$T_l = J.\alpha = J.\frac{(N_1 - N_2).2\pi}{(t_1 - t_2).60} \tag{4.7}$$

The load decelerate and reach to zero final speed (N_2) in the time t as shown in (4.8).The deceleration rate and deceleration time are discussed in literature [79].

$$t = J.\frac{(N_1).2\pi}{60.T_l} \tag{4.8}$$

The moment of inertia of load with motor is key parameter for finding time of acceleration and deceleration also.The relationship between mechanical power (P_m) and the energy (E) equation for the three phase induction motor is discussed [78]. The kinetic energy during regenerative braking is written as (4.9).

$$E = -J.\omega^2 \int_{s1}^{s2} \left(\frac{Tm}{T_m - T_l}\right).s.ds = -J.\omega^2.\frac{[s_2{}^2 - s_1{}^2]}{2} = M.\left(-\frac{1}{2}.J.\omega^2\right) \tag{4.9}$$

Where the value of slip s_1 and s_2 are corresponded to initial speed (N_1) and final speed (N_2) respectively, S is slip and M is multiplying factor = $\frac{[s_2{}^2 - s_1{}^2]}{2}$. The J is rotational inertia (kg.m^2), T_m and T_l Torque developed by the motor and load torque (Nm) respectively. The load torque is assumed small in compare to the motor torque during acceleration.

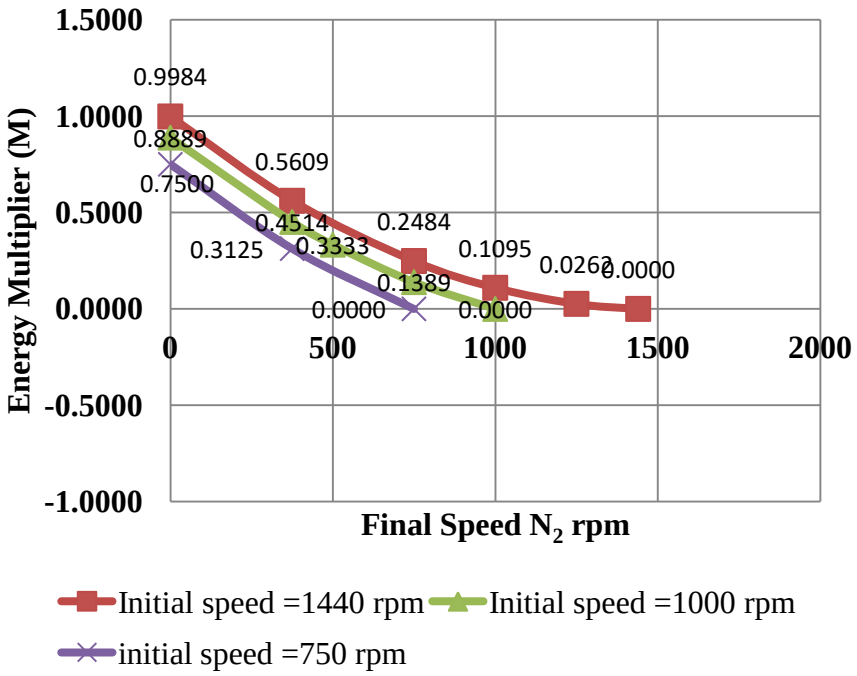

FIGURE 4.5: Energy multiplier (M) versus final speed (N2) rpm for different initial speed (N1) during deceleration of induction motor.

The energy recovery depends on initial speed (N_1) and final speed (N_2) of the motor during deceleration period. To find energy recovery for given initial and final speed of deceleration, it is required to calculate energy multiplier (M). For example, during deceleration for 4-pole, three phase, 50 Hz induction motor considering initial speed (N_1) as 1000 rpm and final speed (N_2) at 0 rpm. Energy multiplier M = 0.89 can be calculated using (4.9). The relation between energy multiplier (M) and final speed (N_2) of deceleration for given initial speed (N_1) is plotted in Fig. 4.5. During deceleration, assuming speed reduction from 1000 rpm to 0 rpm. The recoverable K.E. is multiplied with energy multiplier (M = 0.89) with total K.E. Hence, The recoverable kinetic energy is $E = M*(-\frac{1}{2}.J.\omega^2)$ is available for recovery during deceleration for initial speed (N_1) to final speed (N_2) for 4-pole 3-phase induction motor. Kinetic energy to be recovered by regenerative braking unit and energy need to supply back to the grid.

4.5 Simulation results and discussion

Fig. 4.6 shows a DTC drive for a three phase induction motor connected to the grid with energy recovery system. The simulation motor parameters of 50 HP, 100 HP, 215 HP three phase induction motors are given in Table 4.1, 4.2, 4.3 respectively. The full load torque is 239 Nm for 50 HP three phase induction motor. The simulation results are obtained for following operating conditions shown in Table 4.4. Fig. 4.6 shows block diagram vector decoupling control technique to control DC/AC converter connected to the power grid, which fed back energy during deceleration of the induction motor drive.

TABLE 4.1: Simulation parameters of 50 HP three phase induction motor

Sr. No.	Parameter	Unit	Sr. No.	Parameter	Unit
1	Rated Power	50 HP (37 kW)	2	No. of Pole pairs	2
3	Rated Voltage	400 V	4	Frequency	50 Hz
5	Rated Speed	1480 rpm	6	Stator resistance	0.08233 Ω
7	Rotor resistance	0.0503 Ω	8	Stator leakage inductance	0.724 mH
9	Rotor leakage inductance	0.724 mH	10	Mutual inductance	27.11 mH
11	Rotor Inertia Constant	0.37 $kg.m^2$	12	Friction factor(F)	0.0279 Nms

TABLE 4.2: Simulation parameters of 100 HP three phase induction motor

Sr. No.	Parameter	Unit	Sr. No.	Parameter	Unit
1	Rated Power	100 HP (0kW)	2	No. of Pole pairs	2
3	Rated Voltage	400 V	4	Frequency	50 Hz
5	Rated Speed	1484 rpm	6	Stator resistance	0.0355 Ω
7	Rotor resistance	0.0209 Ω	8	Stator leakage inductance	0.335 mH
9	Rotor leakage inductance	0.335 mH	10	Mutual inductance	15.1 mH
11	Rotor Inertia Constant	1.25 $kg.m^2$	12	Friction factor(F)	0.03914 Nms

TABLE 4.3: Simulation parameters of 215 HP three phase induction motor

Sr. No.	Parameter	Unit	Sr. No.	Parameter	Unit
1	Rated Power	215 HP (160kW)	2	No. of Pole pairs	2
3	Rated Voltage	400 V	4	Frequency	50 Hz
5	Rated Speed	1487 rpm	6	Stator resistance	0.01379 Ω
7	Rotor resistance	0.007728 Ω	8	Stator leakage inductance	0.152 mH
9	Rotor leakage inductance	0.152 mH	10	Mutual inductance	7.69 mH
11	Rotor Inertia Constant	2.9 $kg.m^2$	12	Friction factor(F)	0.05658 Nms

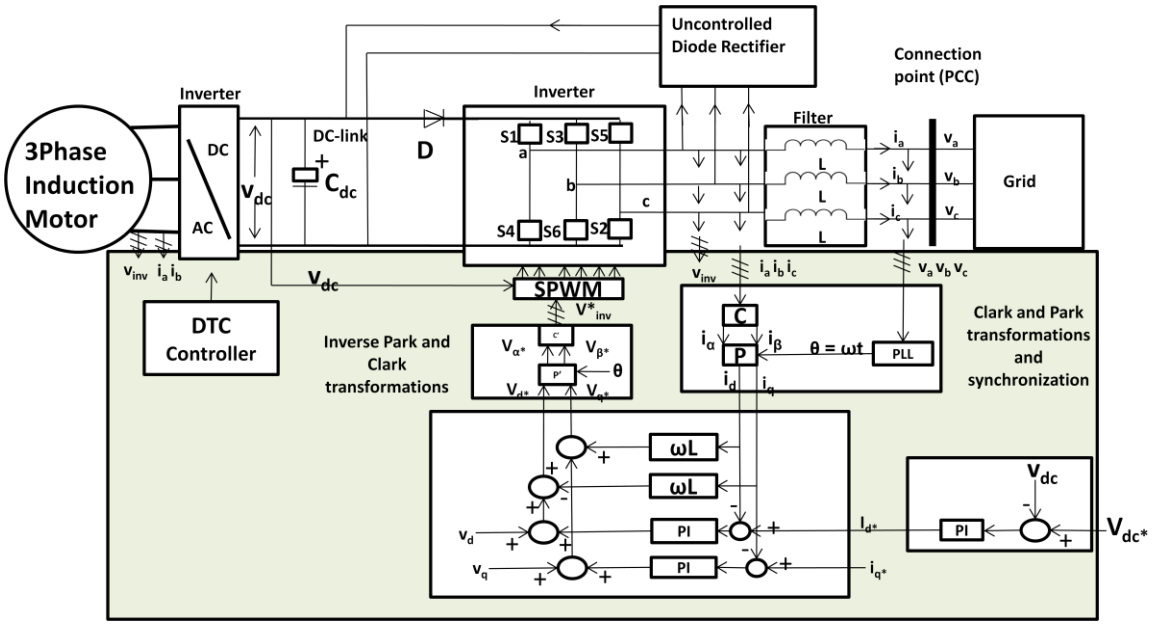

FIGURE 4.6: Block diagram of vector decoupling control of DC/AC converter with DTC based three phase induction motor

TABLE 4.4: Operating conditions for simulations for 50 HP induction motor

Sr. No.	Time (s)	Speed (rpm)	Torque (Nm)
1	0	1000	0
2	0.5	1000 (No Change)	239
3	1	0	239 (No Change)
4	1.5	0	-239

Fig. 4.7 represents stator current (A), rotor speed (rpm), electromagnetic torque (Nm) and Power recovered (kW) for 50 HP three phase induction motor drive. The phase reversal

observed in stator current and negative electromagnetic toque graph found at the point of deceleration started, at t = 1.5 second in Fig. 4.8.

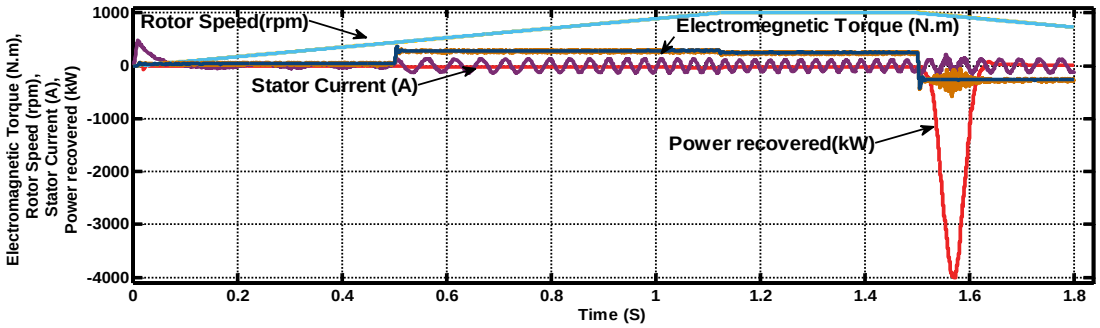

FIGURE 4.7: Waveform of stator current (A), rotor speed (rpm), electromagnetic torque (Nm), and power recovered (kW) for the DTC based three phase induction motor drive.

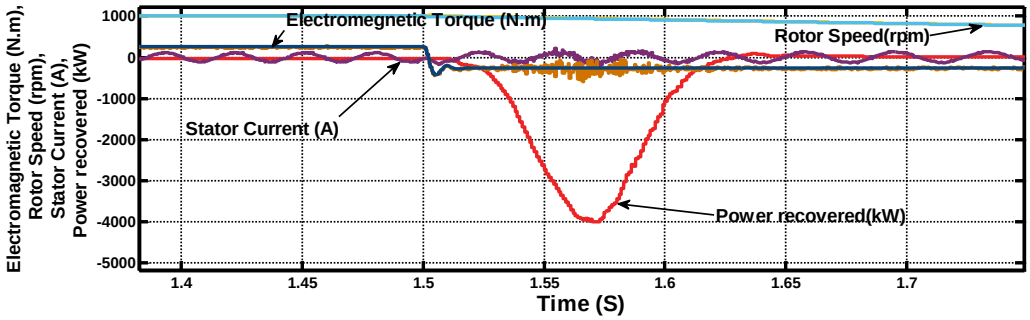

FIGURE 4.8: Enlarge view of waveforms shown in Figure 4.7, for stator current (A), rotor speed (rpm), electromagnetic torque (Nm), and power recovered (kW) for the DTC based three phase induction motor drive.

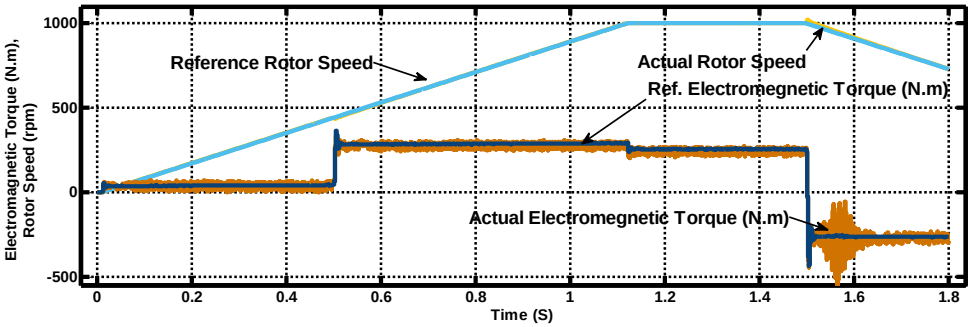

FIGURE 4.9: Waveform of rotor speed (rpm), electromagnetic torque (Nm) respectively for the DTC based three phase induction motor drive.

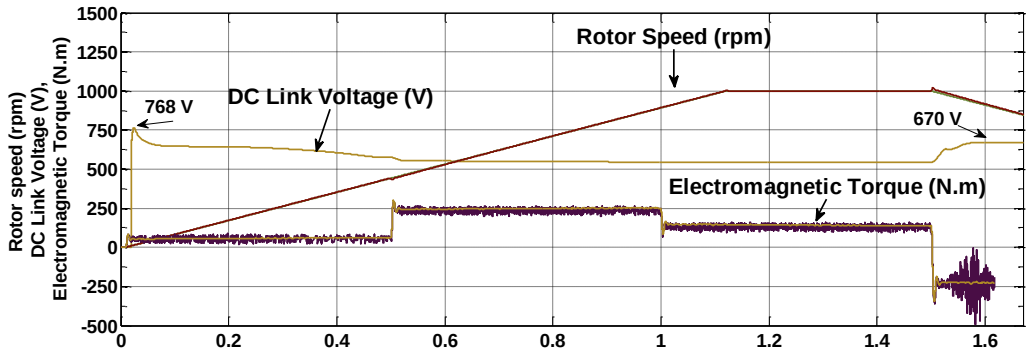

FIGURE 4.10: DC link voltage observation with respect to changes in rotor speed and reference electromagnetic torque for the DTC based three phase induction motor drive.

The rotor speed increases from 0 to 1000 rpm during the acceleration period from 0 to 1 second with rate of acceleration i.e. 900 rpm/s as shown in Fig. 4.9. Fig. 4.10 shows DC link voltage observed increasing 680 V maximum during regeneration started at 1.5 sec. Fig. 4.11 is demonstrated DTC based inverter output voltage which is line voltage fed to three phase induction motor. Due to deceleration starts at 1.5 sec, the line voltage level is increased as shown in Fig 4.11.

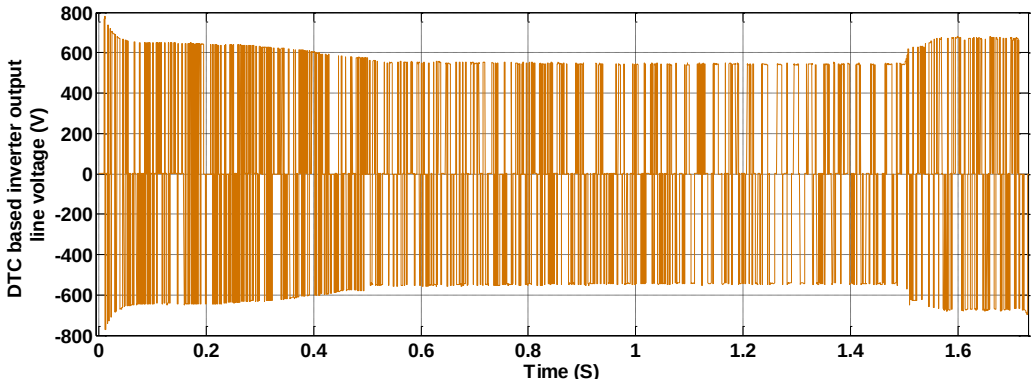

FIGURE 4.11: DTC based inverter output as line voltage fed to 50HP three phase induction motor

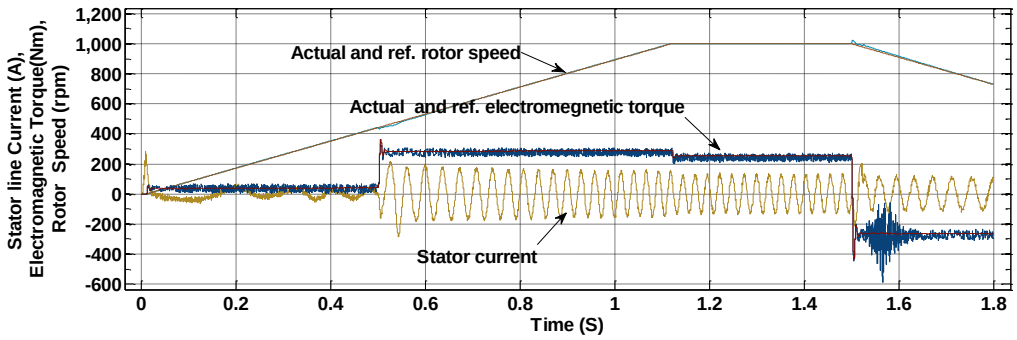

FIGURE 4.12: Stator line current of 50 HP three phase induction motor

Fig. 4.12 shows stator line current of three phase induction motor.it is observed that at 1.5 sec,due to negative torque, phase is reversed at 1.5 sec. Regenerative braking unit (DC/AC

converter) have input side dc link voltage is applied. The inverter output voltage and current (A) are shown in Fig. 4.13 and 4.14 respectively. The current is synchronised and fed back to supply grid.

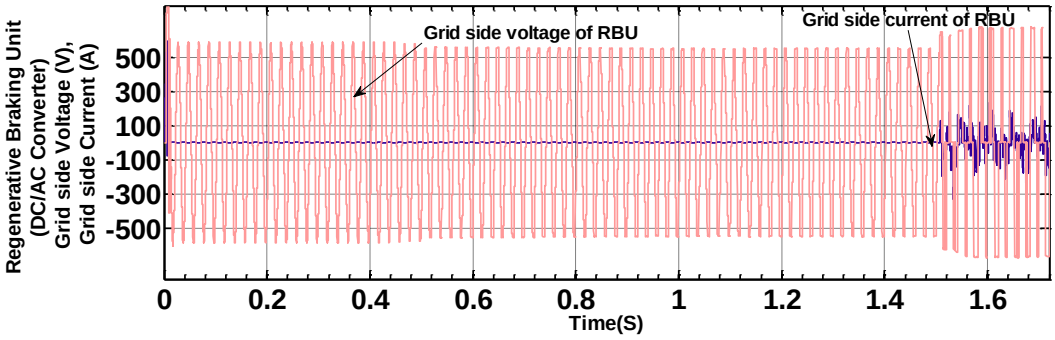

FIGURE 4.13: Regenerative braking unit (DC/AC converter) output voltage and current at grid side

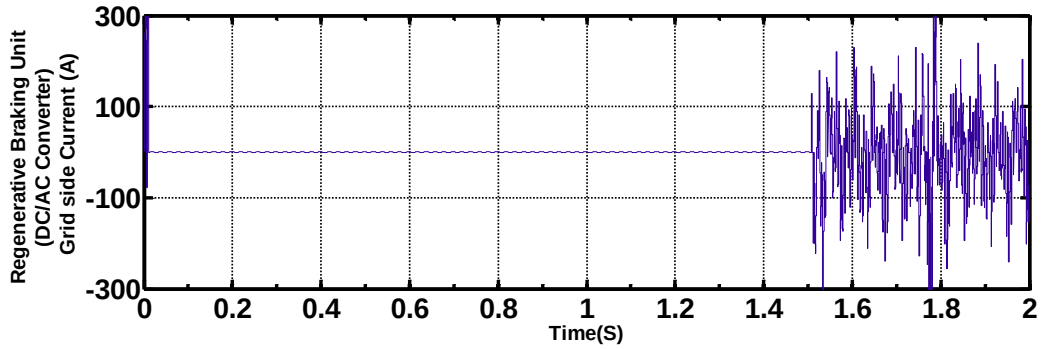

FIGURE 4.14: Regenerative braking unit (DC/AC converter) output current (A) at grid side

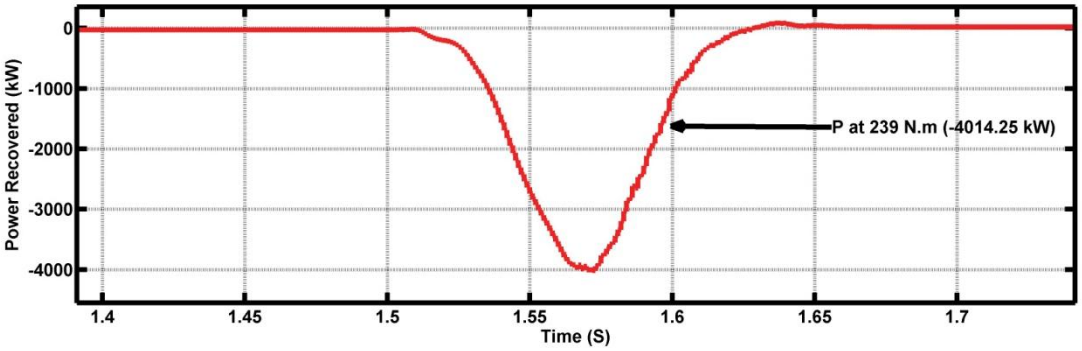

FIGURE 4.15: Power (kW) vs time(s) at grid side of DC/AC converter during deceleration of the 50 HP three phase induction motor

Fig. 4.15 shows power fed to grid during deceleration of induction motor at time t = 1.5 sec. The area covered by the graph in Fig. 4.15 shows energy recovery. The triangle area calculation method is applied to calculate the area of the graph. Total energy fed back during deceleration is 160 kJ using trapazoidal strip integration method. The triangle area calculation method is simple to calculate the area of the graph. Total energy fed during

this deceleration is = 0.5*0.082*4014.25 = 164.58 kJ. It need to find base and perpendicular hight of triangle accurately. During Speed reduction from 1000 rpm to 0 rpm, from the total K.E.= $\frac{1}{2}.J.\omega^2$ = 250 kJ , the recoverable K.E.=M*K.E.= 0.888*250 = 222.22 kJ.The energy recovery efficiency η = 164/222.22 = 74 %. Further, the trapazoidal strip integration method is used to calculate power area for better accuracy,which shows recoverable energy =160 kJ and energy recovery efficiency η = 160/222.22 = 72 %. All simulations done for 215 HP,100 HP, 50 HP induction motor, results are shown using trapazoidal strip integration method in Tables 4.5, 4.6, 4.7.

Table 4.5 shows the simulation results with variation in load torque for energy recovery of 50 HP, 100 HP, 215 HP induction motors. From the Table 4.5, it is shown that as load increase, more kinetic energy to be recovered but Load torque increment provoke large motor current and high electrical losses, reduce energy recovery efficiency.

TABLE 4.5: Three phase induction motor for kinetic energy recovery during deceleration with load torque variation (deceleration rate = 900rpm/s)

Sr. No.	Motor HP	power kW	Initial speed rpm	Load Torque (T_l) Nm	Rotational kinetic energy(E) kJ	Recoverable Energy (M*E)	$E_{recovery}$ (kJ) by simulation	Energy recovery Efficiency η%
1	215	160	1000	1033	1081.08	962	145	13
2	215	160	1000	775	810.81	721	182	21.1
3	215	160	1000	516	540.54	481	189	36.38
4	215	160	1000	258	270.27	240	190	79.16
5	100	75	1000	484	506.59	450.3	148	32.87
6	100	75	1000	363	475.08	422.82	239	56.52
7	100	75	1000	242	226.72	201.78	169.63	84.07
8	100	75	1000	121	158.36	140.94	131	89.9
9	50	37	1000	239	250	222.22	160	72
10	50	37	1000	179	187.5	166.87	154.27	85
11	50	37	1000	120	104.67	93.15	80.1	86
12	50	37	1000	60	62.8	55.89	50.5	90.3

Table 4.6 shows the simulation results for energy recovery of 50 HP, 100 HP, 215 HP induction motor with initial speed (N_1) of deceleration variation. Initial speed (N_1) of deceleration, if higher, losses are higher, hence recovery efficiency is lower.

Table 4.7 shows percentage energy recovery with change of deceleration rate for 50 HP induction motor, with different load for regenerative braking with initial speed (N_1) fixed 1000rpm to final speed (N_2) is 0 rpm. Faster deceleration rate means, current increases more during deceleration, hence higher electrical losses. Higher deceleration rate cause to rise DC link voltage faster, Low deceleration rate means the motor have to decelerate for long time, due to which diminishing kinetic energy loss increases still stop. In addition to that mechanical losses are higher due to long time to decelerate. It is required to take moderate deceleration rate where energy recovery can be optimised.

Further, effect of variation of load torque, variation in initial speed (N_1) of deceleration, change in deceleration rate on energy recovery are discussed in detail in next chapter.

TABLE 4.6: Kinetic energy recovery during deceleration with initial speed (N_1) variation for three phase induction motor (deceleration rate = 900rpm/s)

Sr. No.	Motor HP	Power kW	Initial speed rpm	Load Torque T_l Nm	Rotational kinetic energy (E) kJ	Energy Multiplier (M)	Recoverable Energy (M*E) kJ	$E_{recovery}$ kJ simulation	Energy recovery Efficiency η%
1	215	160	1480	1033	1607.75	1	1607.63	170	10.57
2	215	160	1000	1033	1081.21	0.89	961.07	145	15.09
3	215	160	500	1033	540.6	0.56	300.34	212	70.59
4	100	75	1480	484	751.78	1	751.69	132	17.56
5	100	75	1000	484	506.59	0.89	450.3	148	32.87
6	100	75	500	484	253.29	0.56	140.72	125	89.38
7	50	37	1480	239	370.23	1	370.16	154	41.06
8	50	37	1000	239	250	0.89	222.22	160	72
9	50	37	500	239	125.08	0.56	69.49	61.4	88.5

TABLE 4.7: % Energy recovery during deceleration with change of deceleration rate (fixed initial speed (N_1) 1000rpm to final speed (N_2) 0 rpm)

Sr. No.	Motor HP	Load Torque T_l Nm	Deceleration rate (rpm/s)	Rotational kinetic energy kJ $E = \frac{1}{2}J.\Delta\omega^2$	Recoverable Energy (M*E) KJ (M = 0.89)	$E_{recovery}$ kJ by simulation method	Energy recovery Efficiency η%
1	50	239	450	250.2	222.22	157.45	71
2	50	239	900	250.2	222.22	160	72
3	50	239	1350	250.2	222.22	157.12	71
4	50	239	1800	250.2	222.22	151.39	68
5	50	179	450	187.5	166.9	126	76
6	50	179	900	187.5	166.9	135	81
7	50	179	1350	187.5	166.9	130	78
8	50	179	1800	187.5	166.9	125	75
9	50	120	450	104.67	93.15	77.31	83
10	50	120	900	104.67	93.15	80.1	86
11	50	120	1350	104.67	93.15	77.50	83.2
12	50	120	1800	104.67	93.15	75.45	81
13	50	60	450	62.8	55.89	47.5	85
14	50	60	900	62.8	55.89	48.3	86.5
15	50	60	1350	62.8	55.89	47	84
16	50	60	1800	62.8	55.89	46.6	83.5

4.6 Chapter Conclusion

- In this chapter, simulation results for energy recovery of DTC based Induction motor drive using DC/AC converter are discussed.
- The block diagram is presented for energy fed back to supply grid during deceleration of induction motor. The waveforms of electromagnetic torque, rotor speed, power, stator current etc. are observed and remarkable results of energy recovery during deceleration are observed.
- The power fed back to the grid is calculated theoretically and compared simulation results which are approximately same. The significance of energy multiplying factor (M) is discussed.

- From the results, it can be concluded that the energy recovery depends on load torque, initial speed of starting of deceleration, motor power rating and deceleration rate.
- The energy regeneration of an induction motor is presented in simulation results during deceleration. The overall efficiency of the DTC based induction motor is improved using energy recovery during braking.

In the next chapter, effect of different variables on energy recovery during deceleration for three phase induction motor is discussed.

CHAPTER-5

5 Effect of different variables on energy recovery during deceleration for three phase induction motor

5.1 Introduction

In this chapter, the effect of various variables on energy recovery is analysed with Taguchi method. The aim of this chapter is to understand the most influential variable to optimise the energy recovery efficiency. The variables like load torque, initial speed of starting of deceleration, motor power rating and deceleration rate are considered to analyse their effect on energy recovery.

5.2 Effect of load torque variation on energy recovery during deceleration for three phase induction motor

Simulation results are obtained by varying load torque for 50 HP induction motor which are represented in Fig. 5.1, to inspect the effect of it on energy recovery during deceleration. The power fed to grid during deceleration measured at grid side of DC/AC converter. The load torque is varied in step of 25% of full load as shown in Fig. 5.2. In the Fig. 5.2 regenerative power graph of 25%, 50%, 75%, 100% for 50 HP induction motor is represented. Table 5.1 shows operating condition of the simulation.

TABLE 5.1: Simulation operating condition

Sr. No.	Time (s)	Speed (rpm)	Torque (Nm)
1	0	1000	0
2	0.5	1000 (No Change)	239
3	1	0	239 (No Change)
4	1.5	0	-239

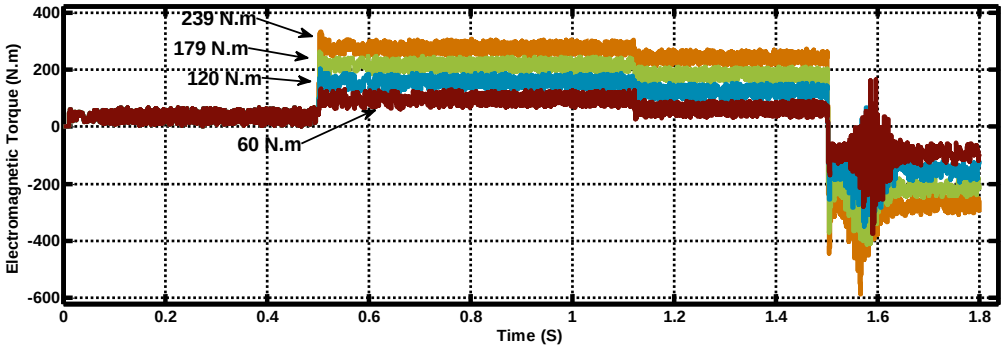

FIGURE 5.1 : Load torque variation for 50 HP induction motor

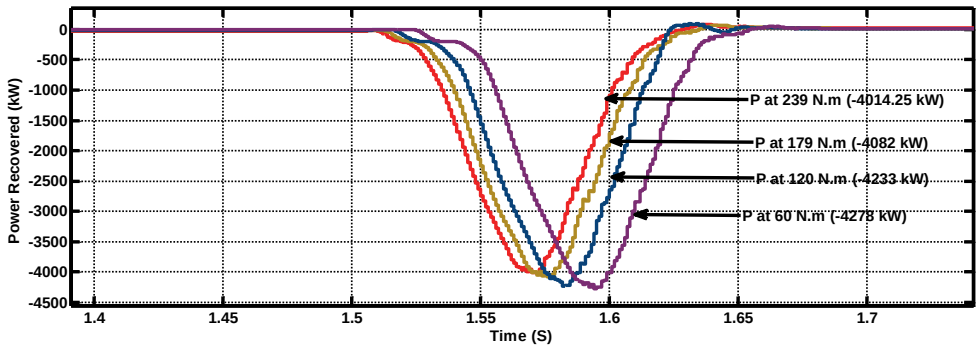

FIGURE 5.2 : Power fed to grid observation with load torque variation for 50 HP induction motor

The Table 5.2 shows percentage energy recovery efficiency for the load torque variation of 50 HP induction motor. During energy recovery cycle, numbers of losses occur during deceleration in the system. Significant energy losses during deceleration occur like mechanical losses, electrical losses and diminishing kinetic energy during deceleration.

TABLE 5.2: Three phase induction motor for kinetic energy recovery during deceleration with load torque variation (deceleration rate = 900 rpm/s)

Sr. No.	Induction Motor Parameter	Initial speed (N_1) rpm	Load Torque T_l Nm	Peak Power during deceleration (kW)	Rotational kinetic energy (E) kJ	Recoverable Energy (M*E) kJ	$E_{recovery}$ (kJ) by simulation	Energy recovery Efficiency η%
1	50 HP, 37 kW, 1480 rpm, 239 Nm, 400 V, 50 Hz, 4 pole,3-phase	1000	239	4014.25	250	222.22	160	72
2		1000	179	4082	187.5	166.87	142	85
3		1000	120	4233	104.67	93.15	80.1	86
4		1000	60	4278	62.8	55.89	50.5	90.3

5.3 Effect of initial speed variation during deceleration on energy recovery for three phase induction motor

As shown in Fig. 5.3, for a 50 HP three phase induction motor deceleration starts from initial speed (N_1) to final speed (N_2).At the end of deceleration period the motor reach to final speed (N_2) which is zero for all the three cases. The energy recovery during deceleration of 50 HP three phase induction motor is observed for different initial speed N1. The deceleration rate is fixed to 900 rpm/s during the simulation. The simulation is performed at fixed load torque of 239 Nm which is full load torque of the motor. The Fig. 5.3 shows 50 HP induction motor simulation results in which the motor have different initial speed like 500 rpm, 1000 rpm and 1480 rpm. In Fig. 5.3, the simulation has been carried out for three different cases, results of which are shown in Fig 5.4. Fig. 5.4 shows regenerative power obtained at different initial speed of deceleration i.e. 500 rpm, 1000rpm and 1480 rpm. The operating condition of simulation results are discussed in Table 5.2. The three phase 50 HP induction motor is started at t = 0 sec with no load, with 900 rpm/s deceleration rate. The full load is applied at t = 1 sec in each case. At t =2.5 s applied torque -239 Nm of torque is applied for braking.

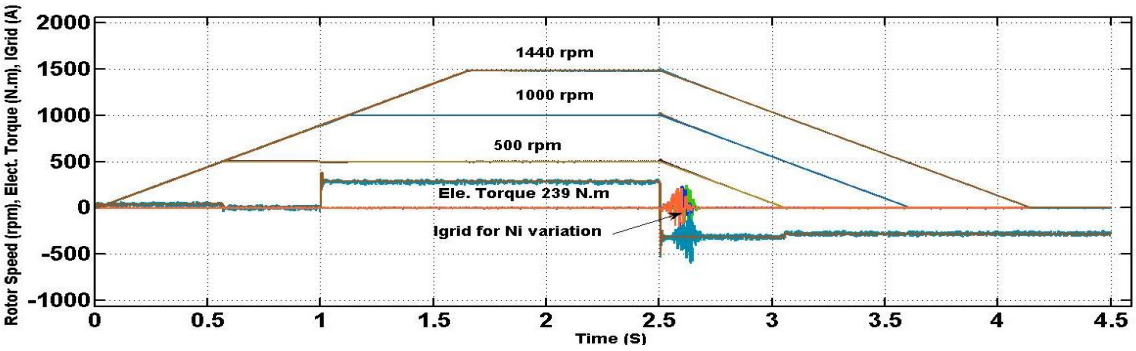

FIGURE 5.3: Grid current observation with initial speed variation for DTC based 50 HP induction motor drive [Fixed Deceleration rate = 900rpm/s and T = 239 Nm]

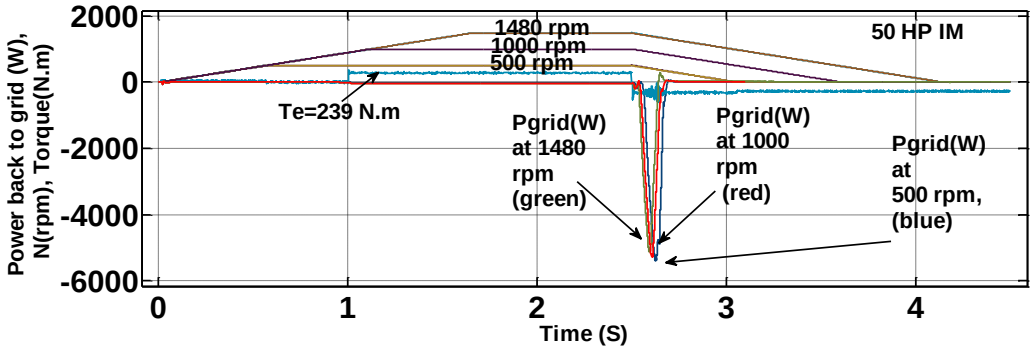

FIGURE 5.4: Power fed to the grid during deceleration from (1) 1480 to 0 rpm (2) 1000 to 0 rpm (3) 500 rpm to 0 rpm, for DTC based 50 HP induction motor drive [Fixed Deceleration rate = 900rpm/s and T = 239 Nm]

TABLE 5.3: Simulation operating condition for initial speed variation

Sr No	Time (sec)	Speed (rpm)	Fixed Acceleration/ Deceleration Rate rpm/sec	Torque applied Nm
1	0	500/1000/1480	900	0
2	1	_	900	239
3	2.5	0	900	-239

From Fig. 5.5, it can be observed that as initial speed increases, the peak of the current found higher and hence I^2R losses are also higher, so energy recovery efficiency decreases. The variation in the initial speed during deceleration, affects energy recovery.

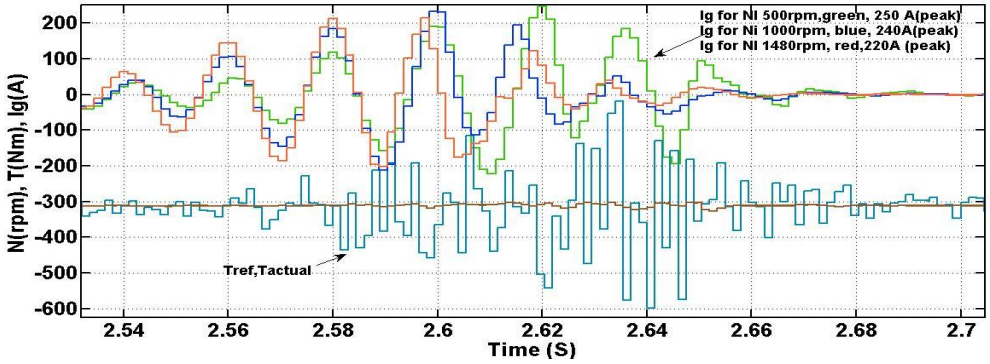

FIGURE 5.5: Grid current variation measured at DC /AC converter during initial speed variation of deceleration in 50 HP induction motor

Table 5.3 represents energy recovery efficiency found during deceleration with for different initial speed. In Table 5.3, the recoverable energy is, $E = M.\left(-\frac{1}{2}.J.\omega^2\right)$, where M is multiplying factor = $\frac{[s_2{}^2 - s_1{}^2]}{2}$, the value of slip s_1 and s_2 are corresponded to initial speed (N_1) and final speed (N_2) respectively.

TABLE 5.4: Kinetic energy recovery of DTC based three phase induction motor drive with initial speed variation during deceleration

Sr. No.	Motor HP	Power kW	Initial speed rpm	Load Torque T_l Nm	Rotational kinetic energy (E) kJ	Energy Multiplier (M)	Recoverable Energy (M*E) kJ	$E_{recovery}$ kJ simulation	Energy recovery Efficiency η%
1	50	37	1480	239	370.23	1	370.16	152	41.06
2	50	37	1000	239	250	0.888	222.22	160	72
3	50	37	500	239	125.08	0.56	69.49	61.5	88.50

5.4 Effect of variation in deceleration rate on energy recovery during deceleration for three phase induction motor

The DTC based three phase induction motor drive for 50 HP motor, has been simulated with different deceleration rate like 450 rpm/s, 900 rpm/s, 1350 rpm/s, 1800 rpm/s, as shown in Fig 5.6. The initial speed of start of deceleration is fixed 1480 rpm. Table 5.4 represents the peak of grid current (Ig_peak (A)) at grid side of the regenerative braking unit during deceleration of three phase 50 HP induction motor at different deceleration rate. If the deceleration rate increases, the mechanical losses decrease and electrical losses

increase. It is possible to find a certain deceleration rate to optimise energy recovery during deceleration of DTC based three phase induction motor drive.

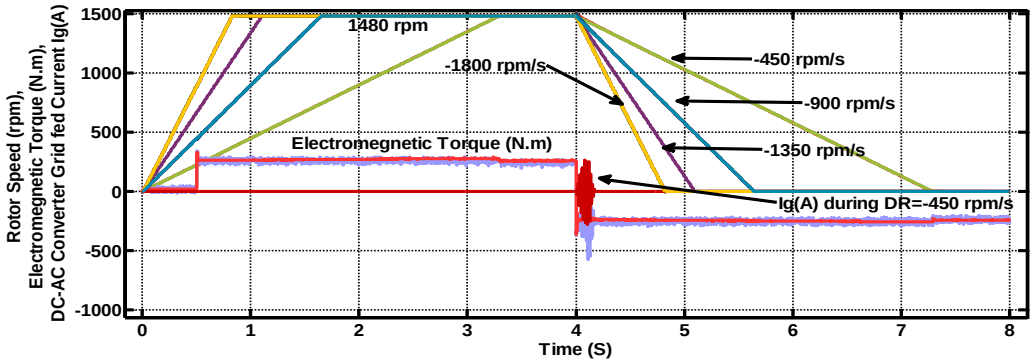

FIGURE 5.6: Rotor Speed (rpm) at different deceleration rate for 50 HP, T = 239 Nm, braking at t = 4 sec

TABLE 5.5: The Peak grid current at DC- AC converter at grid side (Ig_peak (A)) for different deceleration rate

Sr. No.	Deceleration Rate(rpm/s)	Energy Recovery Efficiency % (at full load = 239 Nm)	Ig_peak (A) 179 Nm	Ig_peak (A) at T= 239 Nm	Comments
1	1800	68	173.5	290	Mechanical loss higher, Electrical loss moderate
2	1350	71	195	308	Mechanical loss moderate, Electrical loss higher
3	900	72	179	305	Electrical loss and Mechanical loss comparatively moderate
4	450	71	178	270	Mechanical losses higher, Electrical losses lower

Table 5.5 represents kinetic energy recovery of DTC based three phase induction motor drive at different deceleration rate with fixed full load and fixed initial speed of deceleration 1000 rpm to final speed 0 rpm. Increase in deceleration rate, decreases the mechanical losses and increase electrical losses, hence tradeoffs required to optimise energy recovery during regenerative braking as the percentage energy recovered is a function of deceleration rate.

TABLE 5.6: % Energy recovery during change of deceleration rate for regenerative braking from initial speed N_1= 1000rpm to final speed N_2 = 0 rpm.

Sr. No.	Motor (HP)	T_{ref} (Nm)	deceleration rate (rpm/s)	Rotational kinetic energy (kJ) $E = \frac{1}{2}J.\Delta\omega^2$	Recoverable Energy (M*E) KJ (M= 0.89)	$E_{recovery}$ (kJ) by simulation method	% recovered energy
1	50	239	450	250.15	222.64	157.45	71
2	50	239	900	250.15	222.64	160	72
3	50	239	1350	250.15	222.64	157.12	71
4	50	239	1800	250.15	222.64	151.39	68

5.5 Energy recovery efficiency and energy losses

Fig. 5.7, Fig. 5.8 and Fig. 5.9 represents percentage recovered energy for different load torque variation, different initial speed (N_1), different deceleration rate respectively. Energy recovery efficiency depends upon number of losses during deceleration.

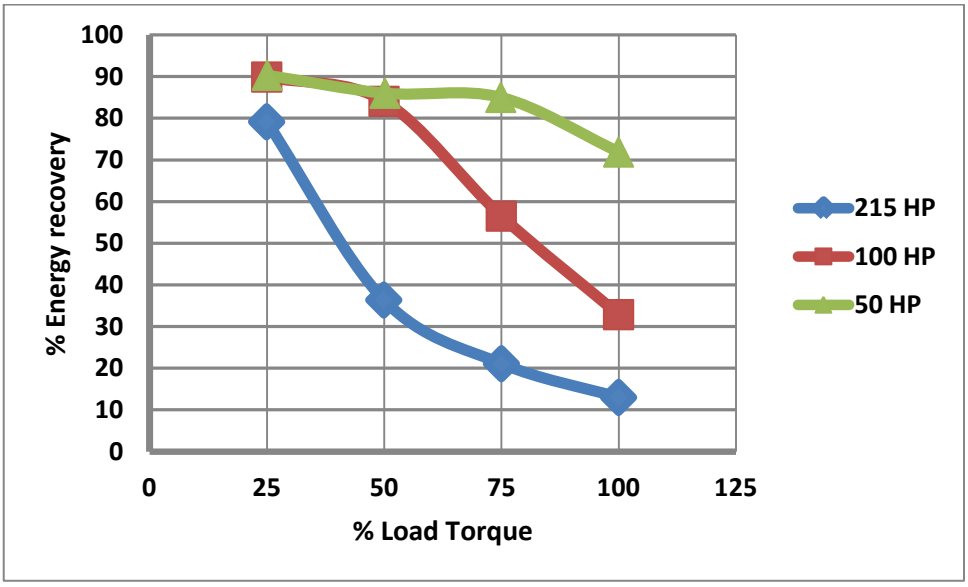

FIGURE 5.7: % Energy recovery vs % load torque for DTC based three phase induction motor drive

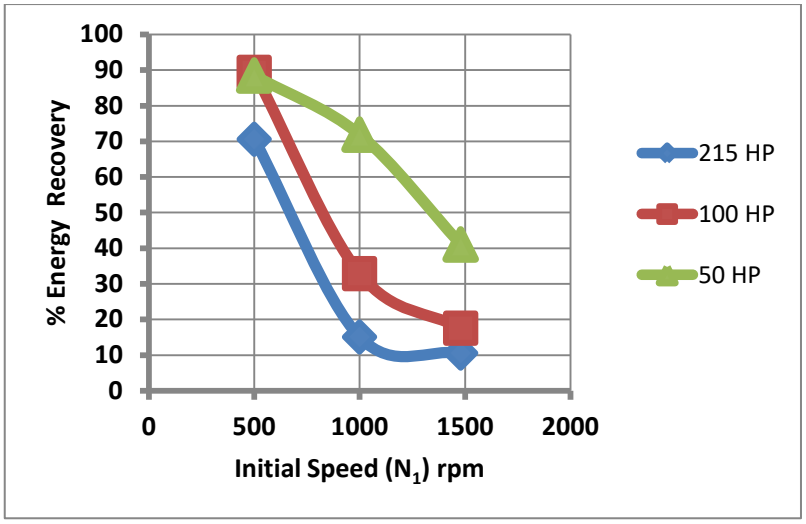

FIGURE 5.8: % Energy recovery with respect to initial speed (rpm) during deceleration for DTC based three phase induction motor drive

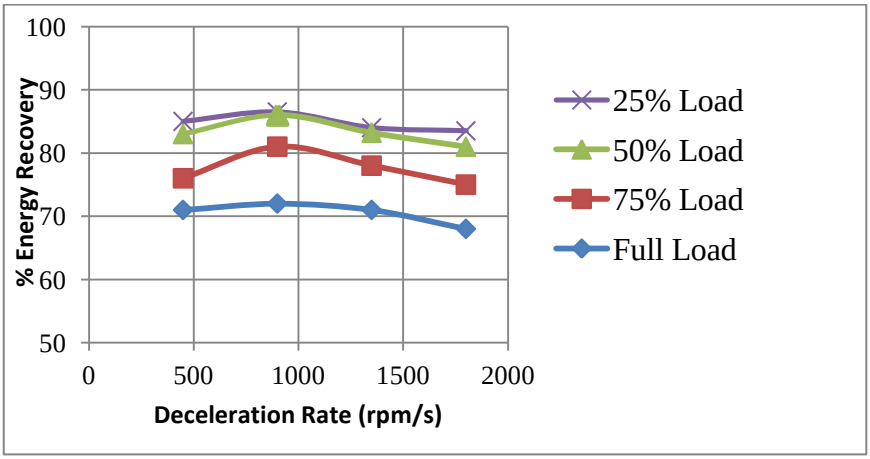

FIGURE 5.9 : % Energy recovery with respect to deceleration rate (rpm/s) for DTC based three phase Induction Motor (50 HP) Drive

5.5.1 Induction Motor losses during deceleration

Energy recovery efficiency depends upon different types of losses during deceleration. Significant energy losses during deceleration occur, like mechanical losses, electrical losses and present kinetic energy losses. Fig. 5.10 represents different losses which are affecting energy recovery efficiency. During the braking period, the motor voltage decreases linearly both in magnitude and frequency. Motor current needs to be estimated. Hence, losses cannot be calculated directly by standard equations applicable at steady state operation.

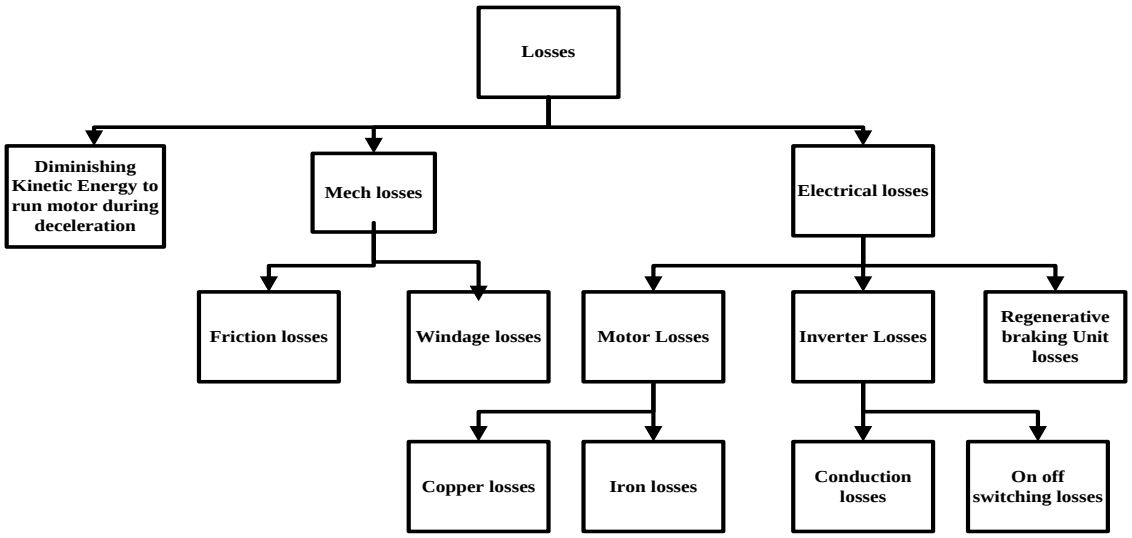

FIGURE 5.10: Different losses during deceleration of the induction motor drive

The total kinetic energy available during deceleration can be given by

$$E = \frac{1}{2} J.\Delta\omega^2 \tag{5.1}$$

The J is total moment of inertia of the system and Δω is the difference of final and initial value of rotor speed. The recoverable energy ($E_{recovery}$) is found after subtracted losses of motor, inverter, converter and consumed kinetic energy during deceleration (E_{ked}).

$$E_{recovery} = \frac{1}{2} J.\Delta\omega^2 - E_{motor\ (elect\ +mech)\ loss} - E_{inv\ loss} - E_{conv\ loss} - E_{ked} \tag{5.2}$$

The recoverable energy ($E_{recovery}$) equation is given in (5.2), The motor electrical losses are the total of copper losses and the iron losses of the motor during the deceleration time. The motor mechanical losses are friction and windage losses of the motor. Further,

$$T_e - T_l - T_{fr} = J\frac{d\omega}{dt} \tag{5.3}$$

The friction torque always reduces speed of the motor. Friction occurs between the interactions of an object and a surface, which depends on the characteristics of both the surfaces. Air friction is a type of frictional force, in which the interaction of a solid body moving through the air as a frictional interaction. Windage losses can be given by (5.4).

$$\text{Windage losses} = \pi.C_d.\rho.R^4\omega^3.L \tag{5.4}$$

where C_d is skin friction coefficient, ρ is medium density, R is a radius, ω is the angular velocity, and L is cylinder length of the motor [80].

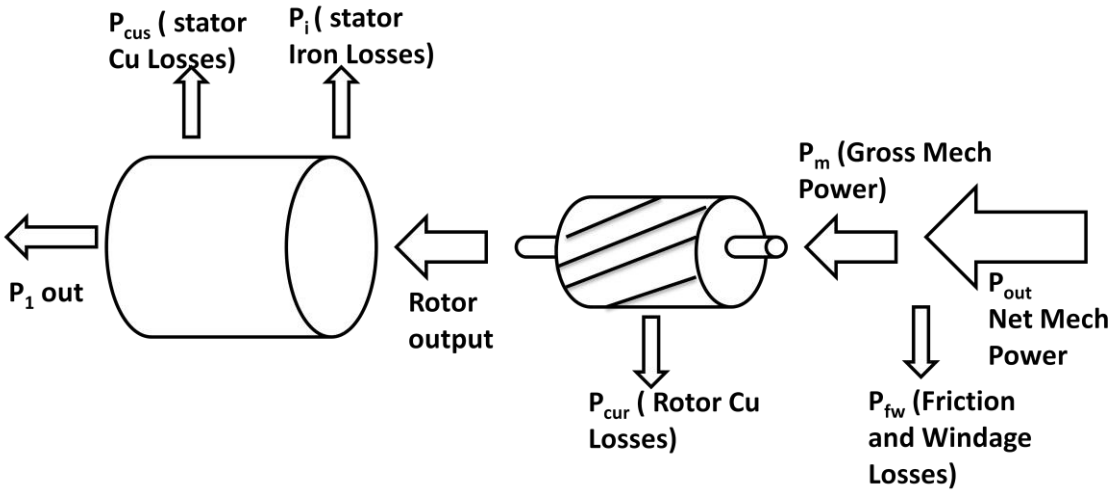

FIGURE 5.11: Motor losses during energy recovery

5.5.2 Inverter and converter losses

Inverter and converter have mainly switching losses and conduction losses. The current flowing through the converter during deceleration time determines these losses. The conduction losses depend on load. The switching loss for the diode is constant. However, the switching losses in the switch, are load dependent with respect to the voltage and current.

5.5.3 Loss modelling in the switch

The conduction loss (P_{cond}) and the switching loss (P_{sw}) of the MOSFET or IGBT switches are given below [81].

$$P_{swt} = P_{cond} + P_{sw} \tag{5.5}$$

$$P_{cond} = I_{sw,avg}.V_{CE} + I_{sw,rms}^2 R_{CEon} \tag{5.6}$$

Where,

P_{swt} = total switching losses

P_{cond} = conduction losses of the MOSFET or IGBT switch

P_{sw}= switching losses of the MOSFET or IGBT switch

$I_{sw,rms}$= switch RMS current

R_{CEon}= switch on-state resistance

V_{CE} = constant voltage drop of the switch

$I_{sw,avg}$ = switch average current

Assuming pulse width modulation (PWM) type controller strategy in the inverter. For the three phase inverter, the conduction losses can be calculated as in (5.7).

$$\mathrm{P}_{condsw} = (\frac{1}{8} + \frac{M}{3\pi}\cos\emptyset R_{CEon} I_{sw}^2 (\frac{1}{2\pi} + \frac{M}{8}\cos\emptyset) V_{CE} I_{sw} \quad (5.7)$$

Where,

M = Modulation index

cosØ = Power factor

I_{sw} = Switch current

P_{condsw} = switch conduction losses

The average switching losses in the switch can be calculated as in (5.8)

$$\mathrm{P}_{sw} = \frac{V_{sw} I_{sw}}{2} f_{sw} (t_{onsw} + t_{offsw}) \quad (5.8)$$

Where,

V_{sw} = switch Voltage

I_{sw} = the stator current of the motor

t_{onsw} = turn on rise time

t_{offsw} = Turn off fall time

f_{sw} = switching frequency

5.5.4 Loss modelling of anti-parallel diode

The duty cycle of the anti-parallel diode is different from the duty cycle of the switch since when the switch is off in a lagging circuit, the flow of current in diode is positive until the current reaches zero and consequently the diode will be still on even when the switch is off. The conduction loss in diode, $P_{D,cond}$ can be calculated as in (5.9) [81].

$$P_{D,cond} = (\frac{1}{8} - \frac{M}{3\pi}\cos\emptyset R_{Don} I_D^2 (\frac{1}{2\pi} - \frac{M}{8}\cos\emptyset) V_D I_D \quad (5.9)$$

Where,

R_{Don} = diode on state resistance

V_D = Diode Voltage

I_D = Diode current

Besides the conduction loss, the prominent component in diode switching losses is the reverse recovery losses while the other components in diode switching losses are quiet small and negligible [18]. The switching losses of the anti-parallel diode, P_{swD}, can be calculated as in (5.10).

$$P_{swD} = \frac{f_{sw} V_R}{2S} \left(\frac{dI_f}{dt}\right) (\frac{S.t_{rr}}{S+1}) \quad (5.10)$$

Where,

V_R = the RMS reverse voltage (V)

S = the snappiness factor, (assumed 0.6)

$\frac{dI_f}{dt}$ = the rate of fall forward current (A/s)

t_{rr} = the reverse recovery time (s)

Finally, the total inverter losses can be calculated by multiplying the total losses in one switch and one diode by a factor of six in a typical three phase bridge inverter drive.

5.6 Approach to Design of Experiments (DOE):

The motivation towards design of experiments (DOE) is for identifying the effect of different variables on energy recovery using Taguchi method. Hence, to determine the parameter which are most influential on the response. To identifying the effect of inputs and its levels for best/desired output.

5.6.1 Identification of most significant variable on energy recovery using Taguchi method

Energy recovery mainly depends on four variables load torque, initial speed of starting of deceleration, motor power rating and deceleration rate. Taguchi method used to identify most significant variable affecting energy recovery. The Taguchi method [82], [83] is a structured approach for determining the best combination of inputs to get optimum output. The input variables are load torque, initial speed at starting of deceleration, motor power rating and deceleration rate defined, and the output is recoverable energy efficiency in DTC drive during regeneration.

It is essential to separate out the individual effect of the variables. The standard L_9 arrays insist on the way of conducting the minimal number of experiments which could give the full information of all the factors that affect the performance parameter. The influence of 4 different independent variables with each variable need to be explored. By conducting the sensitivity analysis, and performing analysis of variance (ANOVA), one can decide which independent factor dominates over other and the percentage contribution of that particular independent variable.

TABLE 5.7: Variables table for the Taguchi method

Sr. No	Motor Size (HP)	Deceleration Rate (DR)	Load Torque %	Initial Speed (Ni)
1	50	450	25	500
2	100	900	50	1000
3	215	1350	100	1480

The 3 levels 4 variable (L_9) table approach to understand the most influential variables to optimise the energy recovery efficiency is discussed. The 3 levels 4 variable has 81 test required but due to the Taguchi L_9 table only 9 test results required. The Taguchi method is an excellent tool that assists to know the effect of various variables on energy recovery [84]. It is possible to select suitable variables, as shown in Table 5.7, which indicates variables and their levels in the energy recovery, which contains 4 variables, and each variable has 3 levels of variation. The Table 5.8 shows the form of orthogonal array to obtain data from experiments run. For example, According to first run for experiment shown in Table 5.8 that all the four variable have level one as define in Table 5.8 and find the output for the experiment. The Table 5.9 is L_9-orthogonal array [85] for the four defined variables along with results.

TABLE 5.8: L_9-Orthogonal Array [82]

Experiment Run	**Variable Columns**			
	1	**2**	**3**	**4**
1	1	1	1	1
2	1	2	2	2
3	1	3	3	3
4	2	1	2	3
5	2	2	3	1
6	2	3	1	2
7	3	1	3	2
8	3	2	1	3
9	3	3	2	1

TABLE 5.9: L_9-Orthogonal array as per Taguchi method

Variable Columns and Results				
1	**2**	**3**	**4**	**Results**
Motor Size (HP)	**Initial Speed (Ni) during deceleration**	**% Load Torque**	**Deceleration Rate (DR)**	**Recoverable Energy Efficiency %**
50	500	25	450	89.5
50	1000	50	900	88.56
50	1480	100	1350	50.33
100	500	50	1350	83.66
100	1000	100	450	45
100	1480	25	900	82
215	500	100	900	70.59
215	1000	25	1350	57.33
215	1480	50	450	60.33

In Taguchi method, the term signal represents the desired value, and noise represents the undesirable value. Process variables with the highest signal to noise (S/N) ratio always give the best variables with minimum variance. For S/N ratio of each variable, level is calculated by finding the average of S/N ratios at the corresponding level. The variable Table 5.10 shows S/N ratio of energy recovery obtained for different levels of variables. The Table 5.11 represents response table for means of % energy recovery efficiency obtained for different variable levels. Taguchi proposed formula for calculating S/N ratio is

$$SN_i = -10\ log_{10}(MSD) \tag{5.11}$$

Where, MSD = mean square deviation, Means = average of deviation values. For recovery efficiency always larger is better, hence

$$MSD = \frac{1}{n}\sum_{i=1}^{n}\frac{1}{Y^2{}_i} \tag{5.12}$$

Where, Y_i = Experimental value , n = no. of observations

$$\Delta = Max - Min \tag{5.13}$$

The rank can be found from the delta (Δ) value. Higher the delta value, lower the rank. From the Table 5.10 and Table 5.11 by observing the rank, it shows that the load torque is the most significant variable for energy recovery efficiency response followed by deceleration rate (rpm/s), initial speed at starting of deceleration, motor power rating (HP) respectively.

TABLE 5.10: Response Table for Signal to Noise Ratios (Option: Larger is better)

Level	HP	NI	LOAD	DR
1	37.42	38.23	37.92	35.98
2	36.95	35.73	37.67	38.42
3	35.92	36.32	34.69	35.88
Delta	1.50	2.51	3.23	2.53
Rank	**4**	**3**	**1**	**2**

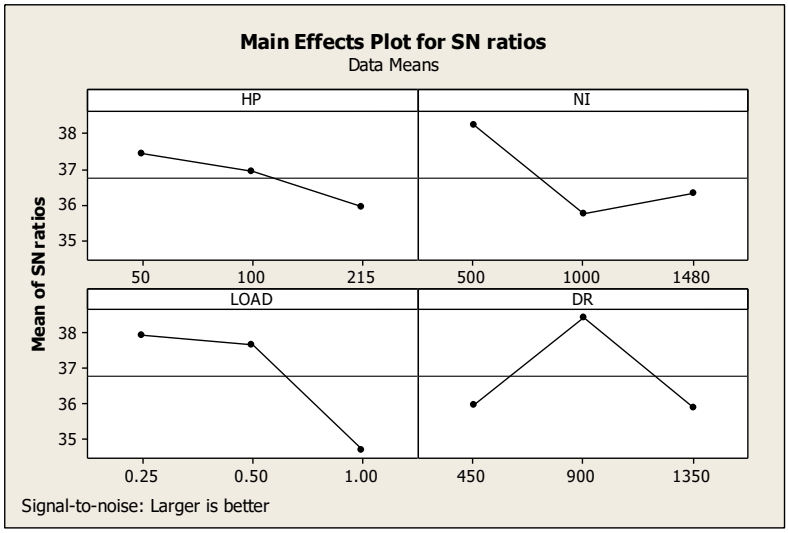

FIGURE 5.12: Main Effect plot for SN ratios

TABLE 5.11: Response Table for Means

Level	HP	NI	LOAD	DR
1	76.96	82.08	80.63	65.78
2	73.74	63.63	77.52	83.90
3	62.75	67.74	55.31	63.77
Delta	14.21	18.45	25.32	20.13
Rank	**4**	**3**	**1**	**2**

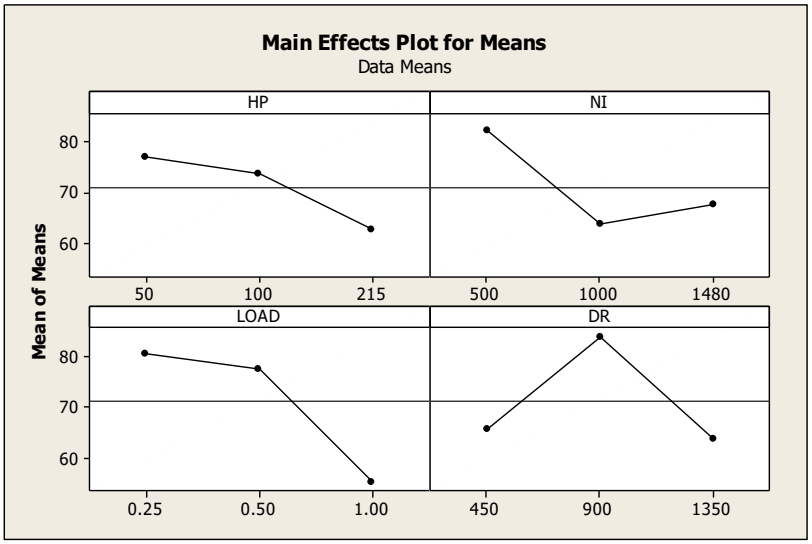

FIGURE 5.13: Main effects plot for means

As per the Rank given by MINITAB software, load torque is most significant factor for energy recovery efficiency response and then deceleration rate (rpm/s), initial speed, motor power rating (HP) respectively.

Regression Equation:

From Main effects plot, relation of energy recovery efficiency (Eff.) versus motor power rating (HP), initial speed (NI), load torque (LOAD) and deceleration rate (DR) is given below.

$$\text{Eff.} = 119 - 0.0878\ \text{HP} - 0.0148\ \text{NI} - 35.3\ \text{LOAD} - 0.0022\ \text{DR} \qquad (5.14)$$

Linear regression is allowed to predict the outcome with a relatively small amount of error. Above regression equation find approximate energy recovery efficiency for a given variable value. The predicated output may vary up to 5% using this equation. It determines relationship between input variable to output with small amount of error. It is more useful to predict energy recovery efficiency in relation with load, initial speed of deceleration, deceleration rate variation and motor power rating.

5.7 Chapter Conclusion

- In this chapter, the effects of different variables on energy recovery are explained and most significant variable affect to energy recovery efficiency among the four variables are observed.
- The influence of different factor on the losses and hence energy recovery efficiency is analysed using the Taguchi approach.
- The improvement of recovery energy efficiency during deceleration of DTC induction motor drive by finding important parameter influences on it.
- Effect of load torque, initial speed of starting of deceleration, motor power rating and deceleration rate variation on energy recovery is graphically demonstrated and analysed.
- Load torque has the greatest impact on energy recovery performance, followed by deceleration rate (rpm/s), initial speed, and motor power rating in decreasing order.

In the next chapter, analysis of torque ripple reduction of direct torque control method for induction motor drive is discussed.

CHAPTER-6

6 Analysis of torque ripple reduction of Direct Torque Control method for induction motor drive

6.1 Introduction

In this chapter, different strategies related to torque ripple reduction, especially fuzzy logic controller based DTC and carrier space vector PWM (CSVPWM) DTC are discussed. Torque ripple is produced in three phase motor by air gap flux at one frequency interacting with rotor MMF at a different frequency. The general torque expression as a function of air-gap flux, rotor current, and the phase angle (δ) between the air-gap flux (Ψ_{rm}) and rotor current (i_{1r}).

$$\tau = K\Psi_{rm}.\, i_{1r}.\, \sin\delta \qquad (6.1)$$

where, K is torque constant. The interaction of fundamental flux with the fifth and seventh harmonics currents result in 6^{th} harmonic torque and vice versa.

Sixth harmonic torque can be given as

$$\tau_{6r} = K\Psi_{1m}(I_{7_r} - I_{5r})\sin 6\omega_e t \qquad (6.2)$$

The 6^{th} harmonic torque tend to cause jitter in machine speed. This pulsating torque effect is negligible due to filtering effect of the rotor inertia. Assume pure inertia load, the speed jitter at 6^{th} harmonic torque can be given as

$$\omega_m = \frac{\tau_m}{J6\omega_e} cos 6\omega_e t \qquad (6.3)$$

As (6.3) shows that at higher harmonic frequency and higher inertia (J), the speed jitter to be attenuated. At very low frequency operation of low inertia motor, torque ripples are

dominant. According to (6.3), 50 HP induction motor have rotor inertia (J) comparatively higher than the 5.4 HP induction motor, so 50 HP induction motor has quite low torque ripple. Hence, to understand torque ripple analysis, 5.4 HP three phase induction motor is used for simulation for FLC based DTC and CSVPWM method. The percentage torque ripple can be calculated as (6.4).

$$\%\text{Torque Ripple} = \%\text{TR} = \frac{\text{T}_{\text{emax}} - \text{T}_{\text{emin}}}{\text{T}_{eaverage}} X100\% \tag{6.4}$$

The high frequency pulsating torque component is induced due to PWM control of inverter that produces a ripple current in the phases. To observe the torque ripple in 1 HP induction motor using DTC strategy, laboratory test taken and hardware results obtained as discussed in next section 6.2.

6.2 Torque ripple observation of Direct Torque Control method for induction motor

Hardware results of torque ripple for 1 HP, 415 V, 4 pole, 50 Hz, 3-phase induction motor are observed. The DTC control algorithm is implemented by ARM CORTEX M4 STM32F407VGT6 32-bit microcontroller. The microcontroller generates the digital control signal via PWM outputs. Hall effect sensors measure current and voltage at induction motor terminals. The speed is measured by the proximity sensor to compare reference speed with the actual.

Typical torque response of a DTC drive is shown in Fig. 6.1. It illustrates the hardware results of rotor speed (upper trace) and electromagnetic torque (lower trace). The Torque ripple = 24% observed from Fig. 6.1. The load torque change shown at 10 sec, 25 sec. Fig. 6.2 shows a low-speed operation at which significant torque ripple found.

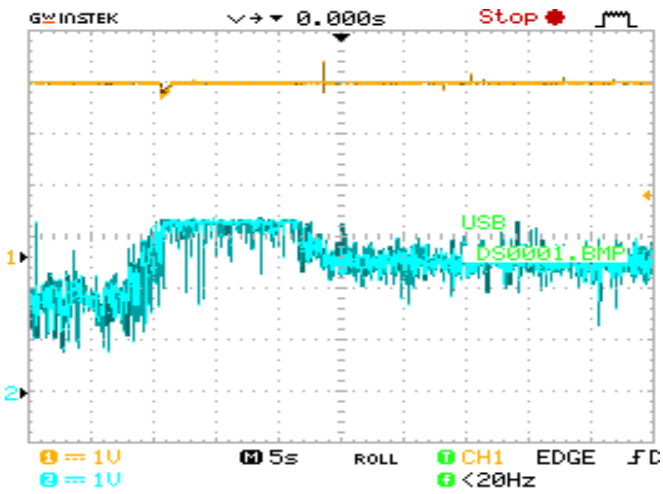

FIGURE 6.1: Speed (1440 rpm) and electromagnetic torque plot with respect to time (Time(s)/div = 5, volt/div = 1, Speed 1440 rpm = 3.3V, Torque 1 Nm/ div, Torque ripple = 24%)

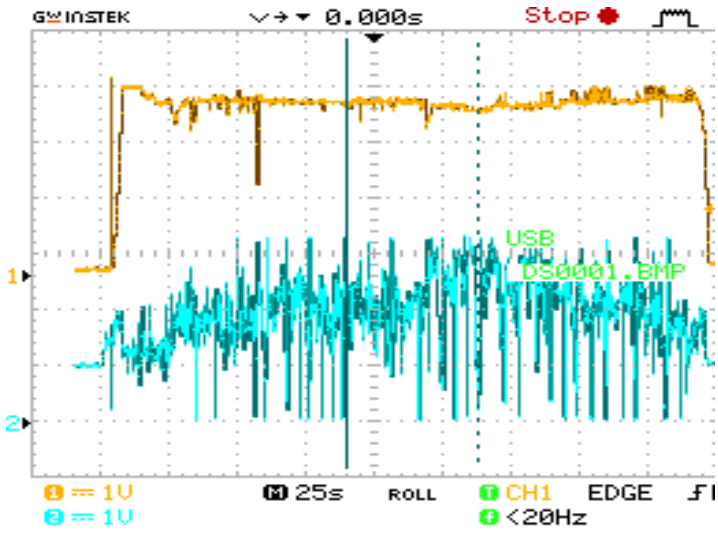

FIGURE 6.2: Low speed operation (150 rpm) with electromagnetic torque pulsation observation (Time/div = 25 sec, volt/div = 1 v, Speed 150 rpm = 3.3V, Torque 1 Nm/Div)

During low speed operation, the torque ripples are dominant. It is necessary to reduce it. In next section, Fuzzy logic controller based DTC and CSVPWM based DTC are discussed.

6.3 Fuzzy logic controller based Direct Torque control Technique

The fuzzy inference System editor of MATLAB^{TM} is used to set input & output variables. It is also used to choose fuzzification and defuzzification methods. Mamdani method for fuzzification and centre of area method for defuzzification are used. Fuzzy logic controller

implemented for speed control for DTC induction motor drive is shown in Fig. 6.3. The fuzzy logic controller block replaces the PI controller of the outer loop and hence problem related to PI controller tuning can be eliminated. The fuzzy logic controller determines the amplitude of reference torque. It is shown that the proposed scheme results in improved stator flux and torque responses under steady-state condition. The main advantage is the reduction of torque and flux ripple during the low-speed. Fig. 6.3 represents the block diagram of fuzzy logic controller based DTC. The Fuzzy logic controller based DTC scheme has been simulated in MATLAB^{TM} /SIMULINK^{TM}.

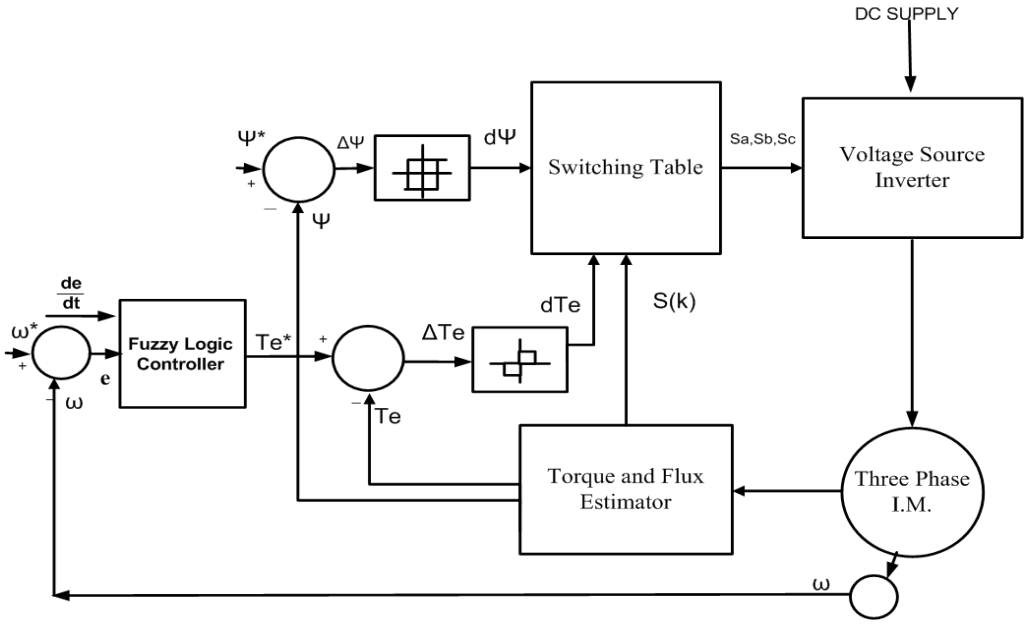

FIGURE 6.3: Block diagram of Fuzzy Logic Controller based DTC

The fuzzy logic controller is generally characterized as follows:

1) Two variable input E and CE and one output u.
2) Seven fuzzy sets for each input and output variables,
3) Fuzzification of inputs using a continuous universe of discourse.
4) Apply fuzzy operator like AND min method and OR max method.
5) Apply Implication method using Mamdani's min operator.
6) Apply the aggregation method for the output values for different condition and occasion.
7) Defuzzify output value using the Centroid method.

The MATLAB^{TM} Fuzzy Interface System (FIS) editor shown in Fig. 6.4 is used to set input & output variables. It is also used to choose fuzzification & defuzzification methods. The five triangular & two trapezoidal membership functions used for the

input variables are exposed in Table 6.1.

TABLE 6.1: Details of input membership functions

Membership Functions	Type	Range
PB (Positive Big)	Trapezoidal	[0.5 1 1 100]
PM (Positive Medium)	Triangular	[0.2 0.5 1]
PS (Positive Small)	Triangular	[0 0.2 0.5]
Z (Zero)	Triangular	[-0.2 0 0.2]
NS (Negative Small)	Triangular	[-0.5 -0.2 0]
NM (Negative Medium)	Triangular	[-1 -0.5 -0.2]
NB (Negative Big)	Trapezoidal	[-100 -1 -1 -0.5]

Fig. 6.4 illustrates the FIS editor toolbox to create MFs for input variables.

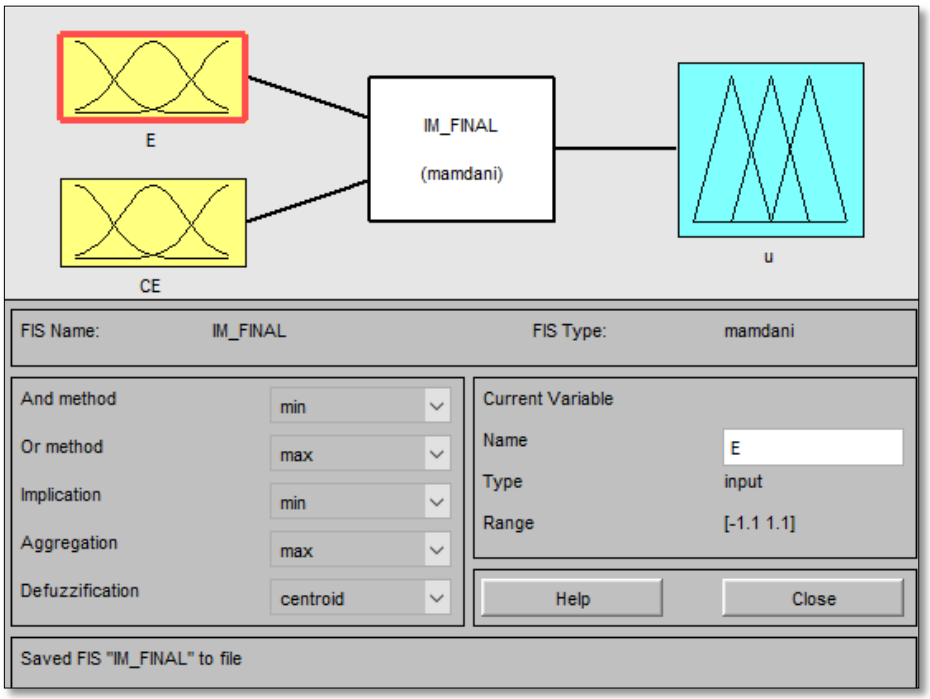

FIGURE 6.4: Membership Functions (MFs) for Inputs to FIS

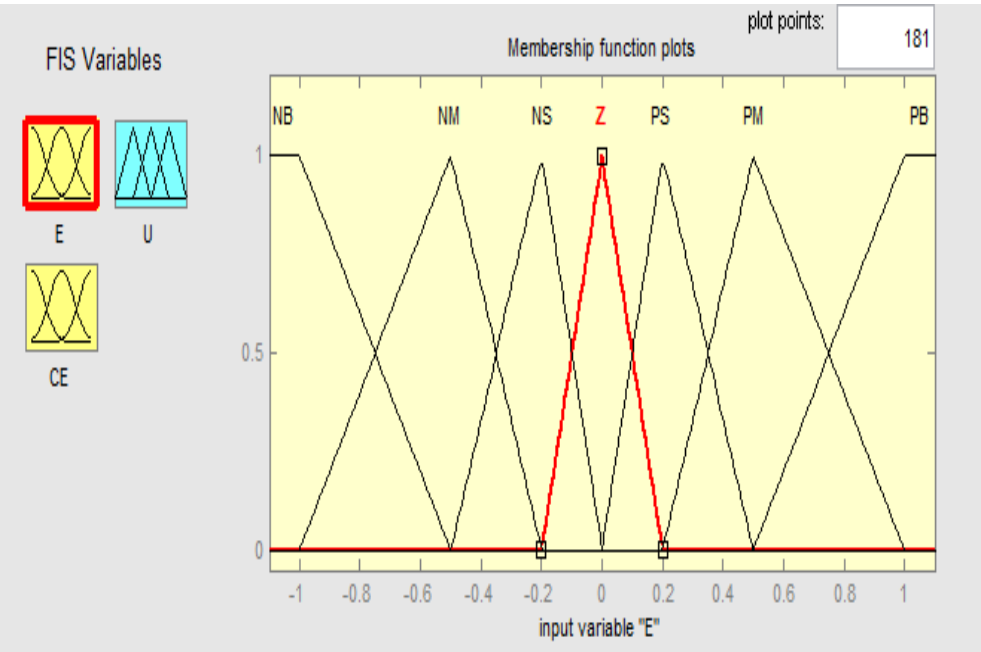

FIGURE 6.5: Membership functions in FIS editor

Seven triangular & two trapezoidal MF have been taken for output u (pu) which are as revealed in Table 2.

TABLE 6.2: Output (u) membership functions

Membership Functions	Type	Range
PB (Positive Big)	Trapezoidal	[0.6 1 1 100]
PM (Positive Medium)	Triangular	[0.3 0.6 1]
PS (Positive Small)	Triangular	[0.1 0.3 0.6]
PVS (Positive Very Small)	Triangular	[0 0.1 0.3]
Z (Zero)	Triangular	[-0.1 0 0.1]
NVS (Negative Very Small)	Triangular	[-0.3 -0.1 0]
NS (Negative Small)	Triangular	[-0.6 -0.3 -0.1]
NM (Negative Medium)	Triangular	[-1 -0.6 -0.3]
NB (Negative Big)	Trapezoidal	[-100 -1 -1 -0.6]

The rules for the fuzzy control are set using Fuzzy Rule Editor, as demonstrated in Table 6.3. Fuzzy rules are relations between input and output fuzzy sets. A FLC converts a linguistic control strategy into an automatic control strategy and fuzzy rules are constructed by expert knowledge or experience database. Firstly, the input speed error (E)

and the change in speed error (CE) have been used as the input variables of the FLC. The output variable (u) converted its numerical value in to linguistic variables by seven fuzzy sets are chosen as in Table 6.2.The rule base matrix for FLC is shown in Table 6.3.

TABLE 6.3: Rule Matrix for Fuzzy Logic Controller

CE \ E	NB	NM	NS	Z	PS	PM	PB
NB	NB	NB	NB	NM	NS	NVS	Z
NM	NB	NB	NM	NS	NVS	Z	PVS
NS	NB	NM	NS	NVS	Z	PVS	PS
Z	NM	NS	NVS	Z	PVS	PS	PM
PS	NS	NVS	Z	PVS	PS	PM	PB
PM	NVS	Z	PVS	PS	PM	PB	PB
PB	Z	PVS	PS	PM	PB	PB	PB

The output surface of the FIS can be visualized by surface viewer available in FIS toolbox. The input variable (E, CE) & output variable (u) along with fuzzy speed control is designed as depicted in Fig. 6.7. The output of the controller is used as a torque reference.

Implementing Fuzzy Logic Control in MATLAB™/ Simulink™ Model:

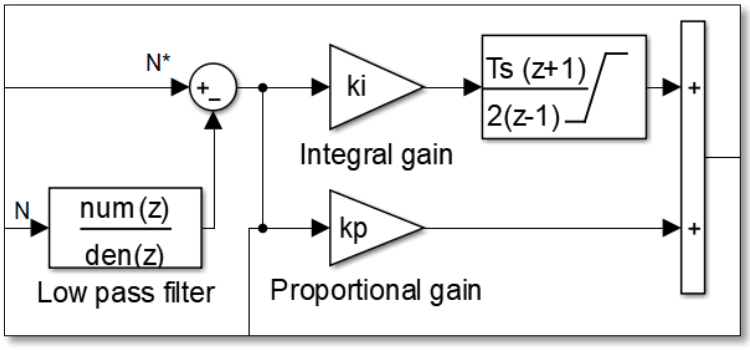

FIGURE 6.6: Conventional PI controller

Fig. 6.6 shows the conventional PI controller implemented for speed control is compared by implementing a fuzzy logic controller, as demonstrated in Fig. 6.7.

The algorithm for fuzzy speed controller can be summarized as the following steps.

(1) Sample the actual speed (ω) and Reference speed (ω*).

(2) Calculate speed error E & change in error CE as follows:

$$E(t) = \omega^* - \omega \quad (6.4)$$

$$CE(t) = E(t) - E(t-1) \quad (6.5)$$

(3) Find per unit or normalised value of error E(t). The error E(t) & change in error CE(t) can be normalised by dividing them with reference base.

(4) Calculate the degree of membership of E (pu) & CE (pu) for relevant fuzzy sets.

(5) Recognize stringent rules & calculate the degree of fulfilment (DOF) of each rule.

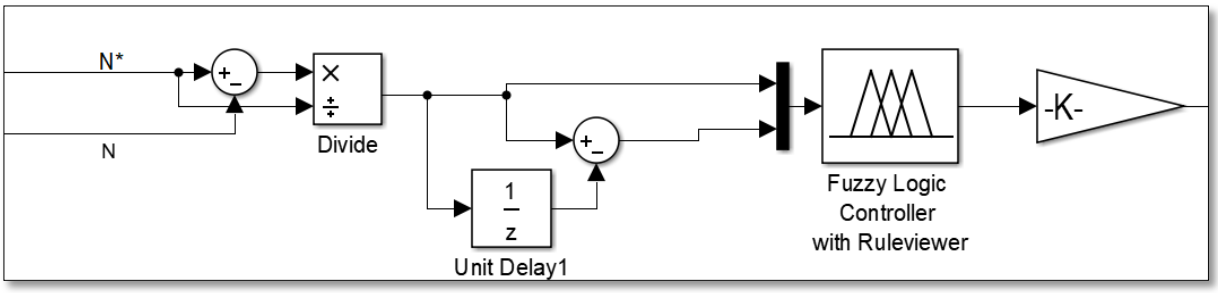

FIGURE 6.7: Fuzzy Logic controller implemented in place of PI controller for speed control

Fuzzy logic controller determinates the desired amplitude of reference torque. It is shown that the proposed scheme results in improved stator flux and torque responses under steady-state condition. The main advantage is the improvement of torque and flux ripple characteristics at the low-speed region.

6.4 Simulation Results of FLC based DTC induction motor drive

Fig. 6.8 shows speed response for conventional DTC. It can be seen in the Fig. 6.9 below that in fuzzy logic control based DTC induction motor drive, there is no overshoot of speed during transient condition as in case of DTC. At very low frequency operation of low inertia motor, torque ripples are dominant. According to (6.3), 50 HP induction motor have rotor inertia (J) comparatively higher than the 5.4 HP induction motor, so it has not significant torque ripple. To understand low speed operation torque ripple problem, here 5.4 HP three phase induction motor is used for simulation.

TABLE 6.4: Parameters of 5.4 HP Induction Motor

Parameters	Ratings
Rated Power	5.4 HP/ 4 kW
Rated Voltage	400 V
Rated Speed	1440 RPM
Pole pairs	2
Stator resistance	1.4 Ω
Stator leakage inductance	5.83 mH
Rotor leakage inductance	5.83 mH
Air gap inductance	0.1722 H
Rotor time Constant(J)	0.00131 kg.m^2
Friction factor(F)	0.002985 Nm.s

TABLE 6.5: Operating condition for 5.4 HP/ 4 kW, 1440 rpm 400 V Induction motor drive

Time (s)	Torque Nm	Speed rpm
0	20	1000
5	27	1000
7	27	1400

The induction motor parameters are given in Table 6.4. The operating condition of 5.4 HP induction motor are given in Table 6.5. The reference speed of motor is changed to 1000 rpm at time t = 0 sec and 1400 rpm at t = 7 sec. From starting at t = 0 sec, the reference torque of 20 Nm is applied. At t = 5 sec, load torque increase to 27 Nm.

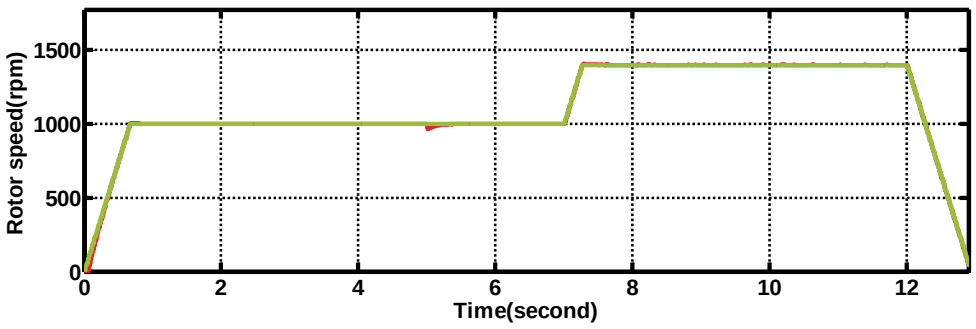

FIGURE 6.8 : Speed response of conventional DTC

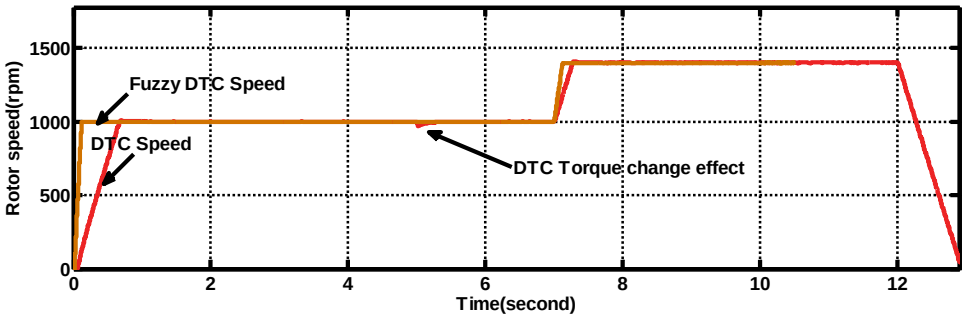

FIGURE 6.9: Rotor speed response comparison of conventional DTC and FLC based DTC

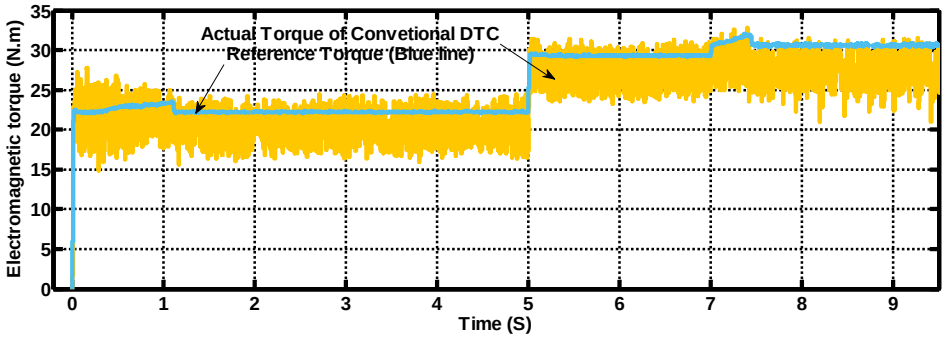

FIGURE 6.10 Torque response of DTC using conventional DTC

The speed change response of Fuzzy DTC is quicker than the conventional DTC. As shown in Fig. 6.8. no more overshoot/undershoot or fluctuation observed in speed due to load change. Fig. 6.9 shows a comparison of DTC and Fuzzy logic controller based DTC for speed response for 5.4 HP induction Motor. Fig. 6.10 shows a conventional DTC torque ripple for 5.4 HP induction Motor. Fig. 6.11 shows a zoom view of conventional DTC torque ripple for 5.4 HP induction motor. Fig. 6.12 shows a comparison of DTC and Fuzzy logic controller based DTC for torque ripple for 5.4 HP induction Motor.

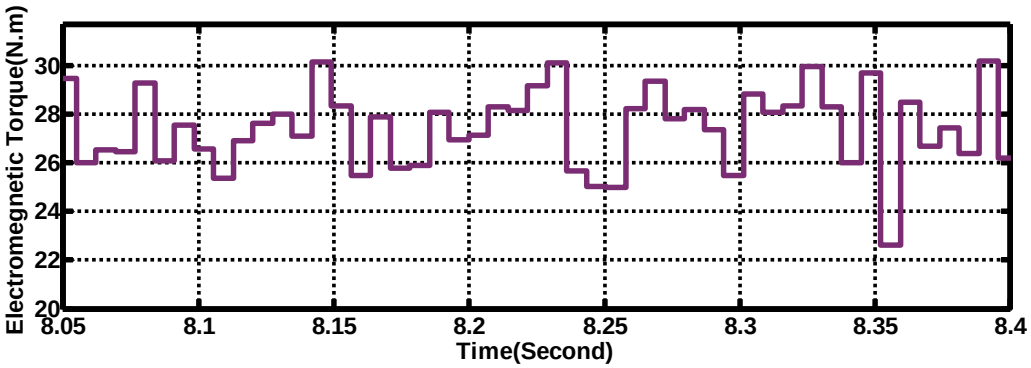

FIGURE 6.11 DTC torque ripple (zoom view) is 6 Nm for 27 Nm applied load (T.R. = 22%)

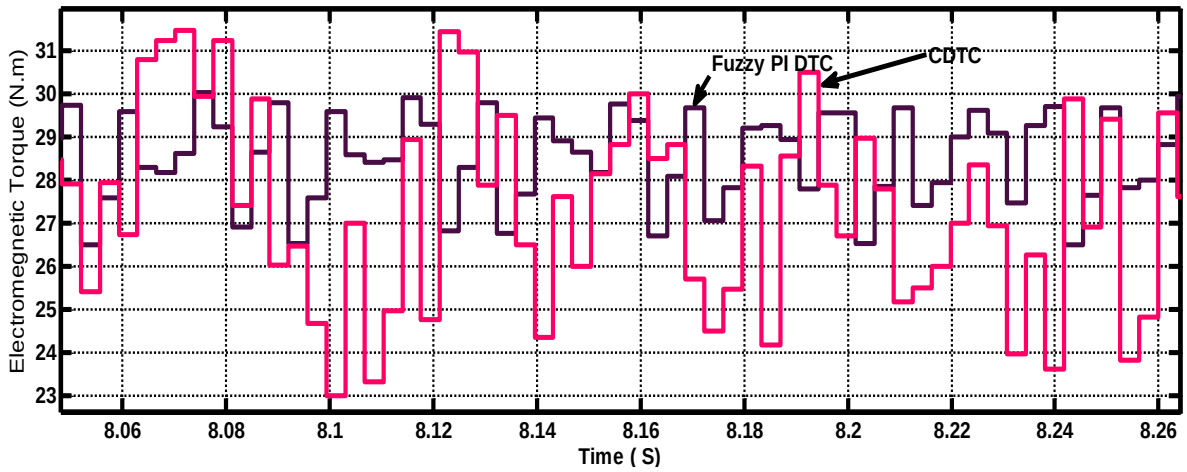

FIGURE 6.12: Comparison of DTC and Fuzzy logic controller based DTC for torque Ripple

6.5 Carrier space vector PWM based DTC (CSVPWM-DTC)

The CSVPWM technique for DTC based induction motor drive is implemented using MATLAB™/SIMULINK™ software. The different magnitude of the common-mode voltage at triplen frequency is added to the sinusoidal and reference signal compared with the triangular carrier signal [86], [87], [88]. Block diagram of CSVPWM based induction motor drive and generation of CSVPWM is presented in Fig. 6.13.

Based on the steps demonstrated above the Carrier Space Vector Pulse Width Modulation (CSVPWM) is generated which in turn used to control the switching of power devices in a three phase full-bridge voltage source inverter. The main purpose is to inspect the consequence of the different level of injecting common-mode voltage on the electromagnetic torque ripple. CSVPWM, DTC, DTC-SVM, Fuzzy speed controller based DTC are compared and analyzed in terms of torque ripple of the three phase induction motor in the next subsection.

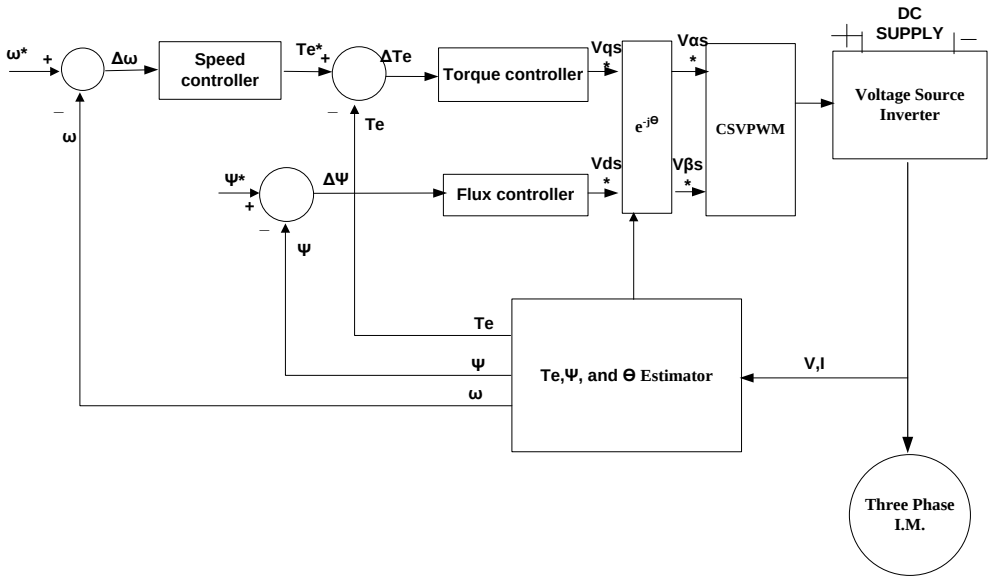

FIGURE 6.13: Block diagram for CSVPWM DTC based induction motor drive

The third harmonic reference signal is added into sinusoidal fundamental reference signal, which leads to a 15.5% increase in the utilization of dc-link voltage [89]. The maximum peak inverter output voltage can be given as

$$V_p = (3.\sqrt{3})/2 * V_m/\pi = 82.7\%V_m \quad (6.5)$$

If rectifier output is smoothed by huge capacitor dc-link input voltage is improved by 4.7% to V_p. Hence the peak inverter output voltage is $V_p = \sqrt{3}/2 * V_m = 86.67\%$ is achieved [89]. By using CSVPWM method, a 15% increase in modulation index can be achieved by incorporating one-sixth third harmonic injection to the fundamental reference waveform [89],[90]. The maximum possible increase in fundamental component by 25% of the target fundamental for optimum third harmonic injection. The Simulation of DTC based Three phase induction motor drive is performed using MATLAB^{TM} software, and the percentage of ripple present in the torque is measured. In the third harmonic injection method, it is challenging to add specific third harmonic voltage during the cycle to cycle. In proposed Carrier Space Vector PWM (CSVPWM) this problem is resolved. The torque ripple is significantly reduced.

6.5.1 Simulation Results of CSVPWM based DTC induction motor drive

The MATLAB™ simulation parameters for CSVPWM simulations are:
Switching frequency: 1050Hz
System frequency: 50 Hz
Three phase induction motor 5.4 HP (4 kW), 50 Hz, 400 V, 4 Pole, 1440 rpm
DC bus voltage: 600V
Modulating index: 1
The parameters and operating condition for 5.4 HP Induction motor CSVPWM based DTC drive are shown in Table 6.4, Table 6.5 respectively.

Reference signal generated by adding 25% common-mode voltage of third harmonic sinusoidal wave to the pure sinusoidal 50 Hz wave. The carrier to reference signal frequency ratio (f_c/f_r) is 21. The simulation results observed and analyze for reference signal generated by adding 35%, 25% and 15% common-mode voltage of third harmonic sinusoidal wave to the pure sinusoidal 50 Hz wave respectively for three cases. At initial 1000 rpm speed command with reference torque, 20 Nm applied. At 5-second load torque increase to 27 Nm and speed increase to 1400 rpm at t = 7 Second. Initially, the motor accelerates from a standstill with 20 Nm load, and it reaches 1000 rpm steady state at t = 0.085 seconds. The torque ripple analysis is done for steady-state condition. Comparison of carrier signal 1050 Hz and reference 50 Hz signal for CSVPWM generation implemented according to Fig. 6.14. The CSVPWM-DTC scheme has been simulated in MATLAB™/ Simulink™. The simulation results analyze for reference signal generated by adding 35%, 25% and 15% common-mode voltage of third harmonic sinusoidal wave to the pure sinusoidal 50 Hz reference signal respectively for all above three cases. The CSVPWM with 15% CMV, 25% CMV, 35% CMV, Fuzzy DTC simulation torque ripple results presented and compared with conventional DTC (CDTC). Fig. 6.15 and Fig. 6.16 show the waveform for CSVPWM generation. Fig. 6.16 demonstrates the comparison of carrier signal 1050 Hz and reference 50 Hz signal for CSVPWM generation. Simulation result for the line voltage and electromagnetic torque pulsation during the steady state is shown in Fig. 6.17. Variation of load torque and its effect is shown in Fig. 6.18. Electromagnetic torque changes as per operating conditions discussed in Table 6.5. The Fig. 6.19 to Fig. 6.22 demonstrated torque responses of different CSVPWM methods.

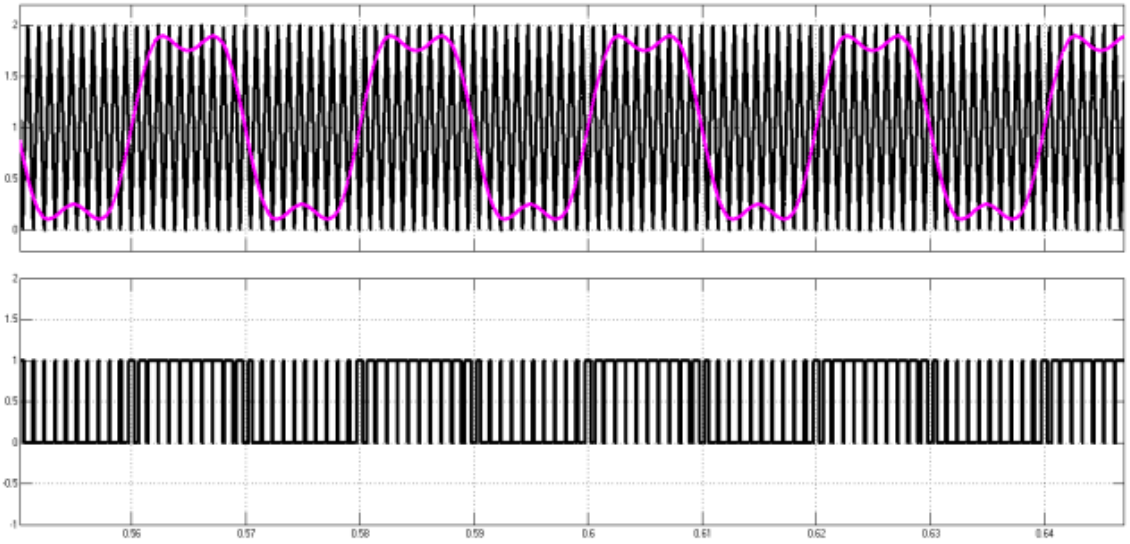

FIGURE 6.14: Comparison of carrier signal 1050 Hz and reference 50 Hz signal for CSVPWM generation

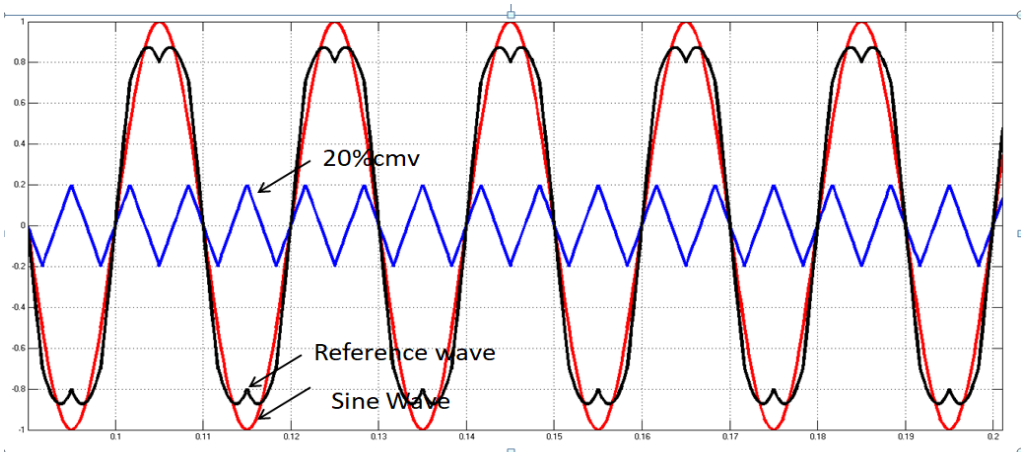

FIGURE 6.15 : CSVPWM modulating signal (Triangular common mode voltage added to pure sinusoidal wave results in reference wave)

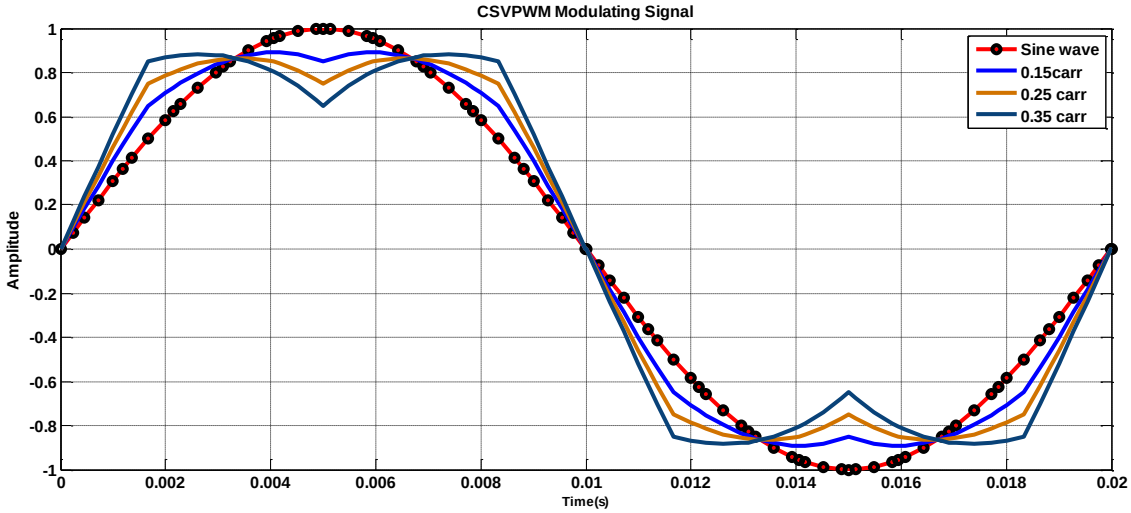

FIGURE 6.16: CSVPWM modulating signal

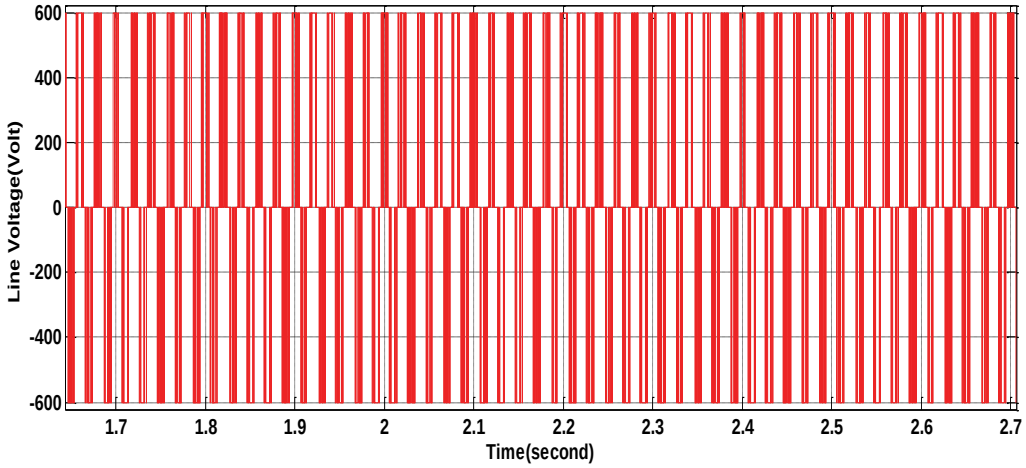

FIGURE 6.17: Line voltage (V_{ab}) of CSVPWM fed induction motor drive

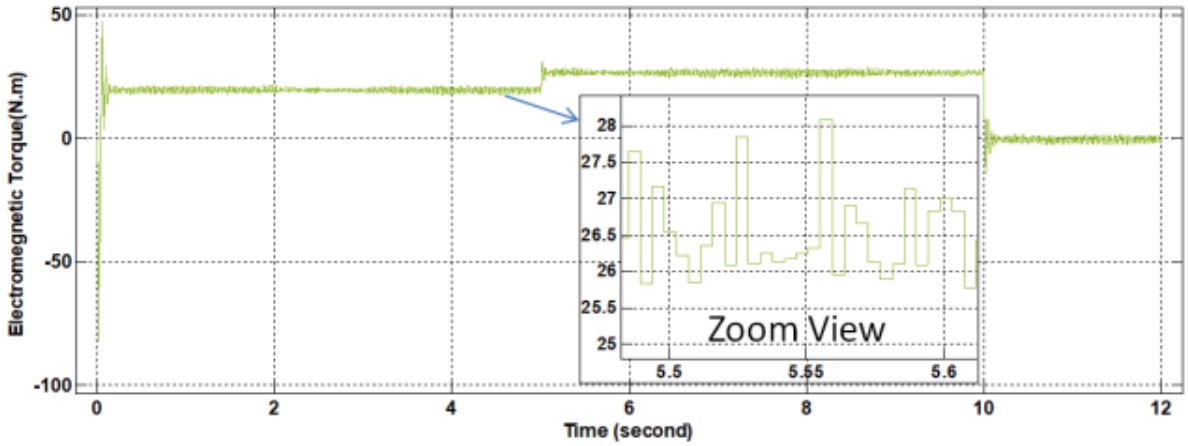

FIGURE 6.18: Torque ripple of CSVPWM fed induction motor with respect to time (sec)

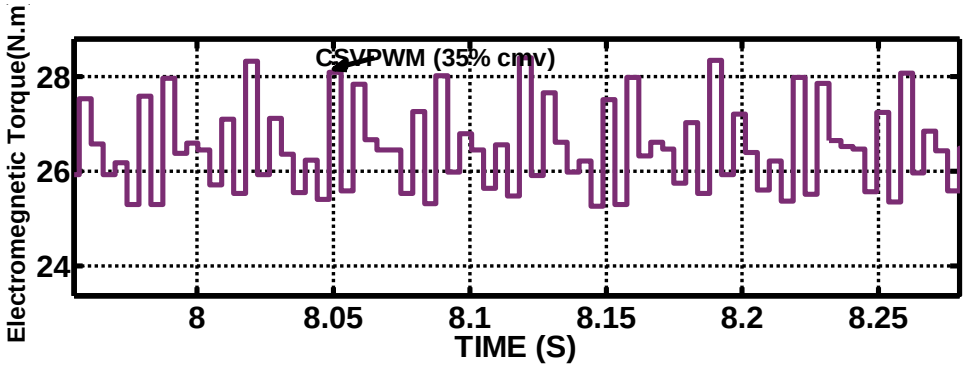

FIGURE 6.19: CSVPWM (35% CMV) torque ripple is 3 Nm for 27 Nm applied torque (TR = 11.11%)

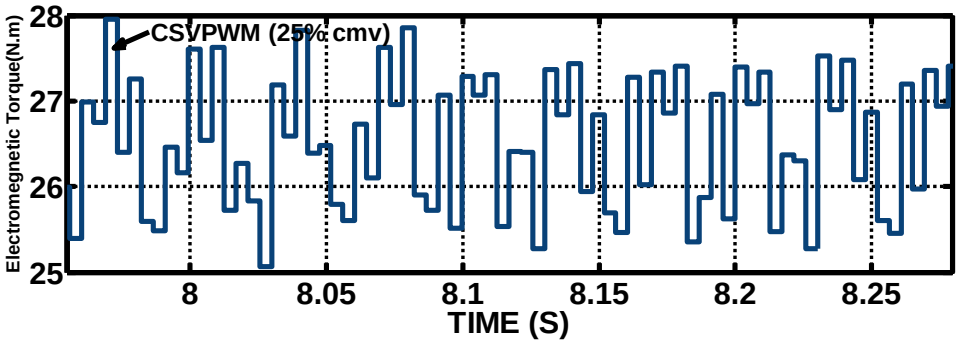

FIGURE 6.20: CSVPWM (25% CMV) torque ripple is 2.5 Nm for 27 Nm applied torque (TR = 9.2%)

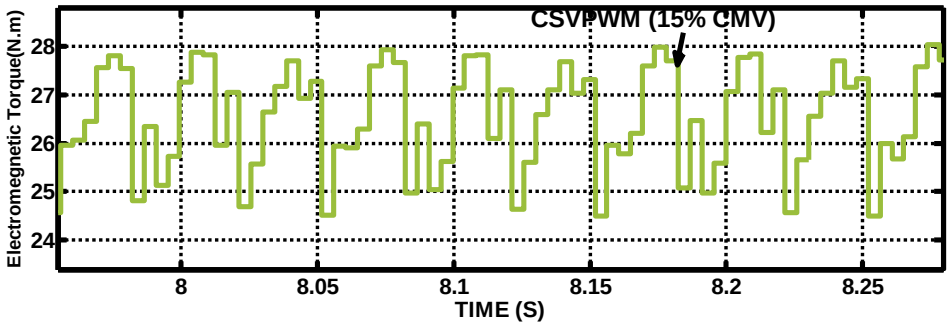

FIGURE 6.21: CSVPWM (15% CMV) torque ripple is 3.5 Nm for 27 Nm applied torque (TR = 12.9%)

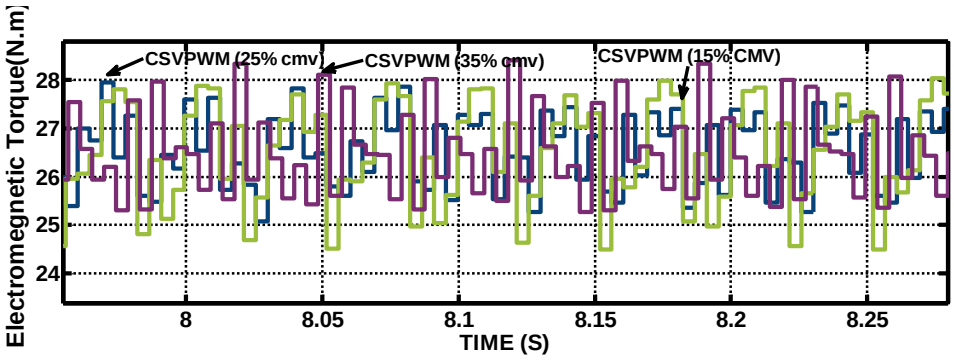

FIGURE 6.22: Comparison of different types of CSVPWM DTC for torque ripple analysis

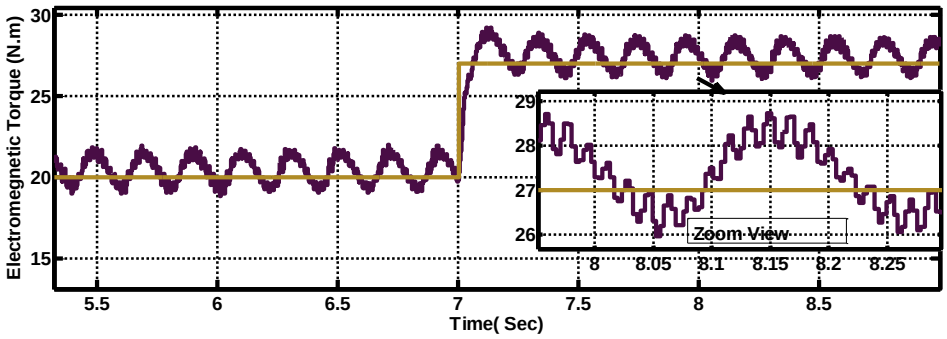

FIGURE 6.23: SVPWM DTC induction motor drive torque ripple observation is 3 Nm over 27 Nm applied torque (TR = 11.11%)

Fig. 6.23 shows the 3 Nm torque ripple of the SVPWM-based DTC technique for a 27 Nm applied torque. Table 6.6 shows torque ripple comparison of all different strategies discussed for 3-phase induction motor drive. The results obtained for CSVPWM (25% CMV) based DTC as shown in Fig. 6.20. The CSVPWM (25% CMV) based DTC the torque ripple of 2.5 Nm for 27 Nm applied load, and which i.e. to 9.2 % of the applied torque. The best result found is Fuzzy Logic Controller based DTC as in Fig. 6.12 as average 2 Nm of torque ripple for full load torque of 27 Nm (TR = 7.4%). Comparisons of DTC, SVPWM-DTC, CSVPWM, Fuzzy logic controller DTC method have been shown in Fig. 6.24 for torque ripple considering same operating condition for three phase induction motor.

TABLE 6.6: Torque ripple comparison for various strategies

Sr. No	Method	Torque Ripple Nm	Base Torque Nm	%Torque Ripple
1	Fuzzy-DTC	2	27	7.4
2	CSVPWM (25% CMV)	2.5	27	9.2
3	CSVPWM (35% CMV)	3	27	11
4	SVPWM-DTC	3	27	11
5	CSVPWM (15% CMV)	3.5	27	12.9
6	Conventional-DTC	6	27	22.22

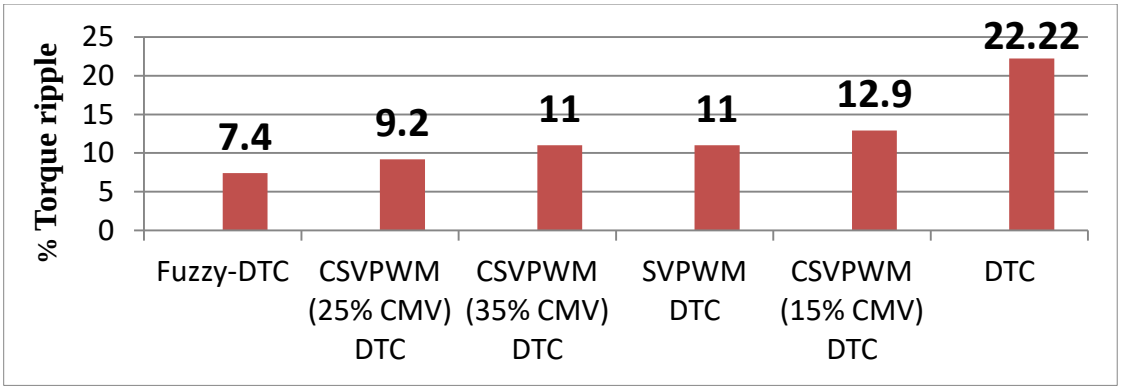

FIGURE 6.24: % Torque ripple for various DTC based induction motor drive method

6.6 Chapter Conclusion

- In this chapter, the overall performance from the viewpoint of torque ripple for conventional DTC, CSVPWM, Fuzzy Logic Controller based DTC based induction motor drive are evaluated using simulation results.
- The significant torque ripple reduction find for fuzzy DTC during steady state full load. The direct torque control induction motor drive for torque ripple analysis is presented. Torque ripple for DTC drive is compared for analysis and review of different methods to minimize torque ripple is discussed.
- The fuzzy based Direct Torque Control method has nearly 2 Nm torque ripple with respect to 27 Nm full load torque. In this concern, around 2.5 NM (9.2%) low torque ripple by CSVPWM with 25% common mode voltage (CMV) based DTC drive is also achieved.
- From the analysis, it is concluded that CSVPWM gives quality voltage and current wave form as THD get reduced hence torque ripple reduction.
- The toque ripple analysis shows opportunity of artificial intelligence technique further for superior results.

In the next chapter, conclusions and scope of future work of the thesis are discussed.

CHAPTER-7

7 Summary, Conclusions and Scope of Future Work

7.1 Summary

The summary of the research work reported in this thesis is discussed below.

1. The energy recovery strategy of a DTC based induction motor drive with a DC/DC bidirectional converter and a capacitor storage system is analysed and discussed. The control strategy of the bidirectional converter for buck-boost operation is evaluated.
2. Various topologies for induction motor drive for regenerative energy fed to supply grid during deceleration are presented. Energy recovery fed to grid through DC/AC converter for DTC induction motor drive is analysed and discussed with simulation results.
3. A study on energy recovery using DC/AC converter has been explored to maximize energy recovery, depends on several variables like load torque, initial speed of starting of deceleration, motor power rating and deceleration rate are discussed. Load torque is investigated as most significant variable to affect on energy recovery using Taguchi method.
4. Various losses in the energy recovery system are analysed during deceleration of DTC based induction motor drive.
5. Torque ripple reduction techniques for DTC based induction motor drive are explored and found effective torque ripple reduction using Fuzzy logic controller based technique and CSVPWM approach.

7.2 Conclusion

In this thesis, energy recovery and torque ripple analysis of direct torque control based induction motor drive is discussed. From the research work following points are concluded.

1. Enhancement in Energy recovery during deceleration of DTC based three phase induction motor drive through capacitor bank as energy storage device is explored. Around 8 % to 26.68 % energy recovery is found per deceleration cycle in this method.
2. Improved energy recovery using DC/AC converter used to fed back energy to the grid has been observed. The proposed method reduces the losses by removing braking resistor and recovers the energy during deceleration. The energy recovery supply back to grid using DC-AC converter shows energy recovery efficiency from 41% to 90.3% according to given initial speed of deceleration, deceleration rate and load torque condition for 50 HP three phase induction motor DTC drive.
3. The energy recovered during deceleration of the induction motor is a function of load torque, initial speed of starting of deceleration, motor power rating and deceleration rate of the motor. The Taguchi method is used to determine the most significant variable among them, and load torque is discovered to be the most significant variable on energy recovery efficiency. The simulation results show that load torque has a significant impact on energy recovery efficiency; thus, the simulation results are verified using the Taguchi method.
4. Kinetic energy during deceleration cannot be fully recover due to various losses like motor mechanical loss, motor electrical loss, inverter switching loss and kinetic energy consumption loss during deceleration of the induction motor. The overall efficiency of the DTC based induction motor drive is improved by incorporating energy recovery during deceleration of the induction motor.
5. Torque ripple minimization up to 2 Nm (7.5%) by the fuzzy logic controller based DTC induction motor drive is achieved. Torque ripple reduction around 2.5 Nm (9.5%) achieved for 5.4 HP three phase induction motor using DTC-

CSVPWM method. The Overall performance from the viewpoint of torque ripple for conventional DTC, CSVPWM, Fuzzy logic controller based DTC based induction motor drive is evaluated using simulation results. The significant torque ripple reduction is found in Fuzzy logic controller based DTC technique and CSVPWM DTC method.

7.3 Scope of Future Work

There are some recommendations and prospective research directions that extend this work as the scope of future work. The future scopes of the research work are following.

1. Proposed method of recovered energy fed to grid by DC/AC converter during deceleration can be compared with front end converter and matrix converter method.
2. Comparative analysis for energy recovery by bidirectional DC/DC converter can be done along with different energy storage systems with battery, capacitor bank, supercapacitor bank, flywheel, etc.
3. The performance of proposed methods can be evaluated with power quality in terms of power factor, THD and compared to other techniques for power fed to the grid during deceleration.
4. The performance of the proposed method for energy recovery can be evaluated with hardware to check its suitability for specific industrial application, such as traction and electric vehicles.
5. Taguchi's three-level, four-variable (L_9) table approach is used to identify the most important parameters for optimising energy recovery performance. Other optimization techniques can be used to compare the outcomes.
6. Fuzzy, ANN or other AI controllers can be developed for torque ripple reduction of induction motor drive especially for low power ranged motors and for low speed operation.

List of References

[1] M. Dybkowski, “Industrial Drive Systems. Current State and Development Trends,” *Industrial Drive Systems. Current State and Development Trends*, vol. 1, no. 1, pp. 5–25, 2016.

[2] Bimal K. Bose, *Modern power electronics and AC drives*. USA: Prentice Hall PTR, 2002.

[3] G. S. Buja and M. P. Kazmierkowski, “Direct torque control of PWM inverter-fed AC motors - a survey,” *Industrial Electronics, IEEE Transactions on*, vol. 51, no. 4, pp. 744–757, 2004.

[4] T. Ramesh and A. K. Panda, “Direct flux and torque control of three phase induction motor drive using PI and fuzzy logic controllers for speed regulator and low torque ripple,” *2012 Students Conference on Engineering and Systems, SCES 2012*, 2012.

[5] I. Takahashi and T. Noguchi, “A New Quick-Response and High-Efficiency Control Strategy of an Induction Motor,” *Industry Applications, IEEE Transactions on*, vol. IA-22, no. 5, pp. 820–827, 1986.

[6] M. Depenbrock, “Direct self-control (DSC) of inverter-fed induction machine,” *IEEE Transactions on Power Electronics*, vol. 3, no. 4, pp. 420–429, Oct. 1988.

[7] C. M. F. S. Reza, M. D. Islam, and S. Mekhilef, “A review of reliable and energy efficient direct torque controlled induction motor drives,” *Renewable and Sustainable Energy Reviews*, vol. 37, pp. 919–932, 2014.

[8] N. El Ouanjli *et al.*, “Modern improvement techniques of direct torque control for induction motor drives - a review,” vol. 5, 2019.

[9] A. Jidin, N. R. N. Idris, A. H. M. Yatim, A. Z. Jidin, and T. Sutikno, “Torque ripple minimization in DTC induction motor drive using constant frequency torque controller,” *2010 International Conference on Electrical Machines and Systems, ICEMS2010*, no. 8, pp. 919–924, 2010.

[10] Kazmierkowski Marian and Henryk Tunia, *Automatic Control of Converter-Fed Drives*. Amsterdam: Elsevier B.V., 1994.

[11] L. Roman, Constantin Paul; Staretu, Ionel; Bogdan, “Torque and speed in the

actuating of mechatronic systems, a case study," *Robotica & Management*, vol. 20, no. 2, pp. 55–60, 2015.

[12] T. Sutikno, N. R. N. Idris, A. Z. Jidin, and M. Z. Daud, "FPGA based high precision torque and flux estimator of direct torque control drives," *2011 IEEE Applied Power Electronics Colloquium (IAPEC)*, pp. 122–127, 2011.

[13] Bhim Singh, Pradeep Jain, A. P. Mittal, and J. R. P. Gupta, "Direct torque control: a practical approach to electric vehicle," in *2006 IEEE Power India Conference*, 2006, p. 4.

[14] X. Yan and D. Patterson, "Improvement of drive range, acceleration and deceleration performance in an electric vehicle propulsion system," in *30th Annual IEEE Power Electronics Specialists Conference. Record. (Cat. No.99CH36321)*, 1999, vol. 2, pp. 638–643 vol.2.

[15] S. Harada and H. Fujimoto, "Range extension control system for electric vehicles based on optimal-deceleration trajectory and front-rear driving-braking force distribution considering maximization of energy regeneration," in *2014 IEEE 13th International Workshop on Advanced Motion Control (AMC)*, 2014, pp. 173–178.

[16] A. Taut, O. Pop, and E. Ceuca, "System for energy recovering with BLDC motor at deceleration momentum," in *Proceedings of the 36th International Spring Seminar on Electronics Technology*, 2013, pp. 299–304.

[17] J. Rodriguez, J. Pontt, C. Silva, S. Kouro, and H. Miranda, "A novel direct torque control scheme for induction machines with space vector modulation," in *2004 IEEE 35th Annual Power Electronics Specialists Conference (IEEE Cat. No.04CH37551)*, 2004, vol. 2, pp. 1392-1397 Vol.2.

[18] P. Zhang, G. Y. Sizov, and N. A. O. Demerdash, "Comparison of torque ripple minimization control techniques in Surface-Mounted Permanent Magnet Synchronous Machines," *2011 IEEE International Electric Machines and Drives Conference, IEMDC 2011*, pp. 188–193, 2011.

[19] A. M. Trzynadlowski, *Control of induction motors*, 1st ed. USA: academic press, Elsevier, 2001.

[20] S. K. Yadav, S. Shiva Kumar, H. Kumar, and C. Mishra, "Investigation on Energy Recovery Converter using Industrial Motor Drive," in *2019 International Conference on Vision Towards Emerging Trends in Communication and Networking (ViTECoN)*, 2019, pp. 1–4.

[21] P. Binesh Mohan and V. R. Bindu, “Energy Regeneration in Induction Machine Drive During Braking,” in *2018 2nd International Conference on Trends in Electronics and Informatics (ICOEI)*, 2018, pp. 91–95.

[22] I. Karatzaferis, E. C. Tatakis, and N. Papanikolaou, “Investigation of Energy Savings on Industrial Motor Drives Using Bidirectional Converters,” *IEEE Access*, vol. 5, pp. 17952–17961, 2017.

[23] Z. Raud, V. Vodovozov, N. Lillo, and A. Rassõlkin, “Reserves for Regenerative Braking of Battery Electric Vehicles | Anton Rassõlkin - Academia.edu,” in *2014 Electric Power Quality and Supply Reliability Conference (PQ)*, 2014, pp. 189–194.

[24] A. Rassõlkin and V. Vodovozov, “Experimental setup to explore the drives of battery electric vehicles,” *World Electric Vehicle Journal*, vol. 6, no. 4, pp. 1109–1114, 2013.

[25] K. P. Ł. Ek, T. Detka, K. Ż. Ebrowski, and K. M. A. Ł. Ek, “Analysis of Regenerative Braking Strategies,” *Electrotechnical Review*, no. 6, pp. 117–123, 2019.

[26] L. Liu, H. Li, S. Hwang, and J. Kim, “An Energy-Efficient Motor Drive With Autonomous Power Regenerative Control System Based on Cascaded Multilevel Inverters and Segmented Energy Storage,” *IEEE Transactions on Industry Applications*, vol. 49, no. 1, pp. 178–188, Jan. 2013.

[27] Y. Fan, L. Zhang, and M. Wei, “The Improved Direct Torque Control of a New Self-Decelerating Permanent-Magnet In-Wheel Motor for Electric Vehicles,” in *2013 IEEE Vehicle Power and Propulsion Conference (VPPC)*, 2013, pp. 1–5.

[28] A. K. Kaviani, S. Member, B. Hadley, and S. Member, “A Time-Coordination Approach for Regenerative Energy Saving in Multiaxis Motor-Drive Systems,” *IEEE Transactions on Power Electronics*, vol. 27, no. 2, pp. 931–941, 2012.

[29] S. Di Cairano, J. Doering, I. V Kolmanovsky, and D. Hrovat, “Model Predictive Control of Engine Speed During Vehicle Deceleration,” *IEEE Transactions on Control Systems Technology*, vol. 22, no. 6, pp. 2205–2217, Nov. 2014.

[30] M. Saleh, Y. Esa, Y. Mhandi, W. Brandauer, and A. Mohamed, “Design and implementation of CCNY DC microgrid testbed,” *IEEE Industry Application Society, 52nd Annual Meeting: IAS 2016*, no. October 2017, 2016.

[31] S. K. Kim, J. H. Jeon, C. H. Cho, J. B. Ahn, and S. H. Kwon, “Dynamic modeling

and control of a grid-connected hybrid generation system with versatile power transfer," *IEEE Transactions on Industrial Electronics*, vol. 55, no. 4, pp. 1677–1688, 2008.

[32] F. J. T. E. Ferreira, M. V Cistelecan, A. T. de Almeida, and G. Baoming, "Simple strategy to recovery energy during stopping period in large high-inertia line-fed induction motor driven systems," in *2008 18th International Conference on Electrical Machines*, 2008, pp. 1–6.

[33] S. Geraee, H. Mohammadbagherpoor, M. Shafiei, M. Valizadeh, F. Montazeri, and M. R. Feyzi, "Regenerative braking of electric vehicle using a modified direct torque control and adaptive control theory," *Computers & Electrical Engineering*, vol. 69, pp. 85–97, 2018.

[34] K. Itani, A. De Bernardinis, Z. Khatir, and A. Jammal, "Comparison between two braking control methods integrating energy recovery for a two-wheel front driven electric vehicle," *Energy Conversion and Management*, vol. 122, pp. 330–343, 2016.

[35] L.-H. Björnsson and S. Karlsson, "The potential for brake energy regeneration under Swedish conditions," *Applied Energy*, vol. 168, pp. 75–84, 2016.

[36] N. Apostolidou and N. Papanikolaou, "Energy Saving Estimation of Athens Trolleybuses Considering Regenerative Braking and Improved Control Scheme," *Resources*, vol. 7, no. 3, p. 43, 2018.

[37] K. Y. Lin and K. Y. Lian, "Actual measurement on regenerative elevator drive and energy saving benefits," in *2017 International Automatic Control Conference, CACS 2017*, 2017, pp. 1–5.

[38] A. Pyper and P. S. Heyns, "Evaluating a distributed regenerative braking system for freight trains," *Proceedings of the Institution of Mechanical Engineers, Part F: Journal of Rail and Rapid Transit*, pp. 1–13, 2018.

[39] S. Heydari, P. Fajri, R. Sabzehgar, and M. Rasouli, "A Novel Approach for Maximizing Regenerative Braking Energy Extraction of Electric Vehicles Using Motor Performance Lookup Table," in *2019 IEEE Transportation Electrification Conference and Expo (ITEC), Detroit, MI, USA*, 2019, pp. 1–5.

[40] N. R. Raju, "An SCR-based regenerative converter for VSI drives," in *PESC Record - IEEE Annual Power Electronics Specialists Conference*, 2003, vol. 4, pp. 1770–1774.

[41] C. L. Chu, C. W. Chou, J. R. Chen, H. Y. Chan, and J. H. Fang, "Study of an electric vehicle drive dynamic testing system with energy recovery," *Procedia Engineering*, vol. 23, pp. 608–615, 2011.

[42] A. T. de Almeida, F. J. T. E. Ferreira, and D. Both, "Technical and economical considerations in the application of variable-speed drives with electric motor systems," *IEEE Transactions on Industry Applications*, vol. 41, no. 1, pp. 188–199, Jan. 2005.

[43] K. O. and T. K. Inoue, "A Study on an Optimal Torque for Power Regeneration of an Induction Motor," *22nd European Photovoltaic Solar Energy Conference and Exhibition*, no. 2, p. 3180, 2007.

[44] A. Mohamed, M. Elshaer, and O. Mohammed, "Bi-directional AC-DC/DC-AC converter for power sharing of hybrid AC/DC systems," *IEEE Power and Energy Society General Meeting*, pp. 1–8, 2011.

[45] A. Maiti, K. Mukherjee, and P. Syam, "Design methodology, control and performance of a three-phase grid-Tie PV inverter under maximum power point tracking," *2016 2nd International Conference on Control, Instrumentation, Energy and Communication, CIEC 2016*, pp. 382–386, 2016.

[46] K. R. Rasin and G. Arunkumar, "Regeneration in Variable Frequency Drives and Energy saving Methods," *International Research Journal of Engineering and Technology(IRJET)*, vol. 4, no. 3, pp. 1246–1249, 2017.

[47] A. B. B. Drives, "Technical guide No. 8 - Electrical Braking," no. 8, 2018.

[48] S. K. Sahoo, D. Patel, M. Balamurugan, and A. K. Sahoo, "A control methodology of bidirectional converter for grid connected systems," *Indian Journal of Science and Technology*, vol. 9, no. 38, pp. 1–7, 2016.

[49] A. Parra, D. Tavernini, P. Gruber, A. Sorniotti, A. Zubizarreta, and J. Pérez, "On Nonlinear Model Predictive Control for Energy-Efficient Torque-Vectoring," *IEEE Transactions on Vehicular Technology*, vol. 70, no. 1, pp. 173–188, Jan. 2021.

[50] "Crane duty motors," 2019. [Online]. Available: https://www.menzel-motors.com/crane-duty-motor/. [Accessed: 08-Dec-2019].

[51] "Hoist Duty Motor," 2019. [Online]. Available: https://www.ashokelectromech.com/search.html?ss=Hoist+Duty+Motor. [Accessed: 08-Dec-2019].

[52] "Textile Motors," 2019. [Online]. Available: http://www.starkindustry.com/textile-motors.html. [Accessed: 08-Dec-2019].

[53] D. Telford, M. W. Dunnigan, and B. W. Williams, "A novel torque-ripple reduction strategy for direct torque control [of induction motor]," *IEEE Transactions on Industrial Electronics*, vol. 48, no. 4, pp. 867–870, 2001.

[54] T. G. Habetler, F. Profumo, M. Pastorelli, and L. M. Tolbert, "Direct torque control of induction machines using space vector modulation," *IEEE Transactions on Industry Applications*, vol. 28, no. 5. pp. 1045–1053, 1992.

[55] S. N. Pandya and J. K. Chatterjee, "Torque Ripple Minimization in Direct Torque Control based IM Drive Part-I: Single-rate Control Strategy," *2008 Joint International Conference on Power System Technology and IEEE Power India Conference*, pp. 1–8, 2008.

[56] J. Beerten, J. Verveckken, and J. Driesen, "Predictive Direct Torque Control for Flux and Torque Ripple Reduction," *IEEE Transactions on Industrial Electronics*, vol. 57, no. 1, pp. 404–412, 2010.

[57] S. Kuo-Kai, L. Juu-Kuh, P. Van-Truong, Y. Ming-Ji, and W. Te-Wei, "Global Minimum Torque Ripple Design for Direct Torque Control of Induction Motor Drives," *Industrial Electronics, IEEE Transactions on*, vol. 57, no. 9, pp. 3148–3156, 2010.

[58] Saurabh N. Pandya and J. K. Chatterjee, "Torque Ripple Reduction in Direct Torque Control based Induction Motor Drive Using Novel Optimal Controller Design Technique."

[59] R. Rahmani, N. M. A. Langeroudi, R. Yousefi, M. Mahdian, and M. Seyedmahmoudian, "Fuzzy logic controller and cascade inverter for direct torque control of IM," *Neural Computing and Applications*, vol. 25, no. 3–4, pp. 879–888, 2014.

[60] T. H. Atyia, "Control Techniques of Torque Ripple Minimization for Induction Motor," *Tikrit Journal of Engineering Sciences*, vol. 25, no. 4, pp. 56–62, 2018.

[61] J. Kang and S. Sul, "Torque ripple minimization strategy for direct torque control of production motor," *Conference Record of IEEE-IAS Annual Meeting*, vol. 1, pp. 438–443, 1998.

[62] S. Srivastava and A. K. Jain, "High performance constant switching frequency hysteresis-based direct torque control technique," in *2014 IEEE International*

Conference on Power Electronics, Drives and Energy Systems (PEDES), 2014, pp. 1–5.

[63] K. K. Chouhan and G. B. Buch, "Improved direct torque control of induction motor," in *2015 International Conference on Electrical, Electronics, Signals, Communication and Optimization (EESCO)*, 2015, pp. 1–5.

[64] G. D. Sukumar and G. Srinivas, "D-Q axis voltage ripple minimization of vector control drive using Type-2 NFS controller," in *2017 International Conference on Inventive Computing and Informatics (ICICI)*, 2017, pp. 1098–1102.

[65] A. A. Ahmed, B. K. Koh, and Y. I. Lee, "Torque Control of Induction Motors with Minimal Ripples Based on Continuous Control Set-MPC in a Wide Speed Range," in *2017 IEEE Vehicle Power and Propulsion Conference (VPPC)*, 2017, pp. 1–6.

[66] Y. Cho, Y. Bak, and K. B. Lee, "Torque-Ripple Reduction and Fast Torque Response Strategy for Predictive Torque Control of Induction Motors," *IEEE Transactions on Power Electronics*, vol. 33, no. 3, pp. 2458–2470, Mar. 2018.

[67] M. P. Kazmierkowski and G. Buja, "Review of direct torque control methods for voltage source inverter-fed induction motors," *Industrial Electronics Society, 2003. IECON '03. The 29th Annual Conference of the IEEE*, vol. 1, pp. 981–991, 2003.

[68] D. Casadei, G. Serra, A. Tani, and L. Zarri, "Direct Torque Control for induction machines: A technology status review," in *2013 IEEE Workshop on Electrical Machines Design, Control and Diagnosis (WEMDCD)*, 2013, pp. 117–129.

[69] S. V Jadhav, J. Kirankumar, and B. N. Chaudhari, "ANN based intelligent control of Induction Motor drive with Space Vector Modulated DTC," in *2012 IEEE International Conference on Power Electronics, Drives and Energy Systems (PEDES)*, 2012, pp. 1–6.

[70] S. Gdaim, A. Mtibaa, and M. F. Mimouni, "Design and Experimental Implementation of DTC of an Induction Machine Based on Fuzzy Logic Control on FPGA," *IEEE Transactions on Fuzzy Systems*, vol. 23, no. 3, pp. 644–655, 2015.

[71] F. D. R. Figueroa and A. V. M. Caeiros, "Genetically Enhanced Intelligent Speed Control for Induction Machines Using Direct Torque Control," in *2011 IEEE Electronics, Robotics and Automotive Mechanics Conference*, 2011, pp. 35–40.

[72] J. Yuan, X. Ma, and J. Liu, "Simulation research of induction motor based on SVM-DTC with three-level inverter," *ICEIEC 2015 - Proceedings of 2015 IEEE 5th International Conference on Electronics Information and Emergency*

Communication, pp. 410–413, 2015.

[73] R. Sadhwani and Ragavan K., "A comparative study of speed control methods for induction motor fed by three level inverter," in *2016 IEEE 1st International Conference on Power Electronics, Intelligent Control and Energy Systems (ICPEICES)*, 2016, pp. 1–6.

[74] D. Mohan, X. Zhang, and G. H. B. Foo, "Three-Level Inverter-Fed Direct Torque Control of IPMSM With Constant Switching Frequency and Torque Ripple Reduction," *IEEE Transactions on Industrial Electronics*, vol. 63, no. 12, pp. 7908–7918, Dec. 2016.

[75] K. C. Jana and S. K. Biswas, "Generalised switching scheme for a space vector pulse-width modulation-based N-level inverter with reduced switching frequency and harmonics," *IET Power Electronics*, vol. 8, no. 12, pp. 2377–2385, 2015.

[76] E. Hassankhan and D. A. Khaburi, "DTC-SVM Scheme for Induction Motors Fedwith a Three-level Inverter," *PWASET*, vol. 2, no. 8, p. 10, 2008.

[77] R. Trounce, J.C., Round, S. and Duke, "Comparison by simulation of three-level induction motor torque control schemes for electric vehicle applications," *Singapore: Proceedings of the International Power Engineering Conference*, vol. 1, no. 1, pp. 294–299, 2001.

[78] M. dekker I. N. york Cochran, Paul L., *Polyphase induction motors analysis, design and application*. 1989.

[79] J. Billy, "Modeling and demonstrating regenerative braking of a squirrel cage induction motor with various deceleration rates using V by F control," Naval Postgraduate School, USA, 2010.

[80] J. E. Vrancikpg, *Prediction of windage power loss in alternator*, Note no. 1. Washington DC: NASA Technical note, 1968.

[81] K. Sarrafan, D. Sutanto, K. M. Muttaqi, and G. Town, "Accurate range estimation for an electric vehicle including changing environmental conditions and traction system efficiency," *IET Electrical Systems in Transportation*, vol. 7, no. 2, pp. 117–124, 2017.

[82] C. R. K. G. Garg, *Research methodology : methods and techniques*, 2nd ed. New Age International (P) Limited, New Delhi, 2004.

[83] D. C. Montgomery, *Design and Analysis of Experiments*, June 2019. USA: wiley.

[84] N. H. S. Ray, "Statistical Analyses of Energy and Exergy of a diesel engine using diesel and biogas in dual fuel mode by Taguchi method," vol. 6, no. 8, pp. 1167–1175, 2017.

[85] S. Athreya and Y. D. Venkatesh, "Application Of Taguchi Method For Optimization Of Process Parameters In Improving The Surface Roughness Of Lathe Facing Operation," *International Refereed Journal of Engineering and Science*, vol. 1, no. 3, pp. 13–19, 2012.

[86] S. N. Pandya and J. K. Chatterjee, "Torque ripple minimization in DTC based induction motor drive using carrier space vector modulation technique," in *2010 Joint International Conference on Power Electronics, Drives and Energy Systems 2010 Power India*, 2010, pp. 1–7.

[87] S. N. Pandya and J. K. Chatterjee, "Torque ripple reduction in direct torque control based induction motor drive using novel optimal controller design technique," in *2010 Joint International Conference on Power Electronics, Drives and Energy Systems 2010 Power India*, 2010, pp. 1–7.

[88] M. A. Al-hitmi, S. Moinoddin, A. Iqbal, K. Rahman, and M. Meraj, "Space Vector vs . Sinusoidal Carrier-Based Pulse Width Modulation for a Seven-Phase Voltage Source Inverter," vol. 4, no. 3, pp. 230–243, 2019.

[89] D.G. Holmes; T.A. Lipo, *Pulse width modulation for power converters principles and practices*. IEEE Press, 2003.

[90] B. N. Kar, K. B. Mohanty, and M. Singh, "Indirect vector control of induction motor using fuzzy logic controller," in *2011 10th International Conference on Environment and Electrical Engineering*, 2011, pp. 1–4.

List of Publications

[1] P. D. Patel and S. N.Pandya, “Energy Regeneration during Deceleration of Direct Torque Control of Induction Motor Drive for Electric Vehicles,” in 2019 *IEEE International Conference on Electrical, Computer and Communication Technologies (ICECCT)*, Coimbatore, India, Feb-2019, no. 3, pp. 5–8.

[2] P. D. Patel and S. N.Pandya, “Energy Regeneration in Direct Torque Control Drive of Induction Motor,” *Lecture Note Electrical Eengineering*, Springer Book Chapter, Singapore, ISSN- 1876-1100, Nov- 2020, pp. 179–189.

[3] P. D. Patel and S. N. Pandya, “Regenerative energy fed to the grid by dc-ac converter during deceleration for direct torque control of induction motor drive,” *International Journal of Ambient Energy*, Tayor and Francis, ISSN: 0143-0750, DOI: 10.1080/01430750.2020.1725631, pp. 1–23, Feb-2020.

[4] P. D. Patel and S. N. Pandya, “Analysis of Torque Ripple in Direct Torque Control Drive for Induction Motor” *Inernational conference on advances in Electrical and Computer Technologies 2019(ICAECT 2019)*, Coimbatore, April- 2019.

[5] P. D. Patel and S. N. Pandya, "A comparative study of direct torque control and space vector pwm technique for torque ripple minimization of induction motor", *National Conference on Recent Advances in Automation Control and Power Engineering (RAACPE- 2017)*, SCET, Surat, ISBN: 978-81-933591-4-3.

[6] P. D. Patel and S. N. Pandya, “Torque Ripple Minimization Techniques Of Direct Torque Control Drive Of Induction Motor,” *TEQIP-II Sponsered National conference "Advancements in Electrical and Power Electronics Engineering (AEPEE-16),”* L.E.C. Morbi, 2016.

- **Under review Research Paper**

[1] P. D. Patel and S. N. Pandya, “Comparative analysis of torque ripple of direct torque control based induction motor drive with different strategies,” Australian Journal of Electrical and Electronics Engineering, ISSN no. 1448837X, Under review.

Appendix A

A.1. Hardware setup for study of torque ripple in conventional DTC based induction motor drive

The hardware setup is developed in courtesy of Government Engineering College, Patan.

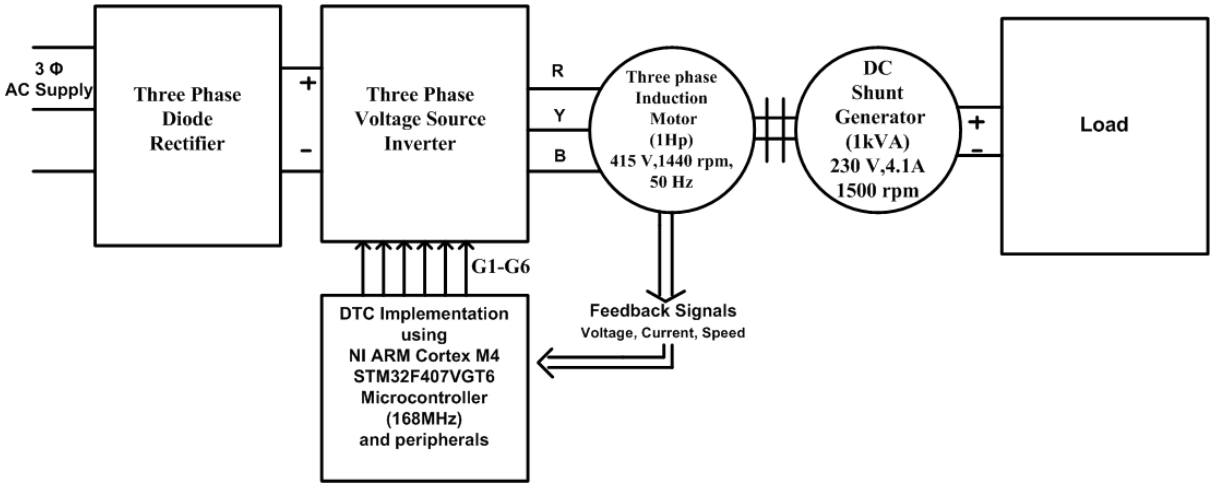

FIGURE A.1 : Block Diagram for Hardware Setup

TABLE. A.1: Parameters of the Induction motor used for Hardware

Parameters	Ratings
Rated Power	1 HP
Rated Voltage	415 V
Rated Speed	1440 RPM
Pole pairs	2
Stator resistance	12.6 Ω
Stator leakage inductance	120.35 mH
Rotor leakage inductance	120.35 mH
Air gap inductance	974 mH
Rotor time Constant(J)	0.08042 $kg.m^2$
Friction factor(F)	0.06 N.m.s

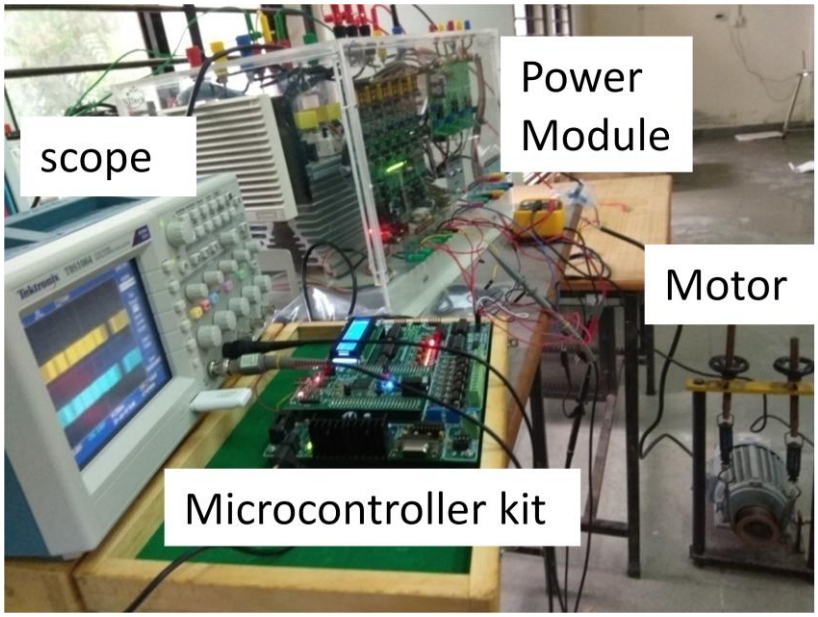

FIGURE A.2 : Hardware Setup for DTC Drive

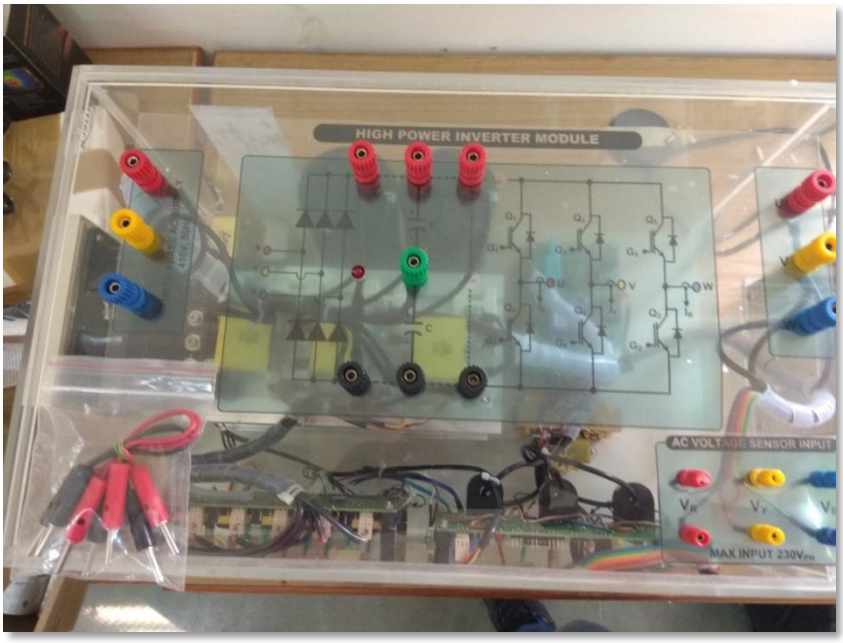

FIGURE A.3 : Power inverter module with voltage and current sensor

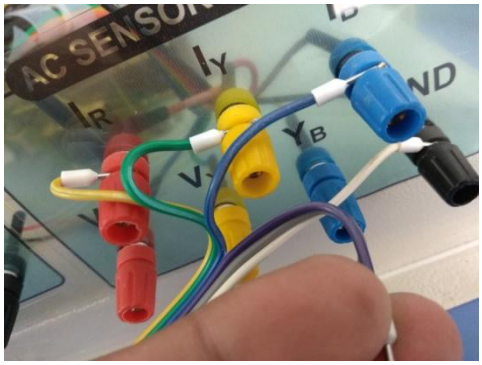

FIGURE A.4 : Current sensing out of three phase Inverter kit

FIGURE A.5 : Proximity sensor for speed sensing

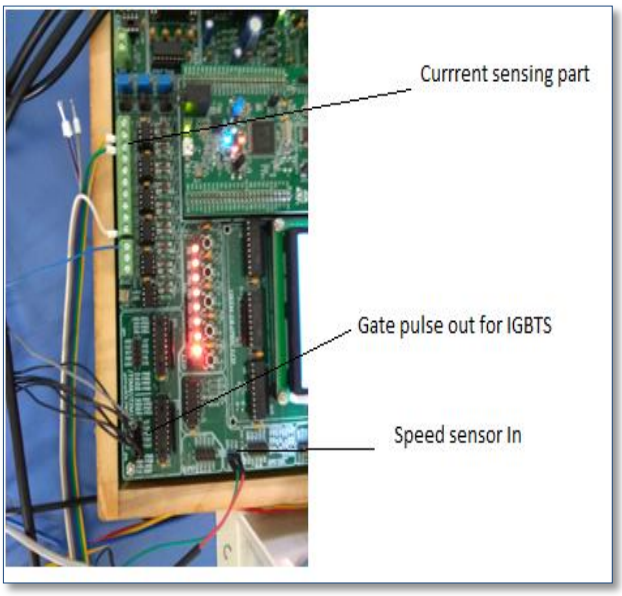

FIGURE A.6 : Microcontroller ARM CORTEX M4 kit

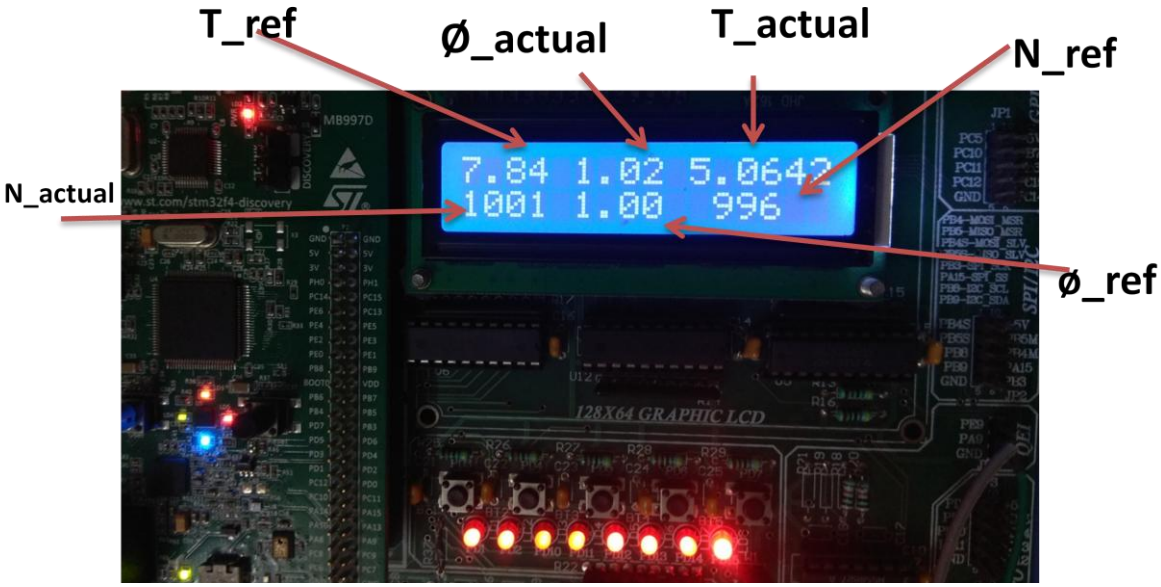

FIGURE A.7 : LED Display for observation of Toque, speed and flux

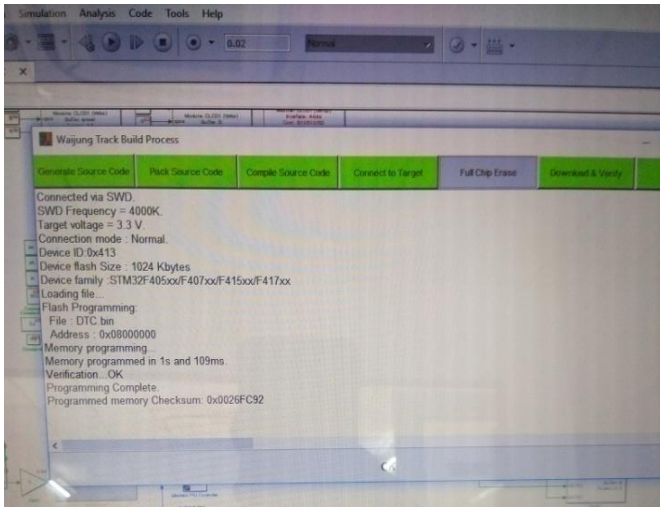

FIGURE A.8 : Screen for WAIJUNG -MATLAB program uploading in controller

A.2. DTC Programming Code

```
%Flux and Torque estimation

function [syi,theta,Te,ids,iqs,vds,vqs,syi_ds1,syi_qs1]=
fcn(ia,ib,sa,sb,sc,vdc,Ts,rds,syi_ds,syi_qs)
%#codegen

ids = ia;
iqs = (ia+(2*ib))/sqrt(3);
vqs =(1/sqrt(3))*(sb-sc)*vdc;
vds = (vdc/3)*((2*sa)-sb-sc);

P=4;%poles
  x =  vds-(ids*rds) ;
  syi_ds  = syi_ds + (x*Ts);
  syi_ds1 = syi_ds;

  y =  vqs-(iqs*rds) ;
  syi_qs  = syi_qs + (y*Ts);
  syi_qs1 = syi_qs;

  syi=sqrt(syi_qs^2+syi_ds^2);
    theta= atan2(syi_qs,syi_ds);

   Te=(3/2)*(P/2)*((syi_ds*iqs)-(syi_qs*ids));
   end


%Torque and Flux controller

function [H_syi,E_syi,H_te1,Ter,i,s,sa,sb,sc]= fcn(te ,te_ref,H_te,syi
,syi_ref,H_syi1,theta)

%Torque loop

HT=0.05; %torque band error 0.012
HB=0.05; %flux band error 0.009
Ter =te_ref-te;

%   if isempty (a)
%   sa=0;
%   sb=0;
%   sc=0;
%   a=0;
% end

if(Ter>HT)
   H_te=1;
elseif(Ter < -HT)
```

```
   H_te= -1;
elseif((Ter>0) &&( Ter<HT))
   if(H_te==1)
      H_te=1;
   elseif(H_te== -1)
      H_te=0;
   end
 elseif((Ter<0)&&(Ter>-HT))
   if(H_te==1)
      H_te=0;
   elseif(H_te== -1)
      H_te= -1;
   end
end
H_te1=H_te;


%flux loop
E_syi = syi_ref - syi;
H_syi=H_syi1;
if(E_syi>HB)
    H_syi = 1;
end
if(E_syi< -HB)
    H_syi = 0;
end
%flux loop ends
%combine results of syi and torque

i =5-3*H_syi-H_te1;

%sector selection


if((theta>= -0.5235)&&(theta<0.5235))%s1
    s=1;

elseif ((theta>=0.5235)&&(theta<1.57079)) %s2
    s=2;

elseif ((theta>=1.57079)&&(theta<2.61799))  %s3
    s=3;

elseif ((theta>=2.61799)&&(theta<3.1415))||((theta>-3.1415)&&(theta< -2.61799))  %s4
    s=4;

elseif ((theta>= -2.61799)&&(theta< -1.57079))  %s5
    s=5;

else ((theta>= -1.57079)&&(theta< -0.5235))  %s6
```

```
    s=6;
end

 % s1=s;
%s selection ends

%s means sector and I means index which gives combine effect of both errors
%#codegen
%s1
%switch status
 if ((s==1)&&(i==1))
sa=1;
sb=1;
sc=0;


 elseif ((s==1)&&(i==2))
 sa=1;
 sb=1;
 sc=1;


 elseif ((s==1)&&(i==3))
sa=1;
sb=0;
sc=1;

 elseif ((s==1)&&(i==4))
sa=0;
sb=1;
sc=0;

 elseif ((s==1)&&(i==5))
sa=0;
sb=0;
sc=0;

 elseif ((s==1)&&(i==6))
sa=0;
sb=0;
sc=1;


%sector2
 elseif ((s==2)&&(i==1))
sa=0;
sb=1;
sc=0;

 elseif ((s==2)&&(i==2))
```

```
sa=0;
sb=0;
sc=0;

 elseif ((s==2)&&(i==3))
sa=1;
sb=0;
sc=0;

 elseif ((s==2)&&(i==4))
sa=0;
sb=1;
sc=1;

 elseif ((s==2)&&(i==5))
sa=1;
sb=1;
sc=1;

 elseif ((s==2)&&(i==6))
sa=1;
sb=0;
sc=1;

%sector3
 elseif ((s==3)&&(i==1))
sa=0;
sb=1;
sc=1;

 elseif ((s==3)&&(i==2))
sa=1;
sb=1;
sc=1;

 elseif ((s==3)&&(i==3))
sa=1;
sb=1;
sc=0;

 elseif ((s==3)&&(i==4))
sa=0;
sb=0;
sc=1;

 elseif ((s==3)&&(i==5))
sa=0;
sb=0;
sc=0;
```

```
 elseif ((s==3)&&(i==6))
sa=1;
sb=0;
sc=0;


%sector4
 elseif ((s==4)&&(i==1))
sa=0;
sb=0;
sc=1;

 elseif ((s==4)&&(i==2))
sa=0;
sb=0;
sc=0;

 elseif ((s==4)&&(i==3))
sa=0;
sb=1;
sc=0;

 elseif ((s==4)&&(i==4))
sa=1;
sb=0;
sc=1;

 elseif ((s==4)&&(i==5))
sa=1;
sb=1;
sc=1;

 elseif ((s==4)&&(i==6))
sa=1;
sb=1;
sc=0;

%sector5
 elseif ((s==5)&&(i==1))
sa=1;
sb=0;
sc=1;

 elseif ((s==5)&&(i==2))
sa=1;
sb=1;
sc=1;

 elseif ((s==5)&&(i==3))
sa=0;
```

```
sb=1;
sc=1;

 elseif ((s==5)&&(i==4))
sa=1;
sb=0;
sc=0;

 elseif ((s==5)&&(i==5))
sa=0;
sb=0;
sc=0;

 elseif ((s==5)&&(i==6))
sa=0;
sb=1;
sc=0;

%sector6
 elseif ((s==6)&&(i==1))
sa=1;
sb=0;
sc=0;

 elseif ((s==6)&&(i==2))
sa=0;
sb=0;
sc=0;

 elseif  ((s==6)&&(i==3))
sa=0;
sb=0;
sc=1;

 elseif  ((s==6)&&(i==4))
sa=1;
sb=1;
sc=0;

 elseif ((s==6)&&(i==5))
sa=1;
sb=1;
sc=1;

 else ((s==6)&&(i==6))
sa=0;
sb=1;
sc=1;

 end
```